Theses and Dissertations

Fall 2020

Local Eigenvalue Modification Procedure for Real-Time Model Updating of Structures Experiencing High-Rate Dynamic Events

Claire Rae Drnek

Recommended Citation

Drnek, C. R.(2020). *Local Eigenvalue Modification Procedure for Real-Time Model Updating of Structures Experiencing High-Rate Dynamic Events.* (Doctoral dissertation). Retrieved from https://scholarcommons.sc.edu/etd/6141

LOCAL EIGENVALUE MODIFICATION PROCEDURE FOR REAL-TIME MODEL
UPDATING OF STRUCTURES EXPERIENCING HIGH-RATE DYNAMIC EVENTS

by

Claire Rae Drnek

Bachelor of Science
University of South Carolina, 2019

_____

Submitted in Partial Fulfillment of the Requirements

For the Degree of Master of Science in

Mechanical Engineering

College of Engineering and Computing

University of South Carolina

2020

Accepted by:

Austin Downey, Director of Thesis

Yi Wang, Reader

Cheryl L. Addy, Vice Provost and Dean of the Graduate School

ABSTRACT

Estimating the state of structures that experience high-rate dynamics requires real-time model updating capabilities. In this work, high-rate dynamic events are characterized by 1) large uncertainties in the external loads, 2) high levels of non-stationarities and heavy disturbances, and 3) unmodeled dynamics generated from changes in system configurations. To achieve real-time model updating, an algorithm must circumvent any pre-calculations and be able to update the structure's state on the timescale of 2 ms or less. This can be accomplished in one of two ways: either by creating a simplified model of a complex structure or by simplifying the calculations needed to determine the state of a complex structure. This work presents a methodology that updates a surrogate model of an experimental testbed experiencing varying dynamics by utilizing the local eigenvalue modification process (LEMP) to numerically simplify solving equations of state. The structure's state is continuously updated by adjusting the associated model through online modal analysis where its future states are estimated using a Bayesian search algorithm to compare the measured signals with selected modal models. New modal models are built based on the enhanced estimate of the structure's state and used for subsequent state estimations.

TABLE OF CONTENTS

LIST OF TABLES

LIST OF FIGURES

LIST OF SYMBOLS

1   Denotes state one or initial state.

2   Denotes state two or altered state.

Δ Denotes the change between state one to state two.

12   Denotes the change between state one to state two.

diag   Denotes a diagonal matrix.

T   Denotes a transpose of a vector or matrix.

c   Denotes a connecting node or participating degree of freedom.

$\boldsymbol{M_\#}$ Mass matrix for state # in physical space.

$\boldsymbol{K_\#}$ Stiffness matrix for state # in physical space.

$\ddot{\boldsymbol{X}}$ Acceleration of system in physical space.

$\boldsymbol{X}$ Displacement of system in physical space.

$\overline{\boldsymbol{M}_\#}$ Modal mass matrix for state #.

$\overline{\boldsymbol{K}_\#}$ Modal stiffness matrix for state #.

$\boldsymbol{P_\#}$ Modal displacement of system for state #.

$\ddot{\boldsymbol{P}}_\#$ Modal acceleration of system for state #.

$\boldsymbol{U_\#}$ Matrix of eigenvectors or modal matrix for state #.

$\boldsymbol{U_{12}}$ Modal participation factors.

$\overrightarrow{u_m^\#}$ m-th modal vector for state #.

$\boldsymbol{\lambda}$ Diagonal matrix of eigenvalues or squares of natural frequencies for the initial state.

Λ Diagonal matrix containing the squares of natural frequencies for the altered state.

ω_m m-th natural frequency of initial system state.

Ω_m m-th natural frequency of altered system state.

$\mathbf{I}$ Identity matrix.

$\mathbf{T}$ Tie matrix.

$\vec{t}$ Tie vector.

$\boldsymbol{\alpha}$ Matrix of scalar values from decomposed stiffness change matrix.

$\mathbf{V}$ Change matrix.

$\vec{v}$ Change vector.

S Arbitrary variable used for simplification purposes.

ρ Density.

A_c Cross-sectional area.

l Length.

$_i$ Elemental property for element i.

E Young's Modulus.

x Selected comparison point for roller location.

B Distribution about previous roller location.

A Distribution about roller location prior to B.

$P(R)$ Probability that roller is moving to the right.

$P(L)$ Probability that roller is moving to the left.

$P(E|B)$ Likelihood that x belongs to B.

$P(E|A)$ Likelihood that x belongs to A.

μ_B Previous roller location.

μ_A Roller location prior to μ_B.

Σ Standard deviation of the normal distribution about the last roller position.

$P(R|E)$ Bayes formula.

$\omega_{true}^{current}$ Current measured frequency.

$\omega_{estimate}^{previous}$ Previous analytical frequency.

a, b Regression parameters.

X Collection of roller locations selected as comparison points.

Y Collection of frequency error at X.

x_c Estimated roller location.

t_m Time trace of measured data.

t_e Time trace of estimated data.

LIST OF ABBREVIATIONS

DOF .... Degree(s) of Freedom

DROPBEAR .... Dynamic Reproduction of Projectiles in Ballistic Environments for Advanced Research

EOM .... Equation of Motion

FEA .... Finite Element Analysis

FFT .... Fast Fourier Transform

GE .... General Eigenvalue

LEMP .... Local Eigenvalue Modification Procedure

PCB .... Printed Circuit Board

PDF .... Probability Density Function

SD .... Standard Deviation

SDM .... Structural Dynamic Modification

TRAC .... Time Response Assurance Criterion

CHAPTER 1

INTRODUCTION

High-rate dynamics is defined as the dynamic response of a system due to a high-rate (<100 ms) and high- amplitude (acceleration> 100 g_n) event such as a blast or impact [1]. Such events are characterized by instantaneous and unpredictable changes in the loading conditions acting upon a system, which alters the magnitude and location of internal and external forces experienced by the structure throughout the event. Because the changes experienced by the structure are sudden and unknown, tracking the state of the structure throughout the event remains a challenge.

One area where real-time modeling could offer comparative advantages is in blast mitigation technology. The purpose of an active blast mitigation system is to minimize the impact of a blast or to counter the effects of the blast after impact. Large forces associated with an incoming blast requires that mitigation systems be capable of calculating the impact in order to deploy the correct countermeasures. Additionally, because most impact blasts originate from short-range threats, the response time for mitigation systems is limited. Active blast mitigation systems must be capable of detecting the presence of a blast threat, determining the magnitude and location of an incoming threat and deploy countermeasures on a millisecond timescale [2]. Additional structures that experience high rate dynamics include manned and unmanned aerial vehicles, ballistic packages, and vehicle airbags.

Due to the large fluctuation in loading conditions over a short time interval, it is essential that the system is tracked throughout the duration of the high-rate dynamic event. One approach to tracking the state of such structures is to utilize structural model updating techniques to update a digitized representation of the system state in real-time. For accurate state estimations the model updating technique must: (1) be flexible in order to adapt and learn the changing external load conditions without relying on pre-trained data, and; (2) be capable of updating within a 2 ms timescale in order to allow for decisions based on real-time data.

Real-time modeling allows for the tracking of complex structures experiencing high rate dynamic events such as in-flight monitoring and impact mitigation technology. In-flight monitoring can be applied to manned and unmanned aerial vehicles as well as space crafts. In the case of an unmanned vehicle, a pilot is not present to monitor the aircraft and operators on the ground must rely on sensor readings to determine the condition of the system. Real-time model updating would allow operating software to receive state data almost instantaneously, enhancing the knowledge of the system and its surroundings allowing for mission critical actions [3]. In the case of manned vehicles and space crafts, the primary mission is to protect the vehicles occupants. Both vehicles are susceptible to damage due to accidental collision with debris or as a result of intentional attacks conducted by foreign or domestic enemies. In the case of manned vehicles, real-time updating of the system would allow for reactions faster than human pilots are capable of. For instance, if the system experiences damage the amount of sensor updates could be overwhelming for a pilot. Between monitoring the craft's speed and flightpath as well as the state of individual components in addition to protecting passenger life and

the mission, pilots will likely not be able to assess the situation and respond accordingly within a critical time frame to avoid losses. Real-time model updating would allow for the incorporation of decision-making software that will respond to changing environments faster than its human occupants can in a time of stress [3].

Additionally, real-time modeling can be applied to impact mitigation whether it is active blast mitigation, as mentioned previously, or airbag deployment. Airbags are an essential safety component in vehicles; however, in some cases, the deployment of airbags can cause additional injuries to passengers. The Delphi Dual Depth airbag is an adaptive airbag which controls the extent of inflation based on factors which as the size and seated position of the passenger as well as the crash severity and location [4]. Crash data must be processed quickly for the airbag to respond adequately to the situation in order to protect occupants. The incorporation of real-time model updating would allow for a response time within 2 ms and allow for additional adaptive measures to be incorporated such as modifying the shape of inflated airbag or adjusting the rate of inflation to maximize protection. In each application, real-time model updating would prioritize occupant's safety and mitigate of damage experienced by the system by providing users with the current state of a system thereby preventing further losses or failure.

Real-time modeling in this work is accomplished using local eigenvalue modification procedure or LEMP which simplifies state calculations when only one change is made to the system. Advantages to applying LEMP are that all variables for the altered state are defined in terms of the initial state and changes made between the two. This reduces the number of calculations required since the solutions for the initial state

equations are constant. Additionally, through LEMP, the original eigenvalue solution is

reduced to a set of second order equations. These advantages reduce the number and

complexity of equations needed to compute the state of the structure allowing for

applications in real-time structural model updating.

CHAPTER 2

LITERATURE REVIEW

Real-time model updating can be accomplished in one of two ways: either by creating a simplified model of a complex structure or by simplifying the calculations needed to determine the state of the complex structure. Previously, Hong et al. estimated system state via a simplified model using adaptive finite element analysis (FEA) techniques [5]. This work aims to maintain the original structure and simplify state calculations by utilizing structural dynamic modification and modal synthesis. Additionally, comparison calculations between the actual state and estimated states can be simplified by implementing reduced search spaces which decreases the number of testing points required. These techniques are further reviewed in the following sections.

2.1 MODAL ANALYSIS: SDM, MODAL SYNTHESIS AND LEMP

Structural dynamic modification (SDM) is a type of modal analysis that identifies physical modifications made to system properties such as mass, stiffness, or damping by monitoring changes in the system's dynamic behavior such as frequencies and mode shapes [6, 7].

SDM utilizes modal synthesis, which was first presented by Hurthy in 1965 [8]. Since then several methods employing the technique have been proposed [9]. Modal synthesis is the principle that any dynamic response of a vibrating structure can be decomposed into a set of individual contributions of single frequencies [10, 11]. The

values of each frequency can be found by computing the general eigenvalue (GE) solution of the state equations. The corresponding eigenvectors, or modal vectors, are used in SDM to model the modal response of the system.

SDM is accomplished by modeling the modified state as a combination of the initial state and the changes made between the two. This is done by incorporating changes in mass, stiffness, or damping matrices into the equation of motion (EOM) for the system. The modified EOM is then transformed to modal space using the GE solution of the initial state. Finally, the updated GE problem is solved to find the new frequencies and mode shapes for the modified structure [12].

SDM utilizes the relationship between the modal properties and spatial properties of a structure. This relationship can be used to simplify state estimations for complex systems by transforming equations from physical space to modal space [6,7]. One advantage of operating in modal space is that the model for the initial structure must only contain information for the degrees of freedom (DOF) where modifications are made, thereby reducing the number of calculations required [12]. However, initial SDM techniques still required processing full GE solutions for matrices which is computationally expensive [13].

The GE equations can be simplified through modal reduction methods [14]. One popular modal reduction technique is LEMP which was originally developed by Weissenburger [15]. LEMP was proposed as a means of further simplifying the state equations constructed using SDM for mass and stiffness changes and later extended to include damping modifications [16, 17]. The benefits of applying LEMP is that the GE equation is reduced to a set of second order equations that require less computational

power and time to solve. Additionally, that the modified frequency roots are bounded by the initial frequencies of the system, which reduces the domain over which the equation is solved [15].

In its early years LEMP was applied to simple structures such as shafts, beams with added support or point masses and systems of mass springs and dampers [18]. Recent works have applied LEMP to larger complex structures such as utility-scale wind turbine blades [19] and flexible multibodies such as vehicles, aircrafts, and manufacturing equipment [20].

2.2 REDUCING SEARCH SPACES: THE BAYESIAN APPROACH

Point selection for comparisons between the actual state and estimated state is based on a Bayesian probabilistic approach. Bayesian approaches are frequently utilized in structural health monitoring applications due to their simplicity, adaptability, and updatable nature [21]. Bayesian approaches are implemented to assess the estimate of the state of the structure given an initial uncertainty about the estimate itself [22]. The assessment reflects the relative degree of belief or uncertainty in the estimates. Not only is the Bayesian approach capable of accounting for uncertainty in the individual predictions (or estimates) made by a model, but also the uncertainty in the model fit itself [22]. Bayesian methods incorporate prior information into a model with limited data to improve the model for future estimations [23]. With each estimation assessment, the resulting posterior distribution becomes a better estimate than the initial prior probability. That posterior then and replaces the initial prior for the subsequent estimate improving the model estimations [24].

Bayesian frameworks have been used to detect the presence, location, and extent of damage in a structure. The applications range from laboratory scale projects such as Papadimitriou's work investigating foundation damage using a small-scaled bridge [24] to full-scale structures such as Moaveni's work investigating earthquake damage in a seven-story building [21]. Bayesian approaches can also be used to predict future operation and lifetime estimations for mechanical and electrical system components. Meeker and Escobar utilized the Bayesian approach in fitting a Weibull distribution to field failure data for estimating the operational lifetime of an aircraft engine bearing cage [23]. While Hamada performed a Bayesian analysis on degradation paths of lasers to estimate remaining lifetime [25].

Bayesian approaches are advantageous because they can be combined with other data analysis techniques to further improve statistical results. Behmanesh and Moaveni identified simulated damage on a footbridge by utilizing an adaptive Metropolis–Hastings algorithm to sample the posterior probability density function (PDF) for updating parameters [26]. Lam et al. extended the concept to detect railway ballast damage under a concrete sleeper. In Lam's approach, damage detection is divided into two phases: model selection and model updating, both of which utilize a Bayesian approach [27]. A similar approach proposed by Madarshahian et al. [28] utilized a two-layer Bayseian approach to minimize the computational cost of estimating prior and posterior distributions. Kurata et al. implemented a Bayesian approach conjointly with branch and bound search techniques to model the crack growth within aluminum hull structures [29].

Bayseian approaches are also advantageous because they can be easily implemented into experimental analysis without changing lab setups. Caicedo et al. [30]

utilized the Acoustic Emission method and a Bayesian approach for estimating crack length in steel test specimens. The Acoustic Emission method is based on the principle that when a crack grows, energy is released in the form of waves. The energy released can be measured by multiple sensors which can determine the location and severity of the crack. The measurements are then used in the Bayesian approach to update the posterior PDF for crack length.

CHAPTER 3

BACKGROUND AND THEORY

This work puts forth and numerically validates an algorithm for estimating the location of an additional boundary condition on the Dynamic Reproduction of Projectiles in Ballistic Environments for Advanced Research (DROPBEAR) testbed and proposes an extension of the theory to removing a boundary condition. This is accomplished by utilizing structural dynamic modification and applying LEMP to the system equations. Further details of the DROPBEAR testbed, analytical model and LEMP are discussed in the following sections.

3.1 DROPBEAR EXPERIMENTAL TESTBED

The model created for this work is based on the DROPBEAR testbed which was initially developed by Joyce et al. [31]. The DROPBEAR was constructed specifically for simulating high-rate dynamic events and features two programable changes: a detachable mass that is secured using an electromagnet, and a movable roller boundary condition attached to a linear actuator, both of which are used to simulate damage to the structure. The DROPBEAR testbed is advantageous when modeling high rate dynamic cases because the setup is capable of repeatedly altering test parameters quickly. Additionally, these parameters can be changed during a test as opposed to between test runs, allowing researchers to gain insight into the system's real-time response. In this work, only the movable roller is utilized, the experimental configuration is shown below in Fig. 3.1 [32].
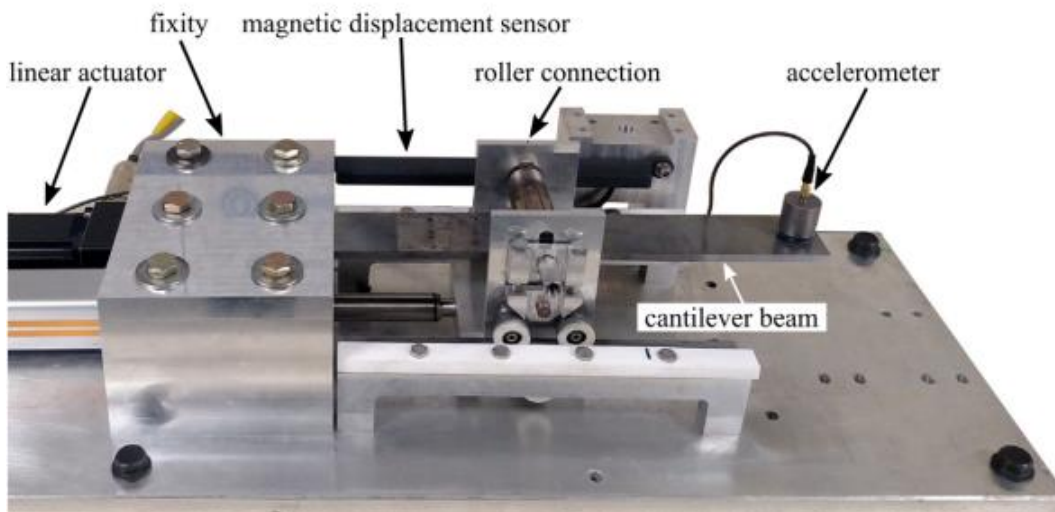
Figure 3.1   Modified DROPBEAR testbed used in this work.

The experimental configuration features an accelerometer (PCB Piezotronics-model 393B04) mounted at the free end of a 51 x 6 x 350 mm steel cantilever beam with Density of 7800 kg/m^3, Young's Modulus of 2e11 N/m^2 and Poisson's Ratio of .26. The design also features a sliding roller cart on a linear actuator that constrains beam bending between 48-175 mm from the fixed end as well as a magnetic displacement sensor that measures the roller's displacement throughout the test. Adjusting the roller location during tests simulates damage to the system by producing a user-defined change to the system input which results in a change to the measured system output (acceleration). The use of rollers ensures the repeatability of each test, as the damage is simulated.

3.2 LOCAL EIGEN VALUE MODIFICATION PROCEDURE (LEMP)

A study conducted by Carroll et al. [33] investigated the computation speeds for various eigenvalue solutions and FEA models of the DROPBEAR testbed. Their work concluded that for a GE solution to accurately estimate the state of the DROPBEAR testbed within a 1 ms timeframe, the FEA model must be limited to 23 nodes. Additionally, for a 23-node model, solving for the system's frequencies accounted for

11

90% of the algorithms iteration time. Furthermore, as the model increased the calculation time grew exponentially as shown on Fig. 3.2, which reports the algorithm timing for a FEA model with 2-100 nodes.
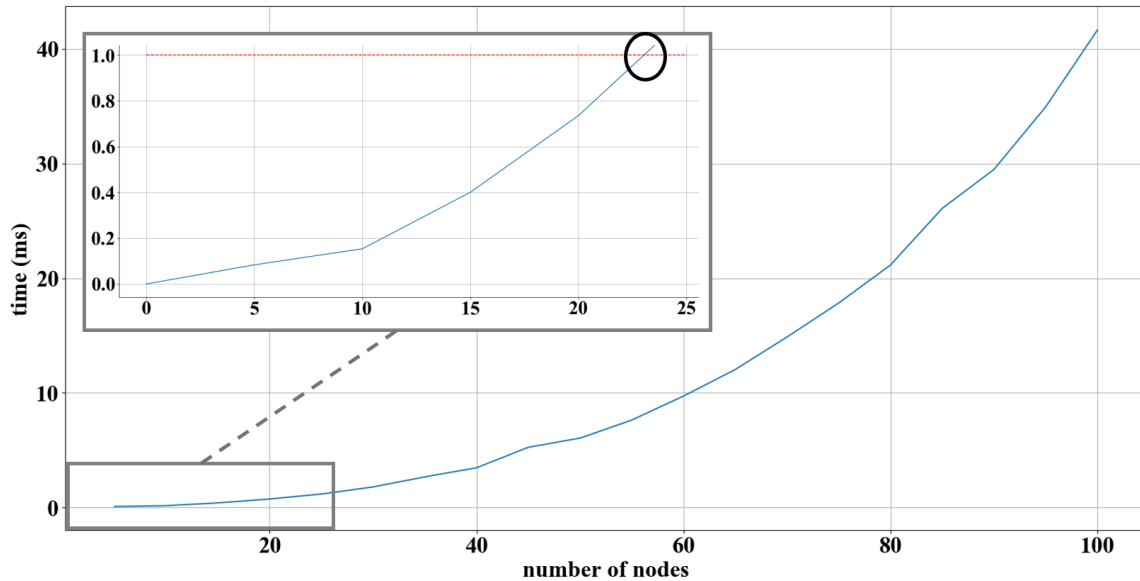
Figure 3.2 Computation speed of GE solutions for various number of nodes.

Accelerating computations would allow for the use of more complex models such as those with additional nodes or various element types. More complex models would greatly enhance the usefulness of physics-informed state estimation of structures experiencing high-rate dynamic events. Moreover, these high-quality models are critical to performing prognostics and enabling decision-making for these structures. One approach for solving state equations with computational efficiency is to avoid eigen solutions all together by applying LEMP for modal analysis.

LEMP is a means of structural dynamic modification to simplify state calculations when only one change to the system is made. In the case of this work, the change is the addition of a roller support, which can be modeled as an increase in stiffness along the beam. LEMP reduces the number and complexity of equations needed to compute the

state of the structure which equates to less computing time than the previously mentioned

GE solutions. To do so, LEMP utilizes a single GE solution for the initial system and

simplifies altered state equations by transforming them into modal space, isolating the

DOFs that contribute to the changes between states and defining equations in terms of the

initial state. A general flowchart illustrating the steps in LEMP is shown in Fig 3.3 and

discussed in further detail throughout this section.
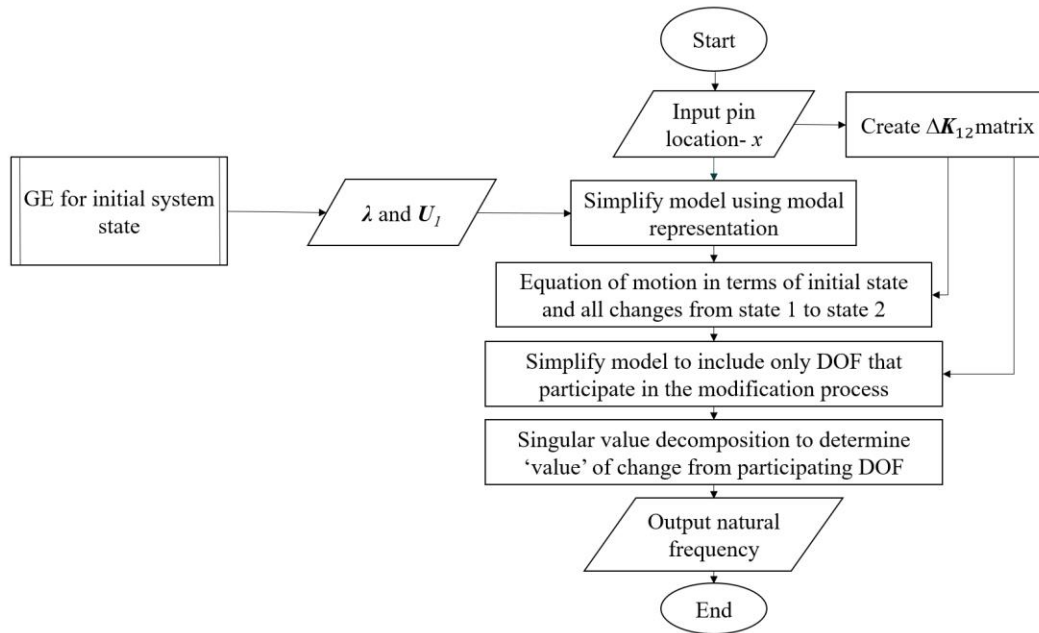
Figure 3.3   Flowchart of LEMP steps.

The EOM for the initial state of a system while ignoring the effects of damping

can be seen in Eq. (1) below.

$$M_1 \ddot{X} + K_1 X = 0 \tag{1}$$

Here, $\ddot{X}$ and X are the acceleration and displacement in physical space. Additionally, M_1

and K_1 are the mass and stiffness matrices of the initial system in physical space. Both

matrices are square symmetric and have dimensions of (n x n) where n is the DOF for the

system.

By definition, the GE problem for Eq. (1) is $K_1 U_1 = M_1 U_1 \lambda$, where λ are the eigenvalues and U_1 are the eigenvectors. The GE problem can be solved using Eq. (2) and Eq. (3) below.

$$\det[K_1 - \lambda M_1] = 0 \tag{2}$$

$$[K_1 - \lambda M_1]U_1 = 0 \tag{3}$$

Which yield the squares of the first n natural frequencies and the first n modal vectors for the system as shown in Eq. (4) and Eq. (5) respectively.

$$\lambda = \begin{pmatrix} \omega_1^2 & 0 & 0 & 0 \\ 0 & \omega_2^2 & 0 & 0 \\ 0 & 0 & \ddots & 0 \\ 0 & 0 & 0 & \omega_n^2 \end{pmatrix} \tag{4}$$

$$U_1 = \begin{pmatrix} \overrightarrow{u_1^1} & \overrightarrow{u_2^1} & \cdots & \overrightarrow{u_n^1} \end{pmatrix} \tag{5}$$

Where ω_n and $\overrightarrow{u_n^1}$ are the n-th frequency and modal vector for the initial state of system. Note that the modal matrix is not equivalent to mode shapes but can be used to calculate them [34].

To simplify future calculations, the system response is transformed from physical space to modal space using relations shown in Eqs. (6) and (7), where P_1 and $\ddot{P}_1$ are the system displacement and acceleration in modal space.

$$X = U_1 P_1 \tag{6}$$

$$\ddot{X} = U_1 \ddot{P}_1 \tag{7}$$

Substituting these equations into Eq. (1) yields Eq. (8) below.

$$M_1 U_1 \ddot{P}_1 + K_1 U_1 P_1 = 0 \tag{8}$$

By multiplying each term by U_1^T the mass and stiffness matrices are normalized in modal space yielding diagonal matrices shown in Eq. (9).

$$\text{diag}(\overline{M_1})\ddot{P}_1 + \text{diag}(\overline{K_1})P_1 = 0 \tag{9}$$

Here $\overline{M_1}$ and $\overline{K_1}$ represent the mass and stiffness matrices in modal space. Additionally, scaling Eq. (9) to unit modal mass yields Eq. (10) where I is the identity matrix.

$$I\ddot{P}_1 + \lambda P_1 = 0 \tag{10}$$

The benefit of scaling to modal mass is that the state equation for the initial state in modal space can be written in terms of the eigenvalues, which were already obtained by Eq. (4).

The equations in modal space above effectively define the initial system of n DOF as a set of n independent single degree of systems as illustrated in Fig. 3.4. Here each DOF responds to one natural frequency of the physical system and is related to physical system response through modal transformations shown in Eqs. (6) and (7).
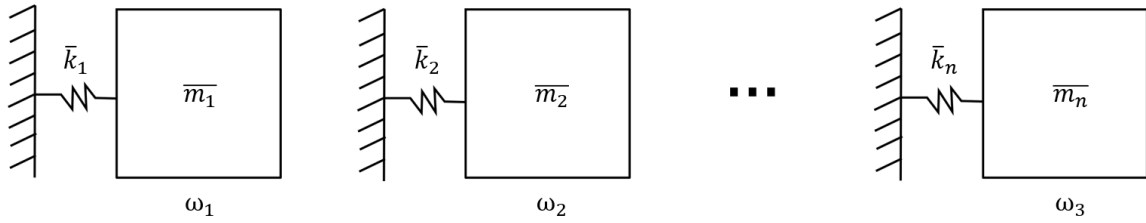
Figure 3.4   *n* independent single DOF systems representing the initial state

The EOM for the altered state, while ignoring the effects of damping can be seen in Eq. (11) below.

$$M_2\ddot{X} + K_2X = 0 \tag{11}$$

Where M_2 and K_2 are the mass and stiffness matrices of the altered state in physical space, respectively. These matrices can be defined in terms of the initial mass /stiffness matrices and the changes made between the two states. In the case of this work, the change between system states is the addition of a roller support. Therefore, there is no

change in the mass matrix, only a change made to the stiffness matrix denoted by ΔK_{12} as shown in Eq. (12) and Eq. (13) respectively.

$$M_2 = M_1 \tag{12}$$

$$K_2 = K_1 + \Delta K_{12} \tag{13}$$

Here ΔK_{12} represents the changes made in the physical space from the initial state to the altered state where diagonal values represent spring stiffness change from each elemental mass to ground and off-diagonal values couple elemental masses together. Because this work utilizes a moving roller, only diagonal values will be affected. Furthermore, for each altered state the only non-zero term in the ΔK_{12} matrix is the diagonal value associated with the DOF where the roller is located.

Substituting Eqs. (12) and (13) into Eq. (11) and transforming the state equation to modal space using Eqs. (6) and (7) yields Eq. (14) below.

$$M_1 U_1 \ddot{P}_1 + (K_1 + \Delta K_{12}) U_1 P_1 = 0 \tag{14}$$

By multiplying each term by U_1^T the mass and stiffness matrices are normalized in modal space which yield the diagonal matrices shown in Eq. (15).

$$\text{diag}(\overline{M_1})\ddot{P}_1 + [\text{diag}(\overline{K_1}) + \overline{\Delta K_{12}}]P_1 = 0 \tag{15}$$

Additionally, scaling Eq. (15) to unit modal mass gives Eq. (16).

$$I\ddot{P}_1 + [\lambda + \overline{\Delta K_{12}}]P_1 = 0 \tag{16}$$

Here $\overline{\Delta K_{12}}$ represents the changes made in modal space from the initial state to the altered state where diagonal values represent spring stiffness change from each system shown in Fig. 3.4 to ground and off-diagonal values couple individual systems together as shown in Fig. 3.5.

16
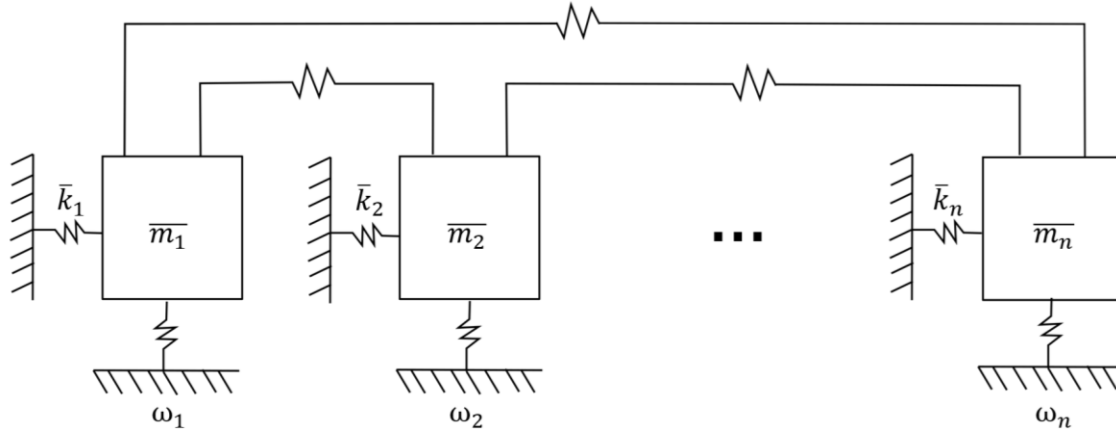
Figure 3.5   Coupled single DOF systems representing altered state.

Additional simplifications occur by truncating the *n* independent single degree of systems to only include the *m* modes of interest. This results in a modal matrix U_I of dimensions (*n* x *m*) which further simplifies the altered state equations.

To solve for the updated natural frequencies that occur as a result from coupling the systems, the following procedure is implemented. The eigen solution of Eq. (16) is set up, but not solved according to Eq. (17) and Eq. (18) below.

$$\det[(\lambda + \overline{\Delta K_{12}}) - \Lambda I] = 0 \tag{17}$$

$$[(\lambda + \overline{\Delta K_{12}}) - \Lambda I]P_{12} = 0 \tag{18}$$

Where the diagonals of Λ are the squares of the updated frequencies and P_{12} is the modal change between the states. The terms in Eq. (18) are then rearranged to yield Eq. (19).

$$[(\lambda - \Lambda) + \overline{\Delta K_{12}}]P_{12} = 0 \tag{19}$$

Noting that the only non-zero values in ΔK_{12} are those associated with the degree(s) of freedom that experience a change in stiffness from the initial to altered state, the equation for $\overline{\Delta K_{12}}$ can also be simplified to only contain information from the contributing nodes. This is accomplished through spectral decomposition of ΔK_{12} as shown in Eq. (20).

$$\Delta K_{12} = T \operatorname{diag}(\alpha) T^{\mathrm{T}} \tag{20}$$

Where $\boldsymbol{T}$ is the tie matrix and $\boldsymbol{\alpha}$ is a matrix of single values obtained from the single

value decomposition of $\Delta\boldsymbol{K_{12}}$. Equation (20) is then transformed to modal space by

multiplying each term by $\boldsymbol{U_1^T}$ as shown in Eq. (21).

$$\overline{\Delta K_{12}} = U_1^T T \operatorname{diag}(\alpha) T^T U_1 \tag{21}$$

The only non-zero or contributing values of $\overline{\Delta K_{12}}$ are found using the rows of $\boldsymbol{U_1}$

associated with the degree(s) of freedom experiencing a stiffness change. This is shown

in Eq. (22), where $\vec{v}$ is the one-dimensional contribution vector as noted in Eq. (23).

$$\vec{v} = U_{1c}^T \vec{t} \tag{22}$$

$$\vec{v} = (v_1 \ v_2 \ldots v_m) \tag{23}$$

Plugging the relation from Eq. (22) into Eq. (21) yields the equation for the modal

stiffness change in terms of contributing nodes only as shown in Eq. (24)

$$\overline{\Delta K_{12}} = \vec{v} \operatorname{diag}(\alpha) \vec{v}^T \tag{24}$$

Plugging in Eq. (24) for the original eigenvalue problem in Eq. (19) yields the following

equations:

$$[(\lambda - \Lambda) + \vec{v} \operatorname{diag}(\alpha) \vec{v}^T]P_{12} = 0 \tag{25}$$

$$(\lambda - \Lambda)P_{12} + \vec{v} \operatorname{diag}(\alpha) \vec{v}^T P_{12} = 0 \tag{26}$$

To further simplify state equations, $\boldsymbol{S}$ is defined as an arbitrary variable according to Eq.

(27).

$$S = \vec{v}^T P_{12} \tag{27}$$

Equation (27) is then plugged into Eq. (26) to yield Eq. (28) below.

$$(\lambda - \Lambda)P_{12} + \vec{v} \operatorname{diag}(\alpha) S = 0 \tag{28}$$

Equation (28) can be rearranged to solve for $\boldsymbol{P_{12}}$ as shown in Eq. (29).

$$P_{12} = \frac{-\vec{v} \operatorname{diag}(\alpha)S}{(\lambda - \Lambda)} \tag{29}$$

Then, Eq. (29) is multiplied by $\vec{v}^{\text{T}}$ to yield Eq. (30).

$$\vec{v}^T \boldsymbol{P_{12}} = \frac{-\vec{v}^{\text{T}} \vec{v} \, \text{diag}(\boldsymbol{\alpha})\boldsymbol{S}}{(\boldsymbol{\lambda} - \boldsymbol{\Lambda})} \qquad (30)$$

Which can be rewritten as Eq (31) using the relation from Eq. (27).

$$\boldsymbol{S} = \frac{-\vec{v}^{\text{T}} \vec{v} \, \text{diag}(\boldsymbol{\alpha})\boldsymbol{S}}{(\boldsymbol{\lambda} - \boldsymbol{\Lambda})} \qquad (31)$$

Since $\vec{v}$ is a one-dimensional vector, $\vec{v}^{\text{T}} = \vec{v}$. Additionally, $\boldsymbol{S}$ on either side cancels

leaving the matrix equation shown in Eq. (32).

$$\frac{-\mathbf{1}}{\text{diag}(\boldsymbol{\alpha})} = \frac{\vec{v}^2}{(\boldsymbol{\lambda}-\boldsymbol{\Lambda})} \qquad (32)$$

Breaking Eq. (32) into components yields the following equation, where the only

unknown is Ω^2 or the natural frequency of the altered system and r ranges from 1 to m,

where m is the number of modes used to describe the system.

$$\frac{-1}{\alpha} = \sum_{r=1}^{m} \frac{v_r^2}{\omega_r^2 - \Omega^2} \qquad (33)$$

In summary, LEMP consists of two main parts: a single GE solution for the initial

state of the system and an eigenvalue modification process for the altered system state

that is updated for each roller position. The eigenvalue modification process consists of

simplifications to state equations accomplished by defining the system in terms of the

initial state and changes made between the two states, utilizing modal representation, and

isolating contributing nodes. An example of LEMP implementation using experimental

values can also be found in Appendix A.

3.3 ANALYTICAL MODEL FOR THE INITAL STATE

Initial state calculations are made using a finite element model and utilizing the

Euler-Bernoulli beam theory. As shown in Fig. 3.6, the modified DROPBEAR testbed is

modeled as a cantilever beam with the far-left end fixed no roller (i.e. support) present

initially. The beam is split into N elements of equal length resulting is $N+1$ evenly spaced nodes along the beam. The selection of N is discussed further in Chapter 4.

n_1 $\qquad$ n_2 $\qquad$ n_3 $\quad$ ... $\qquad\qquad\qquad\qquad\qquad\qquad$ $N+1$

Figure 3.6 $\qquad$ Finite Element Model for modified DROPBEAR testbed.

By definition, each Euler-Bernoulli element is exposed to two forces and two moments as shown in Fig. 3.7. The elemental mass (M_i) and stiffness (K_i) matrices of the element i are defined in Eq. (34) and Eq. (35) respectively.

θ_1 $\qquad\qquad\qquad\qquad\qquad\qquad\qquad\qquad$ θ_2

v_1 $\qquad\qquad\qquad\qquad\qquad\qquad\qquad\qquad\qquad$ v_2

Figure 3.7 $\qquad$ Forces and moments for a Euler-Bernoulli element.

$$M_i = \frac{\rho_i A_{ci} l_i}{420} \begin{pmatrix} 156 & 22l_i & 54 & -13l_i \\ 22l_i & 4l_i^2 & 13l_i & -3l_i^2 \\ 54 & 13l_i & 156 & -22l_i \\ -13l_i & -3l_i^2 & -22l_i & 4l_i^2 \end{pmatrix} \tag{34}$$

$$K_i = \frac{E_i I_i}{l_i} \begin{pmatrix} 12/l_i^2 & 6/l_i & -12/l_i^2 & 6/l_i \\ 6/l_i & 4 & -6/l_i & 2 \\ -12/l_i^2 & -6/l_i & 12/l_i^2 & -6/l_i \\ 6/l_i & 2 & -6/l_i & 4 \end{pmatrix} \tag{35}$$

Where ρ, A_c, l, and E are the material and geometric properties of the experimental testbed as given in Table 3.1.

Table 3.1   Material and geometric properties for modified DROPBEAR testbed.

Density-ρ (kg/m^3)	7800
Cross-sectional area-A_c (m^2)	0.000306
Total length-l (m)	0.35
Elemental length- l_i (m)	$0.35/N$
Young's Modulus-E (Pa)	2E11

These element matrices are combined to construct the global mass (M_1) and stiffness (K_1) matrices for the initial sate. The eigen solution of the global matrices yield the eigenvectors and eigenvalues which are used in modal analysis to compute natural frequencies of the altered structure. Sample calculations for the analytical model can also be found in Appendix A.

3.4 BAYESIAN METHOD

The model updating utilized in this work is based on a Bayesian probabilistic approach which utilizes system parameters that come from past state estimations [21]. Furthermore, each estimate contains a level of uncertainty that is accounted for here by utilizing the likelihood function which represents the error that exists between the "true" structure and the LEMP "estimated" model [23]. In other words, when a new roller location is estimated, that value becomes the mean around which a new Gaussian distribution is created. Values from the updated probability density function (PDF) are selected and either accepted or rejected using the likelihood function and Bayes equation.

These points are then used as comparison points for future state estimations. A flowchart describing the process can be seen in Fig. 3.8 below.
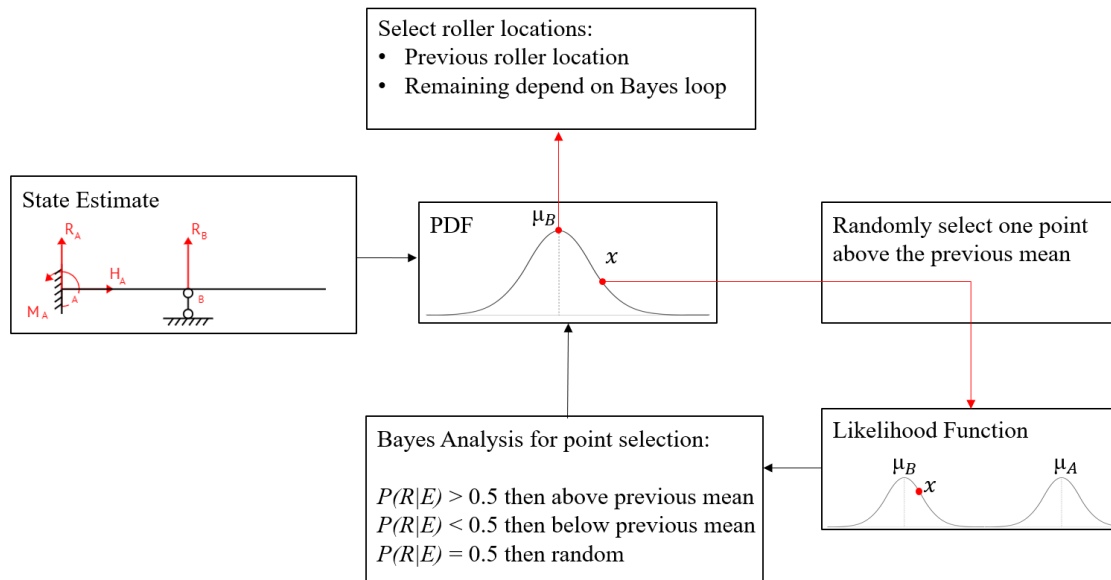
Figure 3.8   Analytical application of the likelihood function and Bayes algorithm.

The following discussion outlines the procedure illustrated in Fig. 3.8. Let R denote that the hypothesis that the direction of roller movement is right. It is initially assumed that the roller is located at the center of the beam and is moving right with a probability $P(R) = .6 (\because P(L) = .4)$; all future calculations assess the probability that the roller will continue to move right. Weighting initial directional probabilities is equivalent of making predictions about the way a system will degrade based on previous knowledge. For example, when modeling structures, the equivalent stiffness will decrease over time as the structure degrades; therefore, the initial weighted prediction and future estimations would assess a decrease in stiffness.

Given a PDF of normal distribution centered about the previous roller position, s roller locations are sampled. The first location is taken to be the previous mean (μ_B), assuming that there is no damage occurring between the two estimations. The second

22

location is a randomly chosen location (x) above the mean value. The likelihood functions for the selected point are calculated according to the two previous distributions Eq. (35) and Eq. (36) respectively where B represents the previous distribution and A represents the distribution prior to that.

$$P(E|B) = \frac{1}{\sqrt{2\pi\sigma^2}} * e^{-\frac{1}{2}*\frac{(x-\mu_B)^2}{2\sigma^2}} \tag{36}$$

$$P(E|A) = \frac{1}{\sqrt{2\pi\sigma^2}} * e^{-\frac{1}{2}*\frac{(x-\mu_A)^2}{2\sigma^2}} \tag{37}$$

Here, σ is the standard deviation of the position distribution, μ_B is the last estimated roller location, μ_A is the estimated roller location from two iterations ago. If $\mu_B > \mu_A$ the roller was last moving right, if $\mu_A > \mu_B$ then the roller was last moving left. The likelihood function is then used in the Bayes' theorem as follows:

$$P(R|E) = \frac{P(R)P(E|B)}{P(R)P(E|B) + P(L)P(E|A)} \tag{38}$$

The output of Eq. (37) is the posterior or updated distribution for the roller location after information regarding the previous location selections and likelihoods are taken into consideration [23]. If $P(R|E) > .5$ then then it is assumed that the roller is currently moving to the right therefore the remaining locations are selected from above the previous mean value. If $P(R|E) < .5$ then then it is assumed that the roller is currently moving to the left therefore the remaining locations are selected from below the previous mean value. If $P(R|E) = .5$ then the remaining locations are selected at random.

CHAPTER 4

SURROGATE MODEL CREATION

Before LEMP is applied, a model must be selected to maximize calculation

efficiently. In other words, the goal is to include enough information about the system

that estimates contain minimal error, but not too much information that calculation time

is negatively affected. Model selection includes determining the number of modes and

nodes to include when modeling the initial and altered systems. Not all initial modes will

contribute equally to altered frequencies, but missing modes that do contribute will

drastically increase the estimation error due to truncation. Therefore, predetermining

which initial modes contribute and how much each contributes to altered states is

essential. The number of nodes determines how refined the solution is, with more nodes

offering a more accurate estimation but requiring a longer calculation time and less nodes

saving time but offering rougher estimates. Mode and node selection are covered further

in the following sections.

4.1 MODE SELECTION

The number of independent single DOF systems used to represent the initial state

(as shown in Fig. 3.2) depends on the participation factors (U_{12}). Recall from Eq. (14) in

Section 3.2 that the EOM for the altered state in modal space is:

$$\text{diag}(\overline{M_1})\ddot{P}_1 + [\text{diag}(\overline{K_1}) + \overline{\Delta K_{12}}]P_1 = 0 \tag{14}$$

The initial modal response can be rewritten as a function of the modal response of

the altered state and the participation factors as shown in Eq. (39).

$$P_1 = U_{12}P_2 \tag{39}$$

If LEMP were not applied, the GE solution of equation 14 given the

transformation shown in Eq. (39) can be solved using Eq. (40) below.

$$\{[\text{diag}(\overline{K_1}) + \overline{\Delta K_{12}}] - U_{12}\,\text{diag}(\overline{M_1})\}P_2 = 0 \tag{40}$$

Where the eigenvectors of Eq. (40) are U_{12}, or the participation factors, which offer

insight into the weight each initial mode carries in defining the altered modes. Values

range between -1 and 1, where absolute values closer to 1 correspond with larger modal

contribution. Prior work by Avitabile explains how the modes of a free-free beam can be

weighted using participation factors and combined to create modes for other beam types

[35]. Figure 4.1 illustrates a matrix of participation factors for the initial free-free and an

altered cantilever beam. The first five modes of the free-free beam are used to create the

first modal response for a cantilever beam (circled in red).

Figure 4.1   Participation factors for two beam types.

Figure 4.2 plots the first five modes of the free-free beam and uses the

participation factors marked in Figure 4.1 to create the first mode for a cantilever beam.

Based on the participation factors, the first and second modes of the free-free beam

contribute most to the first mode of a cantilever with weights of .7967 and .5974

respectively.
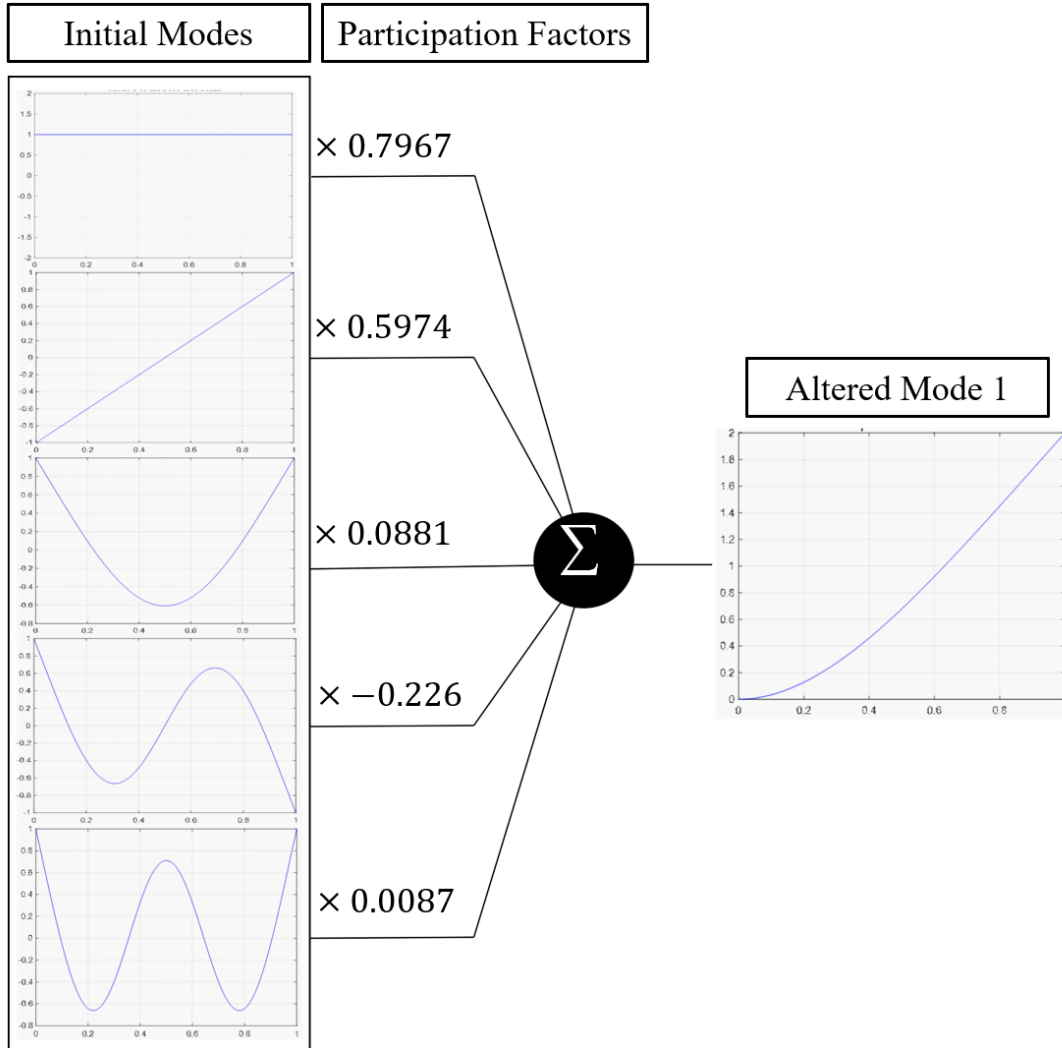
Figure 4.2   Participation factors and modal synthesis for two beam types.

Figures 4.1 and 4.2 illustrate the general concept utilized in this chapter. In the case of this work, the initial system is the modal response of a cantilever beam and altered modes are the responses of the system when a roller is added. To determine the participation factors of the system used in this work, the number of nodes was initially set to 10 which can be seen in Fig. 4.3. This setup yields 20 DOF due to the characterization of the system as a Euler-Bernoulli beam.
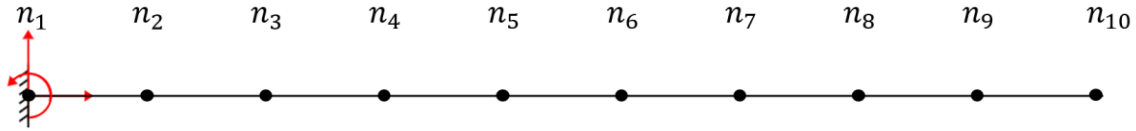
Figure 4.3   Model used to determine participating mode shapes.

The participation factors were then calculated at each node along the beam, excluding n_1 and plotted according to the key in Fig. 4.4. The participation factors were not calculated for the node at the leftmost end of the beam because a fixed boundary condition already exists at that point and adding a roller would not change the system response.

Figure 4.4   Participation weight key.

Figures 4.5 - 4.13 illustrate the modal participation factors for a roller located at nodes ranging from $n_2 - n_{10}$ using the key presented in Fig. 4.4. The initial modes of the cantilever beam are listed on the vertical axes and altered modes of the cantilever beam with a roller placed at a node are listed along the horizontal axes. Boxes are color- coded based on the value of the participation factor where white boxes representing little to no contribution and yellow representing high levels of contribution. Future analysis will focus on contributions greater than 0.2 from initial modes. For example, in Fig. 4.5, the altered modes (horizontal axis) are the modes for the system when the pin is at $n=2$. In this case, the 5th mode for the altered shape can be represented as a combination of modes 4, 5, and 6 from the initial cantilever beam with participation factors of .2383, .7717, and .5489, respectively.

27

Figure 4.5   Modal participation factors for the altered state with roller at n_2.

Figure 4.6   Modal participation factors for the altered state with roller at n_3.
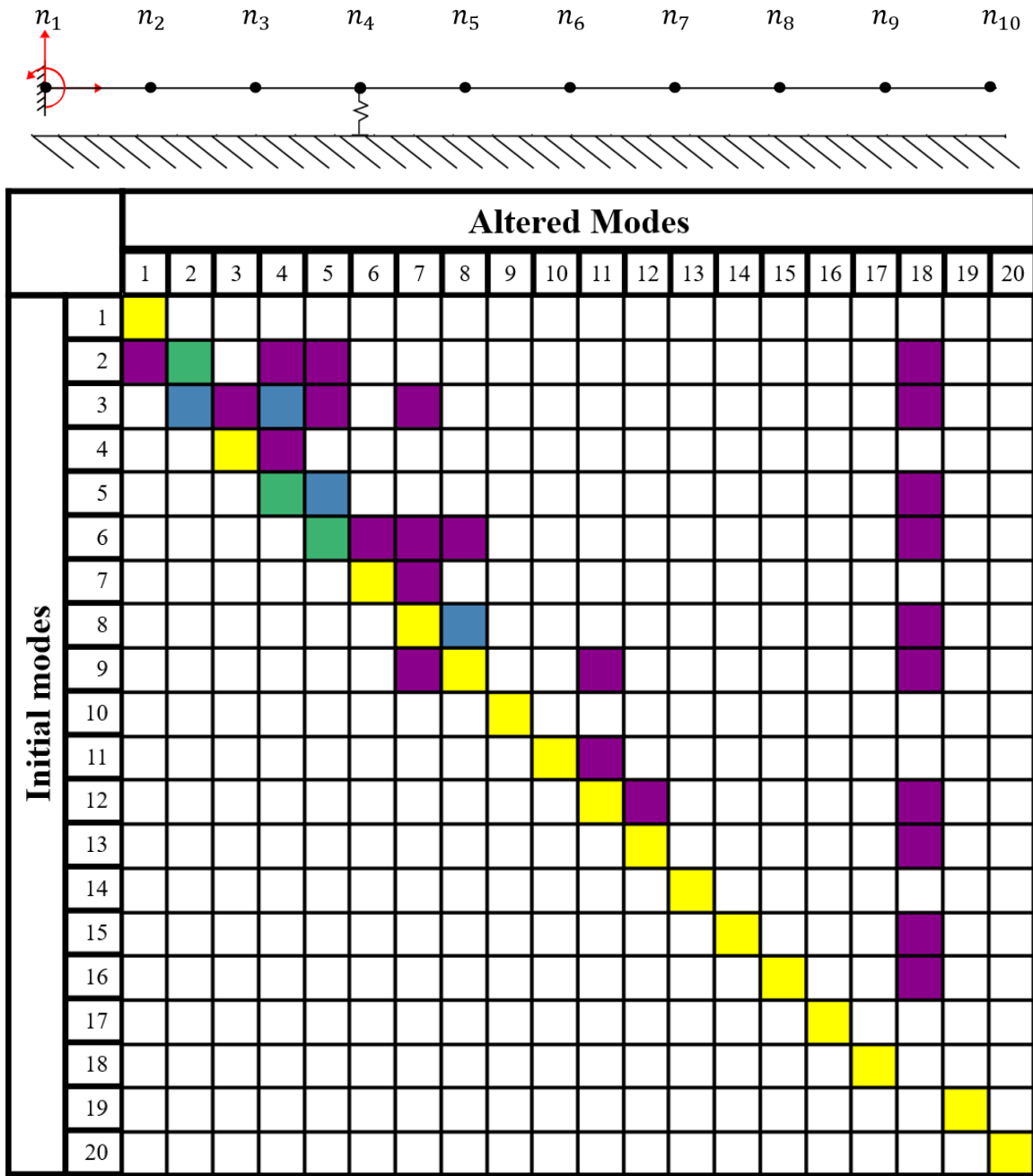
Figure 4.7   Modal participation factors for the altered state with roller at n_4.
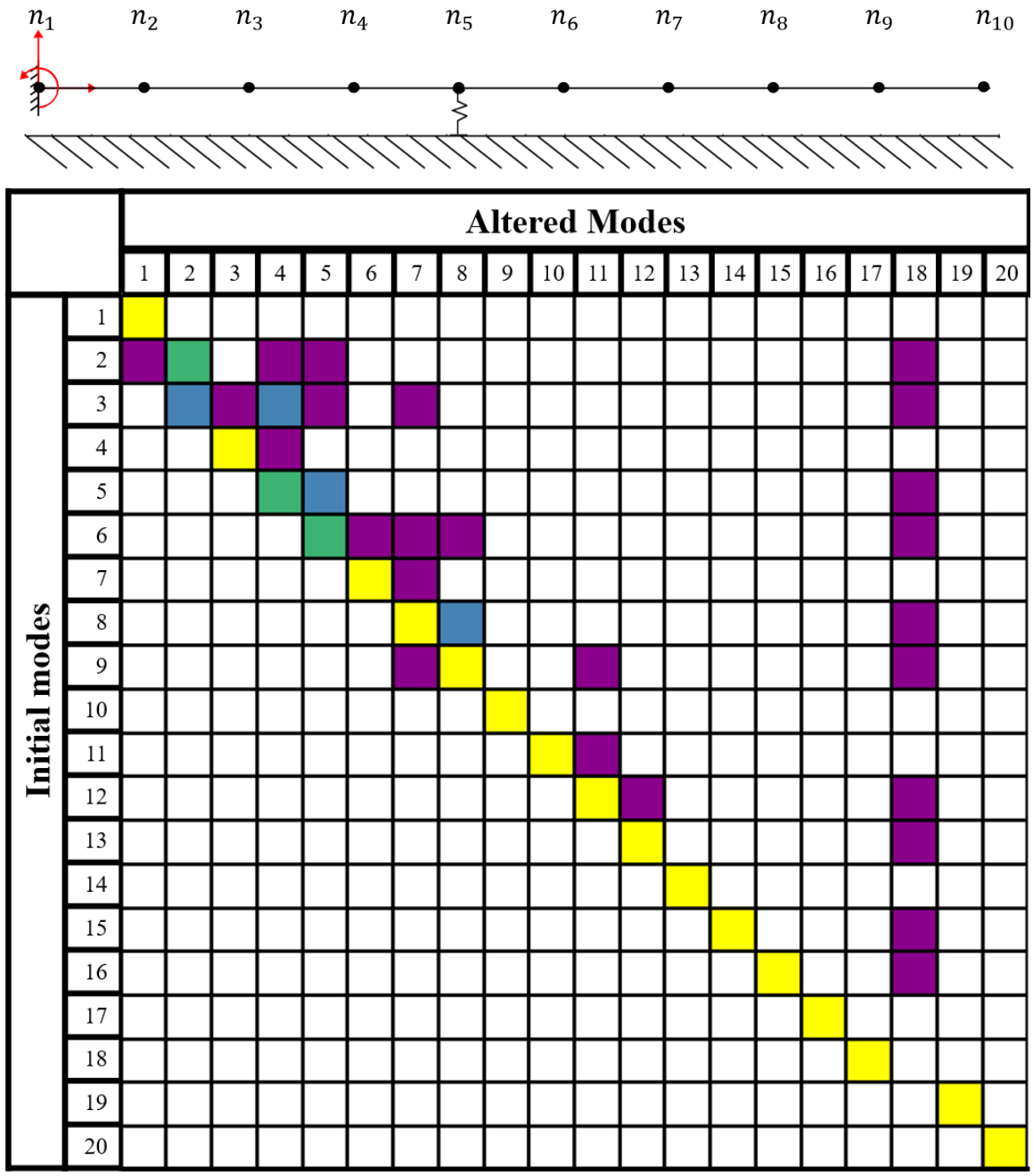
Figure 4.8   Modal participation factors for the altered state with roller at n_5.

Figure 4.9   Modal participation factors for the altered state with roller at n_6.
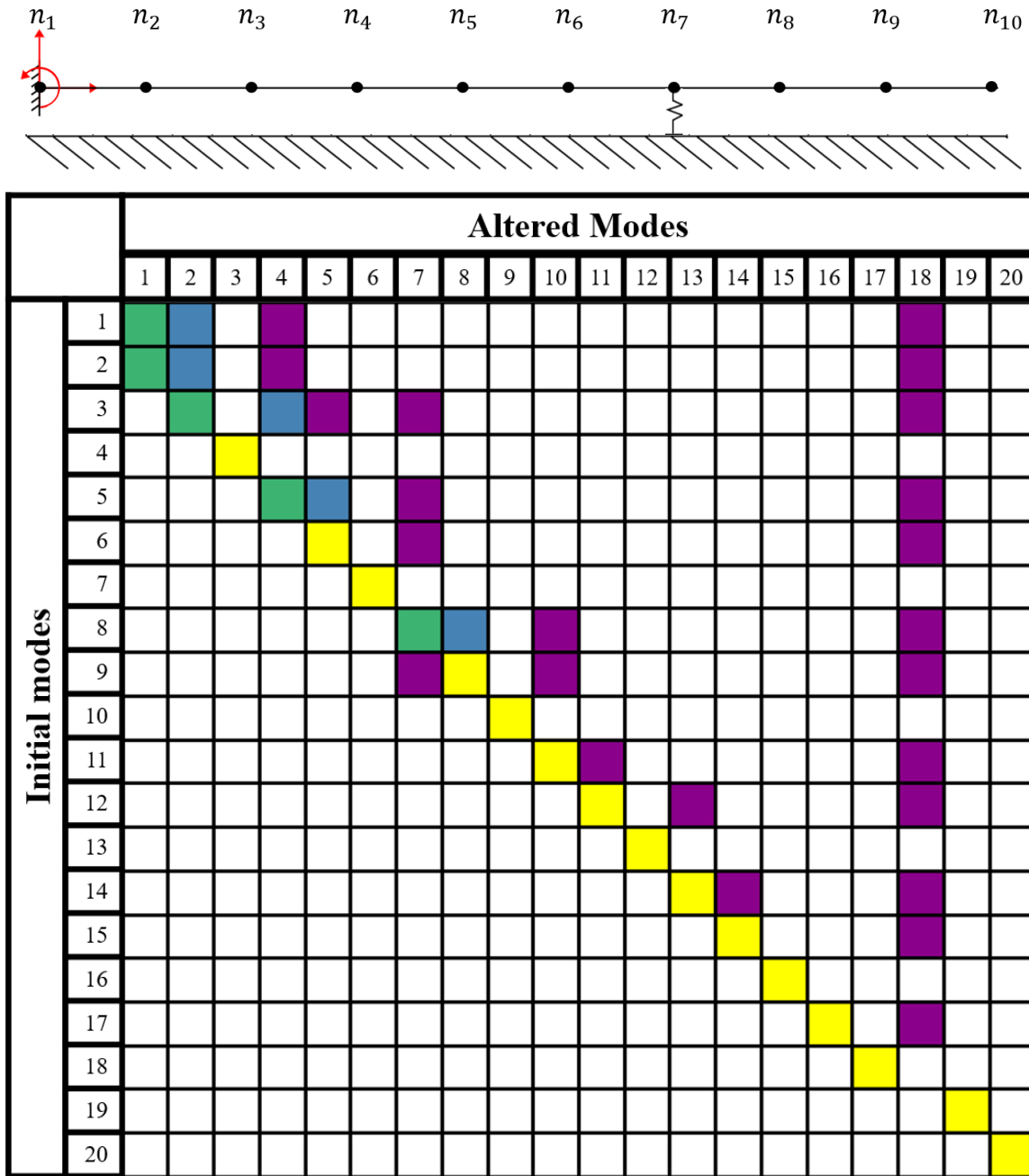
Figure 4.10   Modal participation factors for the altered state with roller at n_7.
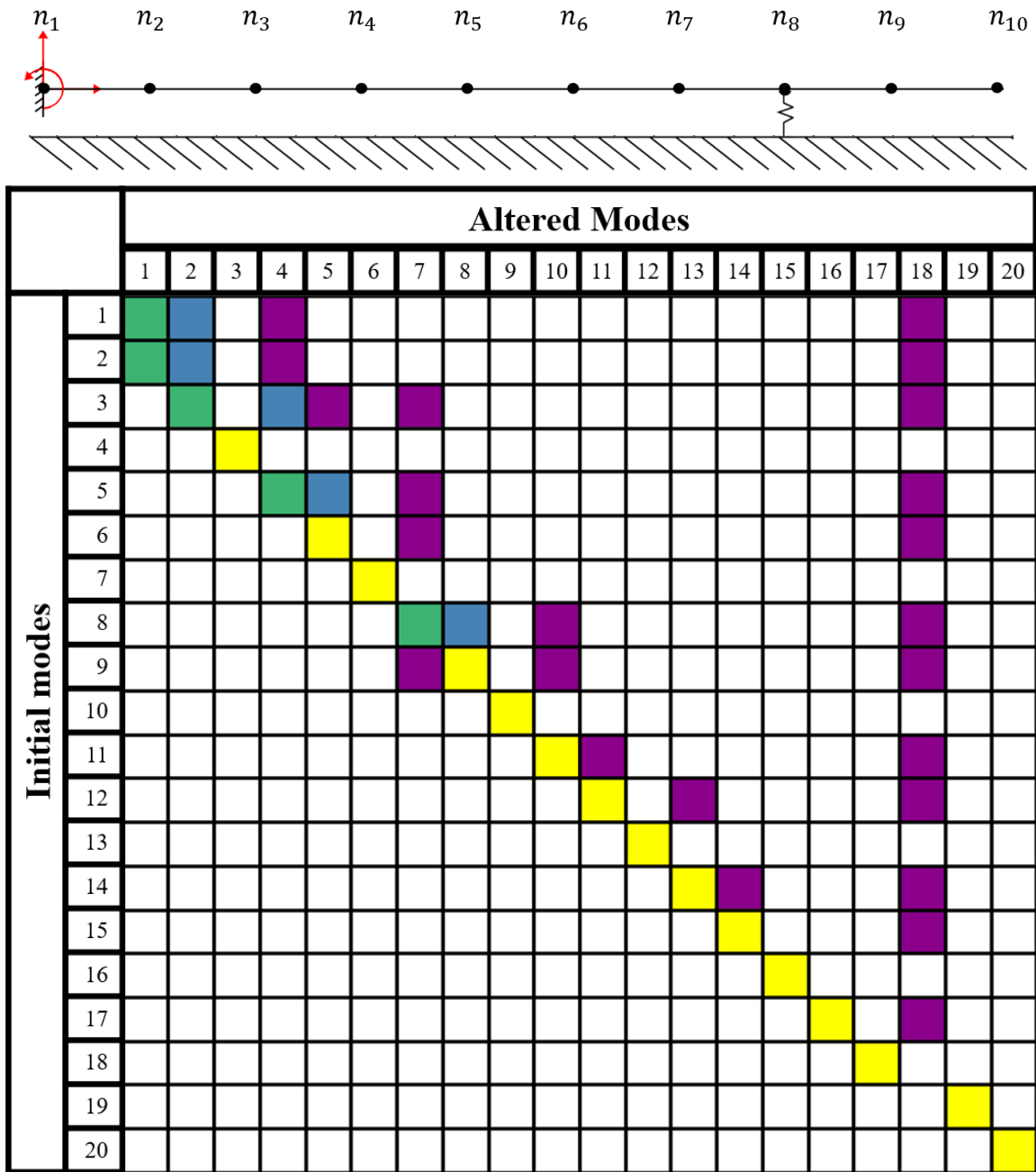
Figure 4.11   Modal participation factors for the altered state with roller at n_8.

Figure 4.12   Modal participation factors for the altered state with roller at n_9.
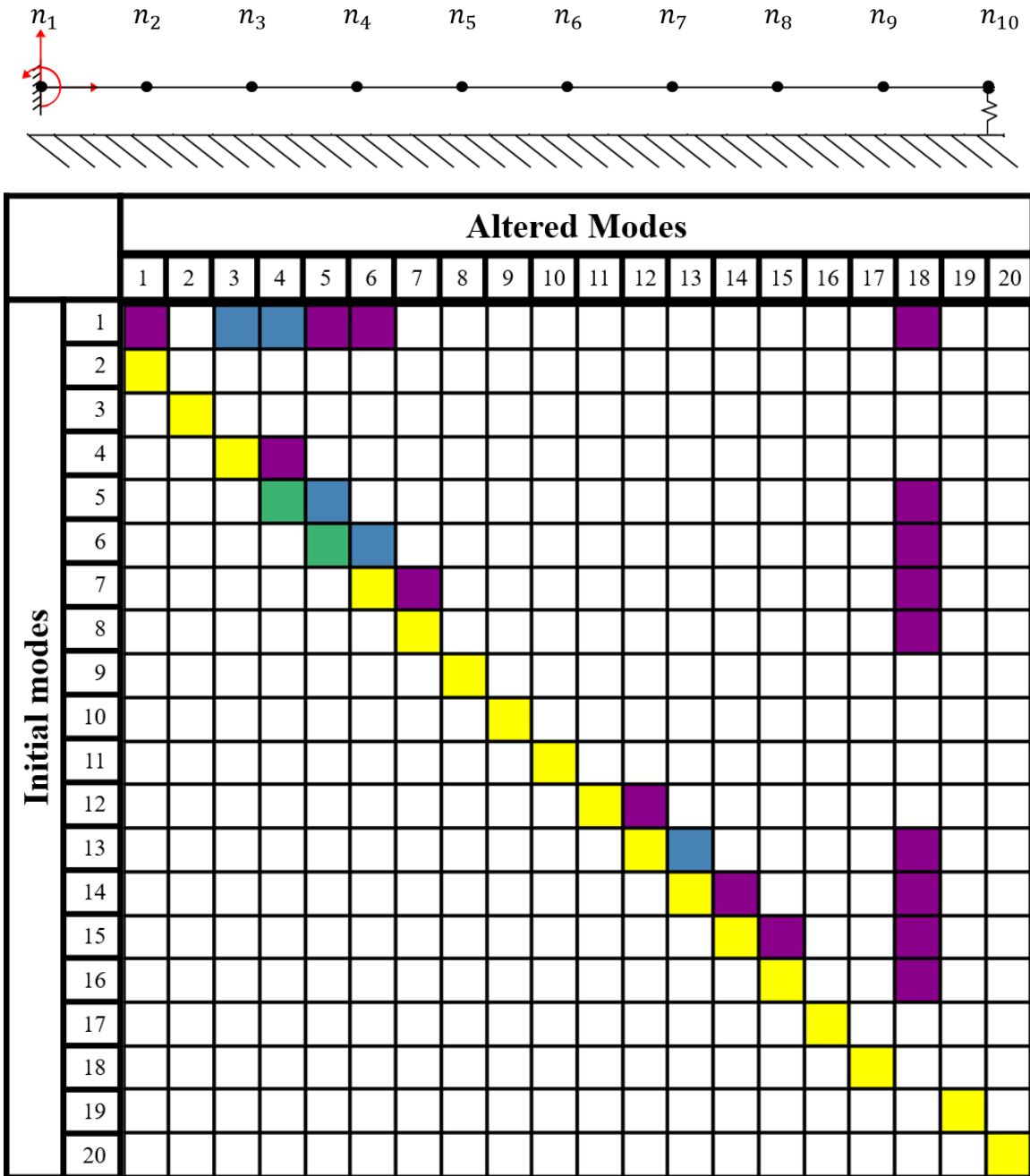
Figure 4.13   Modal participation factors for the altered state with roller at n_{10}.
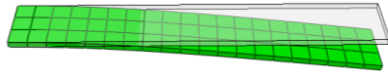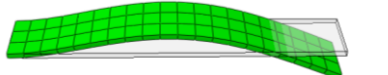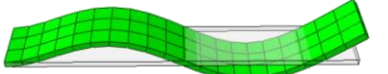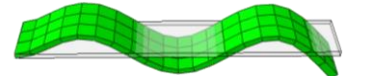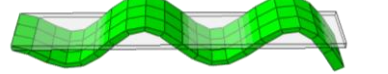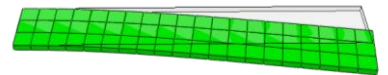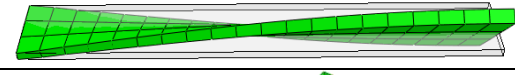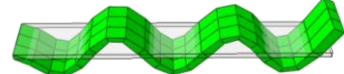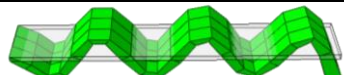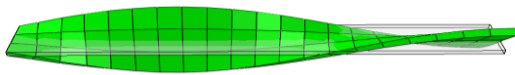
Using Figs. 4.5 – 4.13, the contributions from initial modes were tallied based on participation factors. The total counts and contribution percentage for initial modes whose contribution factors were greater than 0.2 are summarized in table 4.1.

Table 4.1   Counts and percentages for contributing initial modes.

Contributing mode	Participation Factors				Total Counts	Contribution Percentage (%)
	Yellow (.8 - 1)	Green (.6 - .8)	Blue (.4 - .6)	Purple (.2 - .4)		
1	5	2	6	13	26	6.3725
2	4	4	4	18	30	7.3529
3	4	3	6	20	33	8.0882
4	6	2	1	14	23	5.6372
5	2	7	7	15	31	7.5980
6	4	5	3	18	30	7.3529
7	8	1	2	10	21	5.1470
8	5	4	4	13	26	6.3725
9	9	0	1	18	28	6.8627
10	9	0	0	1	10	2.4509
11	9	0	0	8	17	4.1666
12	9	0	0	12	21	5.1470
13	9	0	2	8	19	4.6568
14	9	0	0	9	18	4.411
15	9	0	0	11	20	4.9019
16	9	0	0	7	16	3.9215
17	9	0	0	3	12	2.9411
18	9	0	0	0	9	2.2058
19	9	0	0	0	9	2.2058
20	9	0	0	0	9	2.2058
Total	146	28	36	198	408	100

Participating modes were selected if their contribution percentage was comparatively significant (5% or greater). Therefore, initial modes 1-9, and 12 were selected. However, in addition to participation factors, modes representing the initial state are also limited by the experimental setup. To utilize a mode in state estimations, the data acquisition system must be capable of measuring that mode experimentally. Therefore, it is important that each mode type and frequency be considered when selecting modes. The experimental setup in this work utilizes a single-axis accelerometer mounted at the far end of the beam which limits measurable modes to those with bending in the Y direction. Mode shapes are shown for all participating modes in Table 4.2.

Table 4.2   Participating mode numbers, types, and shapes.

Mode	Frequency (Hz)	Mode type	Shape
1	37.6956	Bending-Y	
2	248.561	Bending-Y	
3	713.463	Bending-Y	
4	1416.4	Bending-Y	
5	2353.62	Bending-Y	
6	3519.66	Bending-Z	
7	4918.5	Torsional	
8	6569.9	Bending-Y	
9	8422.02	Bending-Y	
12	15420.6	Torsional	

From this table the possible modes were further reduced to modes 1-5, 8 and 9. Additionally, the accelerometer used in this work has a maximum frequency range (±3 dB) of 0.02 - 1700 Hz [36], which encompasses the natural frequencies for modes 1-4 as shown in Table 4.2. Therefore, the first four modes were selected to model system states and used to determine the number of nodes required in subsequent chapters.

4.2 NODE SELECTION

From the previous section, it was determined that the system would be modeled using the first four modes; however, the number of nodes to be used in the model is still unknown. To determine the number of nodes required, the first four natural frequency responses are plotted as the roller moves along the beam for models with varying node numbers. The "true" frequency is defined using LEMP with 101 nodes which is then plotted against a reduced model containing 50, 25, or 21 nodes. The first four natural frequencies of the system plotted using a 51-node reduced model are shown in Figs. 4.14-4.17. Those using a 26-node reduced model are shown in Figs. 4.18-4.21 and those with a 21-node reduced model are shown in Figs. 4.22-4.25.

Figures 4.14 - 4.25, show that the relative error between the true and reduced models increases as the number of nodes decreases. However, the relative error does not exceed the maximum allowable error of 15 mm until the number of nodes is reduced to 21. Therefore, the reduced model with 25 nodes is selected to represent the system.

4.3 MODEL CREATION

Based on the results from Section 4.1 and 4.2, the model selected to represent the system is composed of 4 modes and 25 nodes. This initial model is illustrated in physical and modal space by Figs. 4.26 and 4.27 respectively.
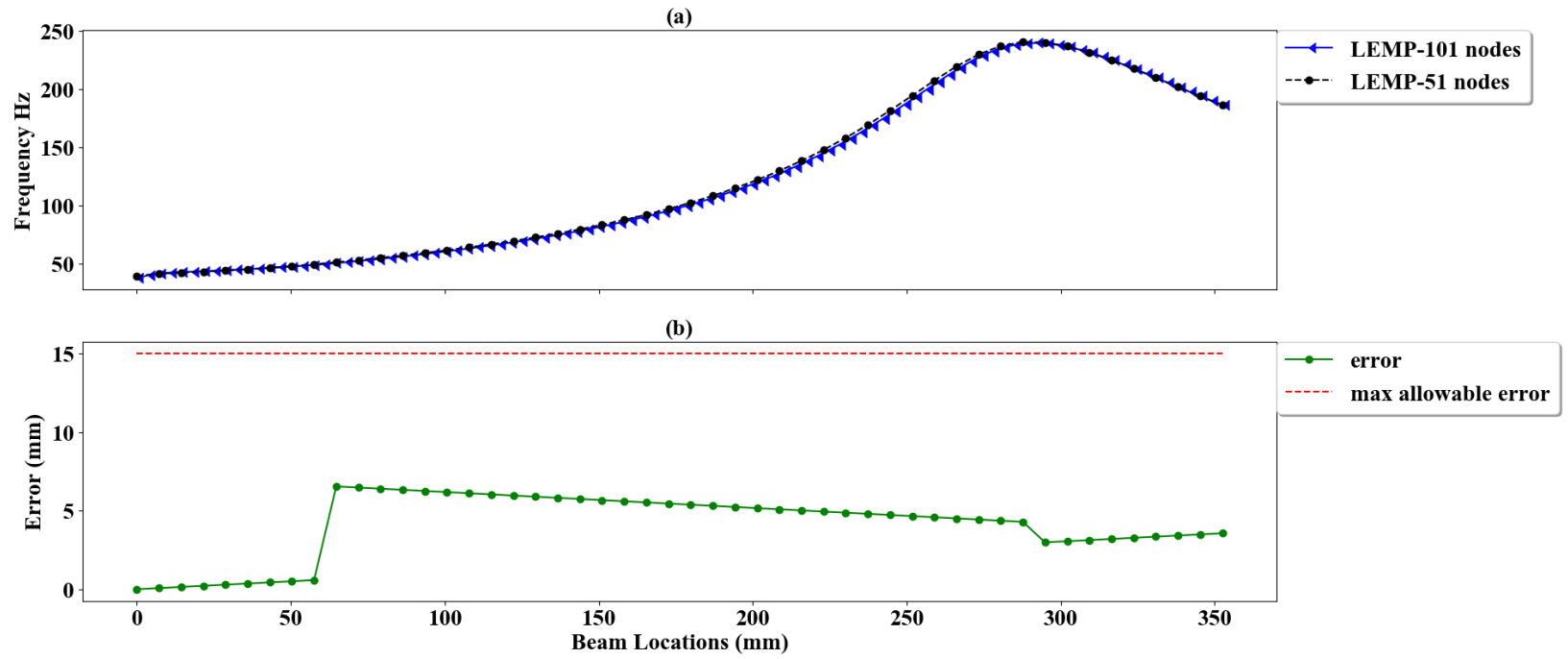
Figure 4.14   First frequency response for a 51-node model (a) and relative error (b).
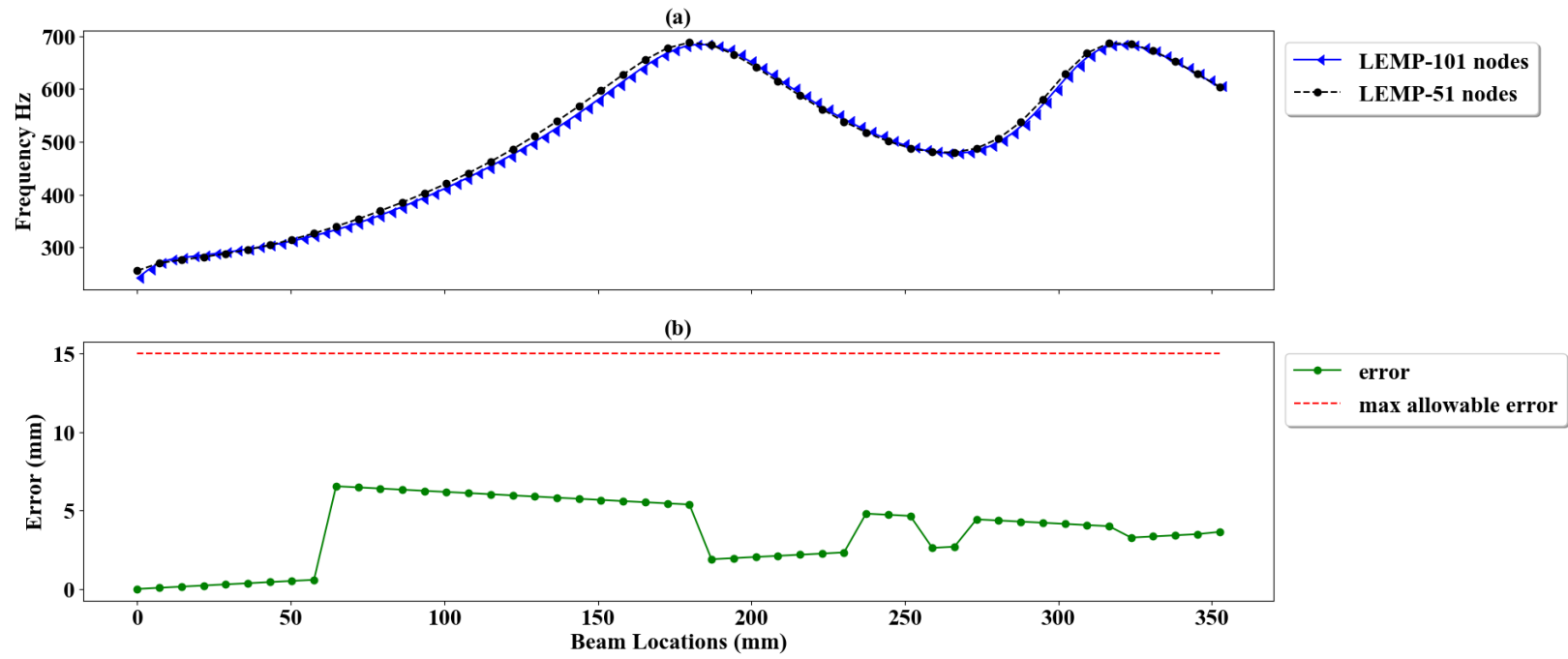
Figure 4.15   Second frequency response for a 51-node model (a) and relative error (b).
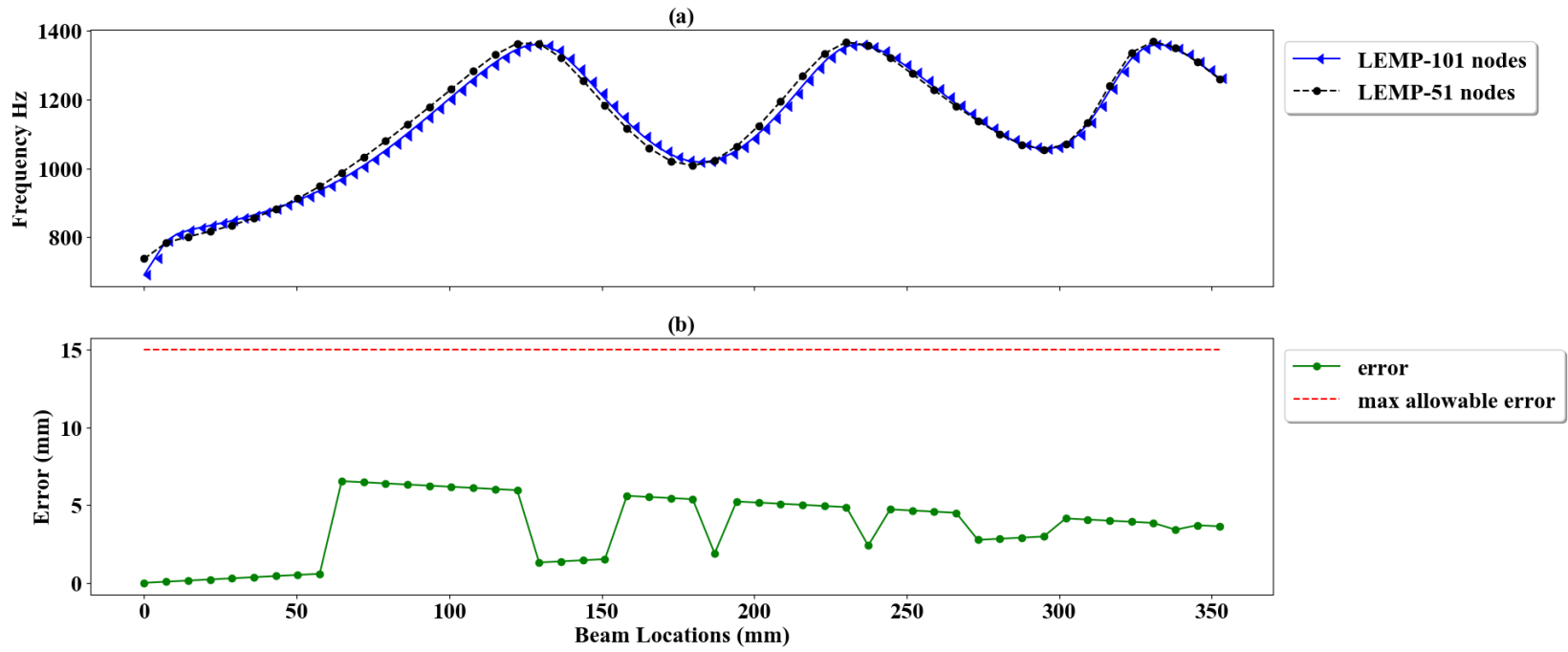
Figure 4.16   Third frequency response for a 51-node model (a) and relative error (b).
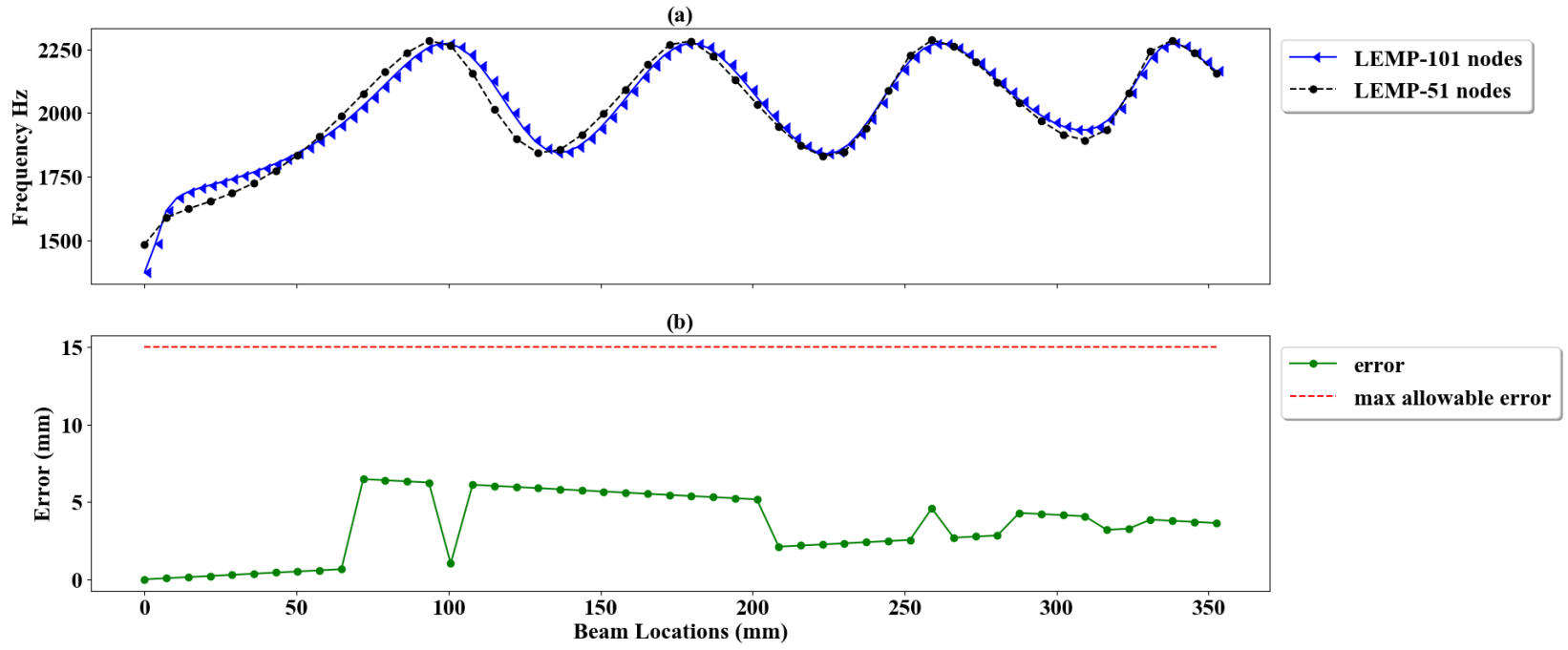
Figure 4.17   Fourth frequency response for a 51-node model (a) and relative error (b).
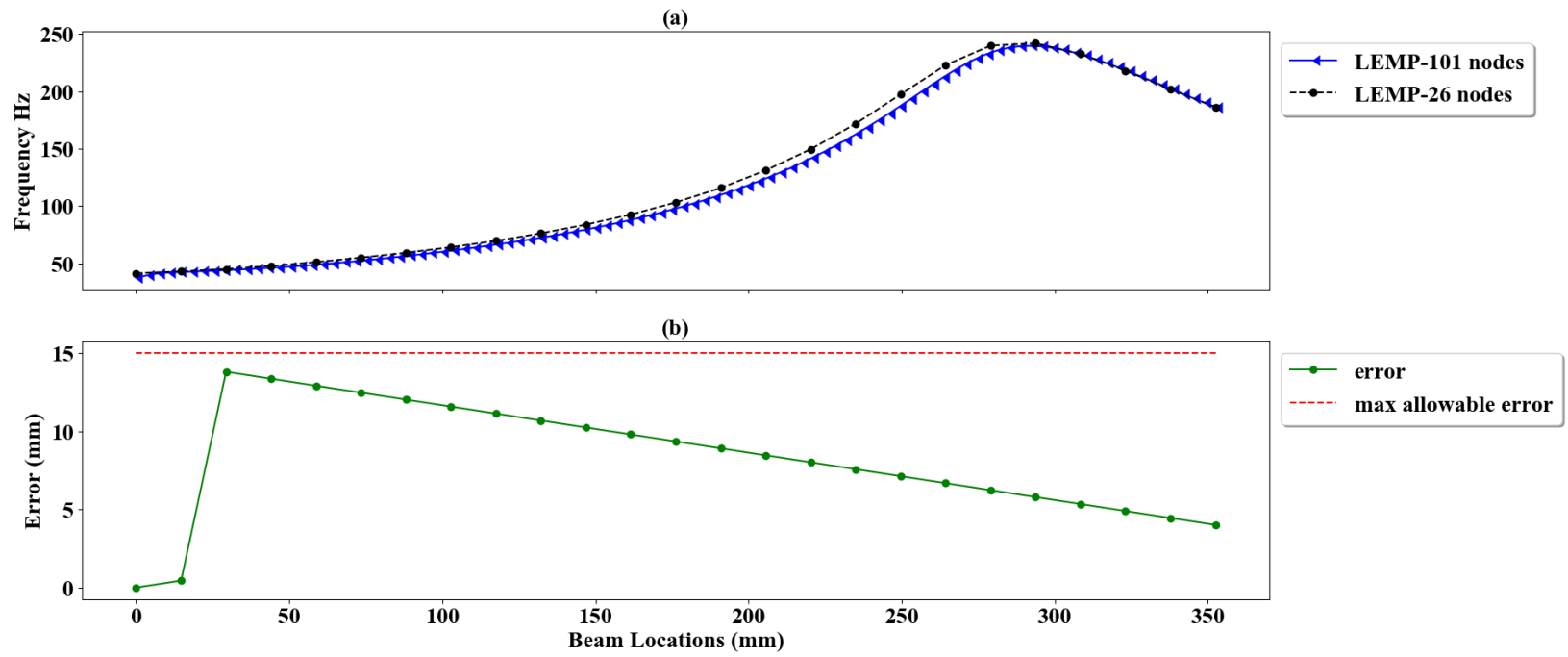
Figure 4.18   First frequency response for a 26-node model (a) and relative error (b).
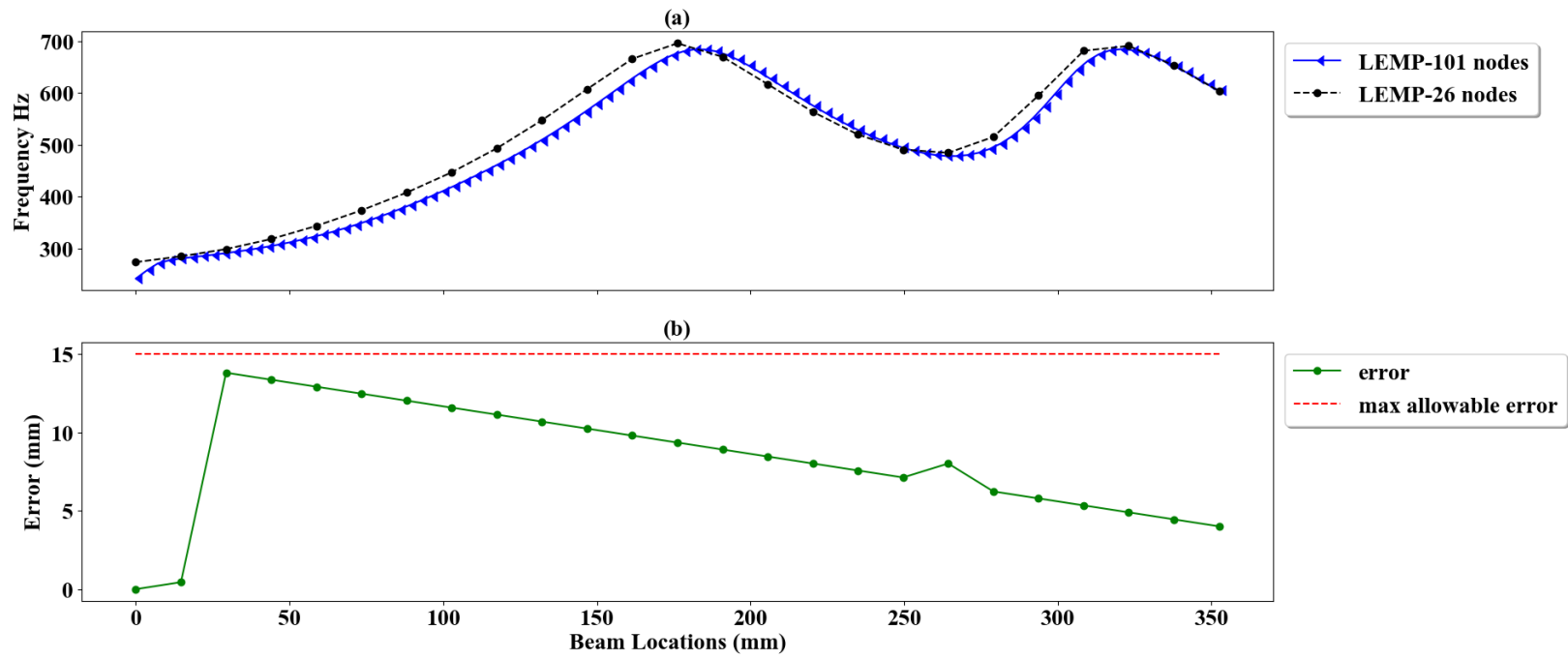
Figure 4.19   Second frequency response for a 26-node model (a) and relative error (b).
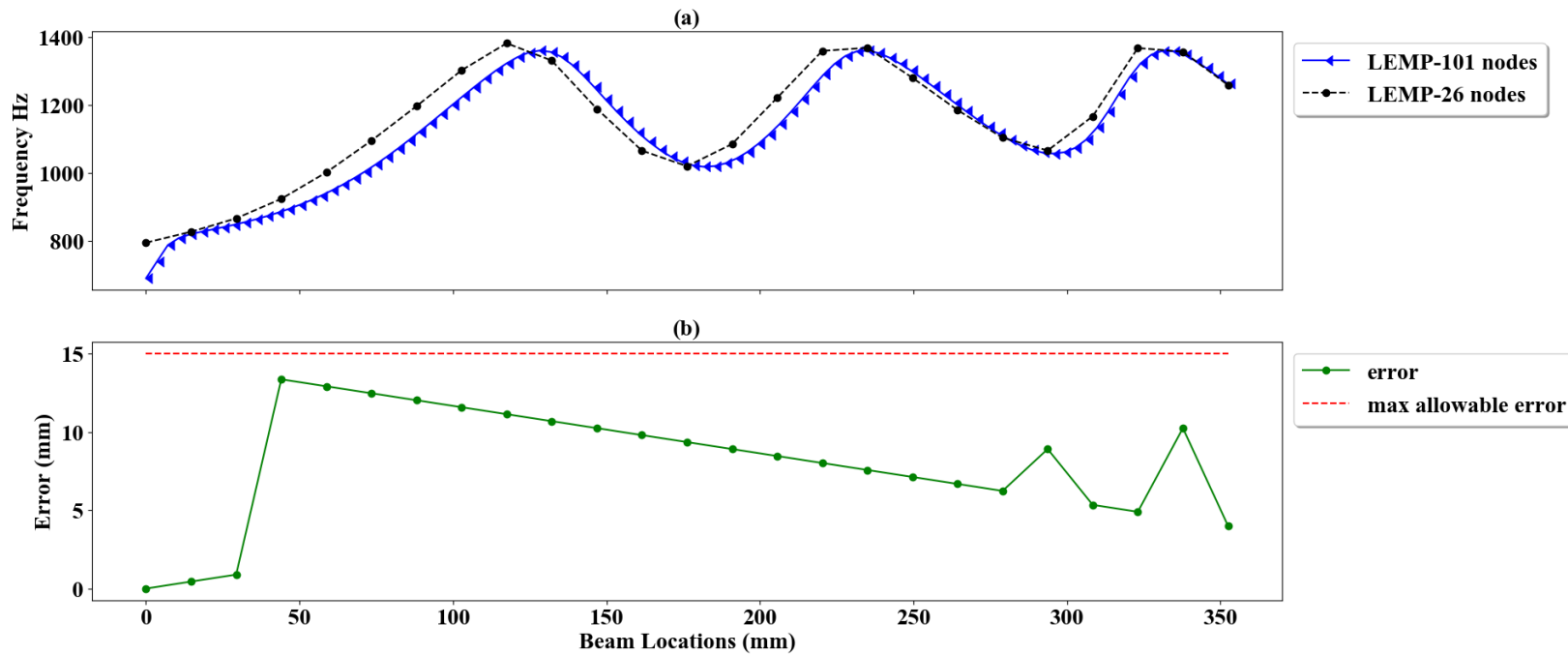
Figure 4.20   Third frequency response for a 26-node model (a) and relative error (b).
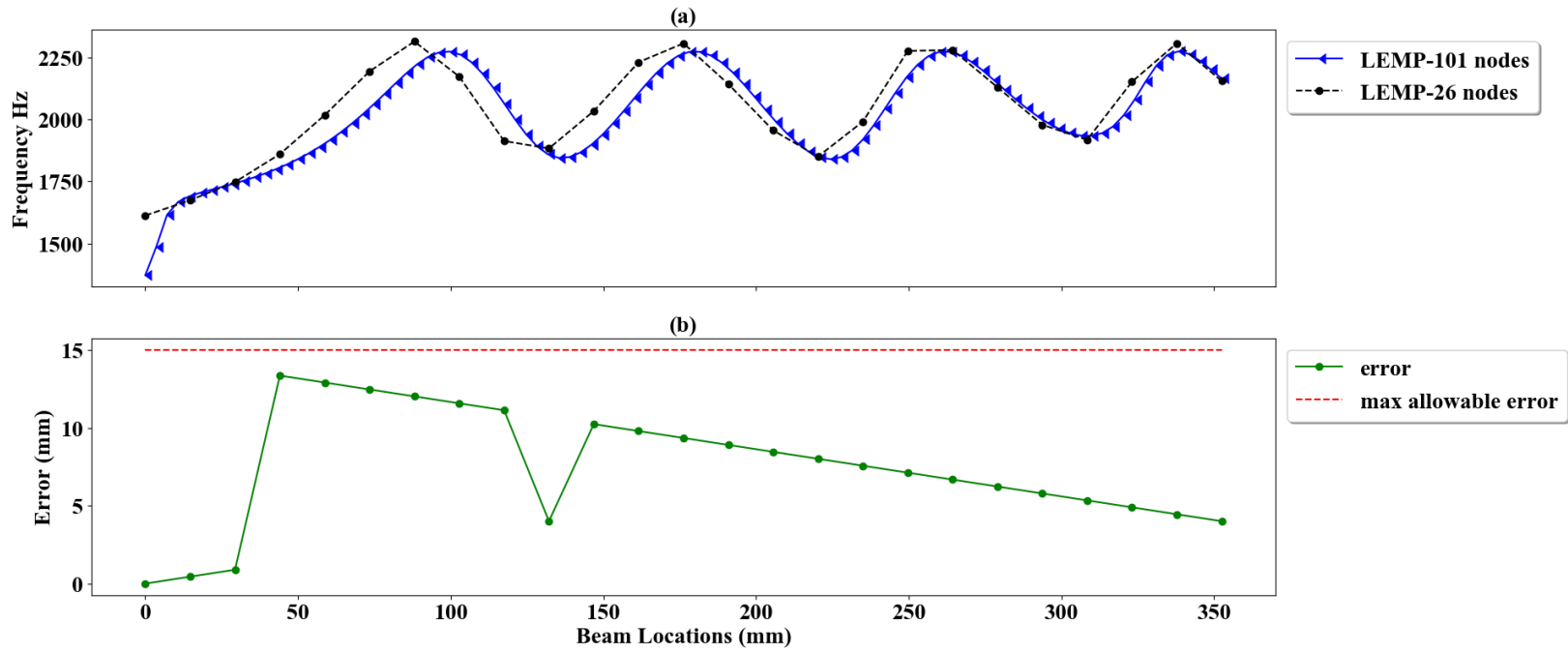
Figure 4.21   Fourth frequency response for a 26-node model (a) and relative error (b).
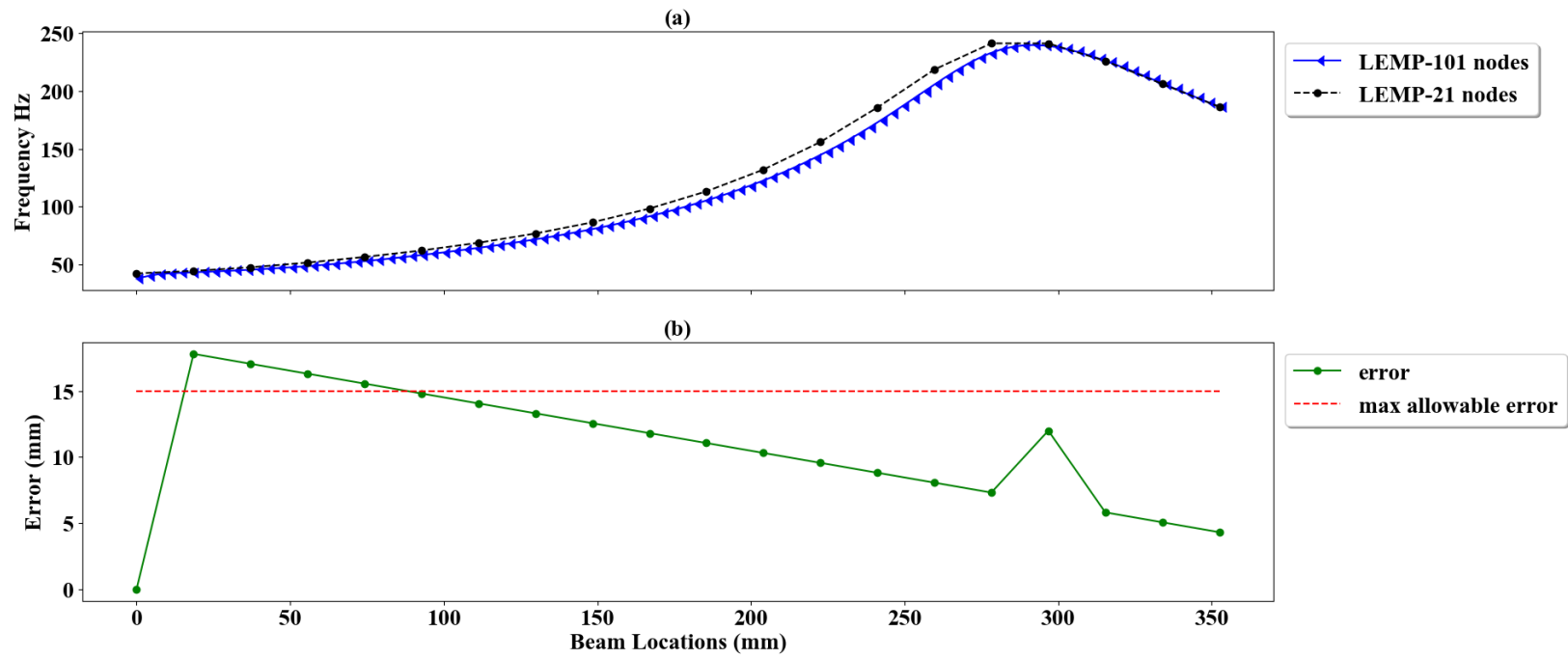
Figure 4.22　First frequency response for a 21-node model (a) and relative error (b).
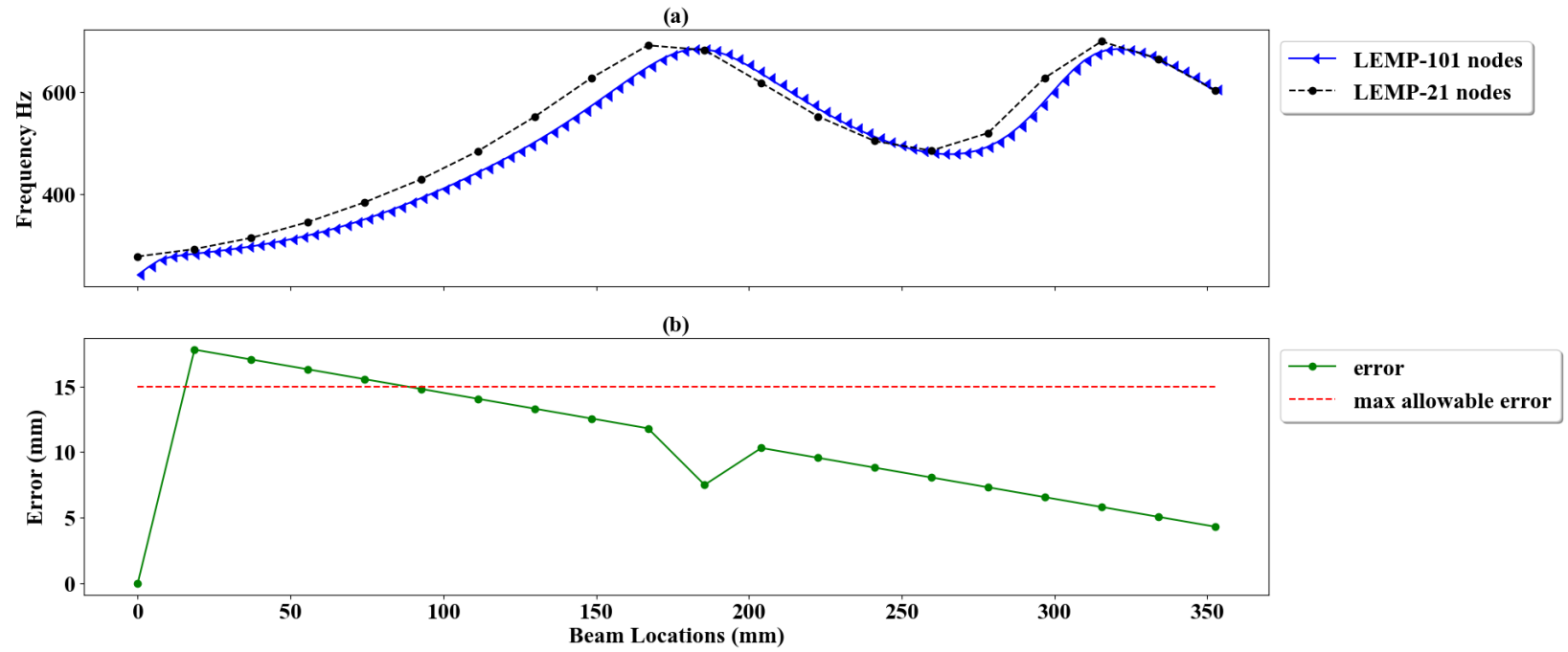
Figure 4.23   Second frequency response for a 21-node model (a) and relative error (b).
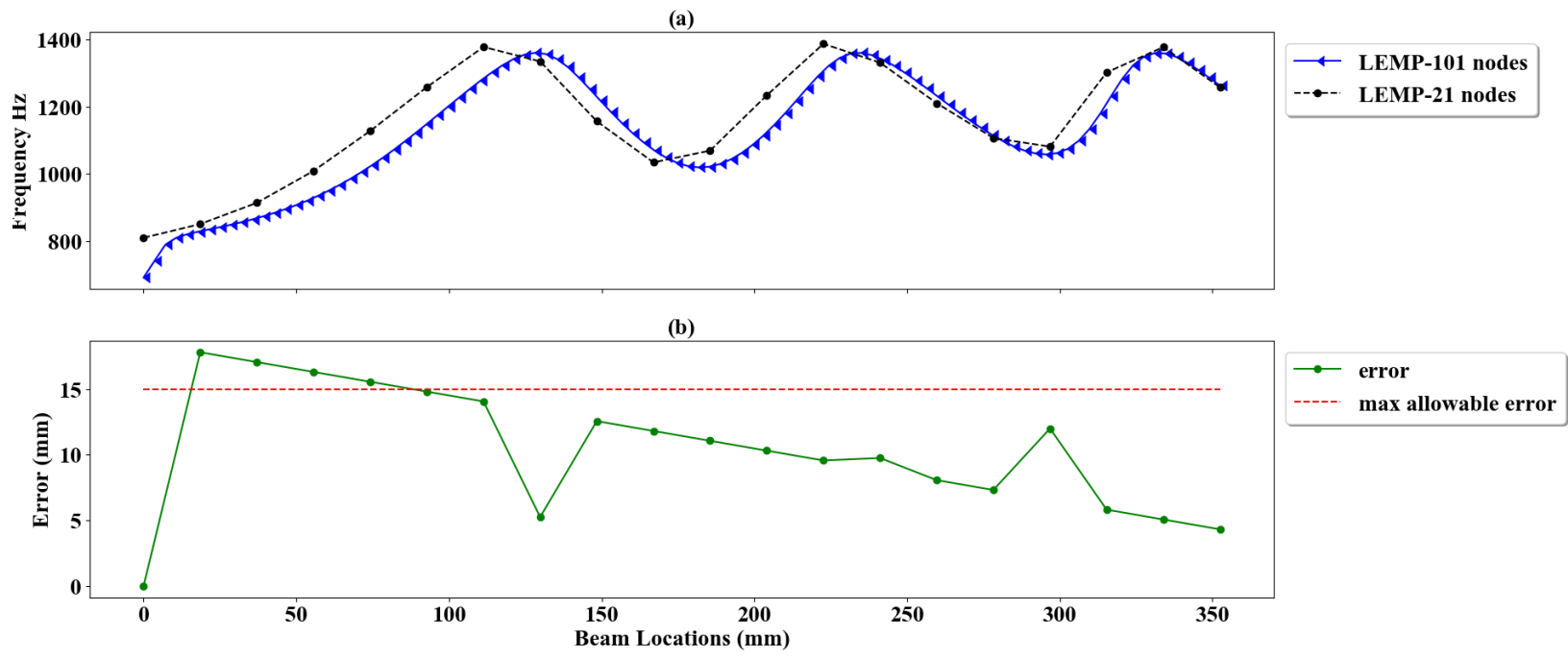
Figure 4.24   Third frequency response for a 21-node model (a) and relative error (b).
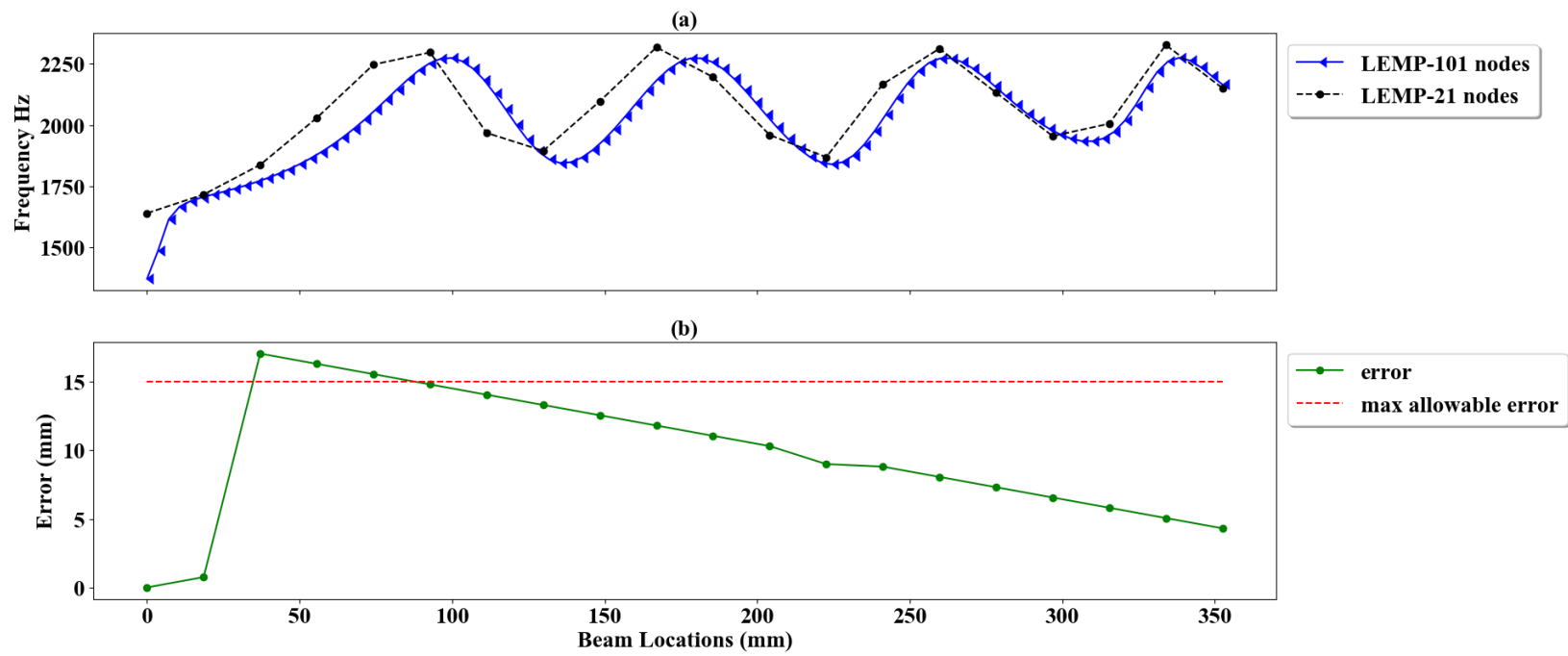
Figure 4.25   Fourth frequency response for a 21-node model (a) and relative error (b).

n_1 n_2 n_3 n_4 n_5 n_6 n_7 n_8 n_9 $n_{10}n_{11}n_{12}n_{13}$ n_{14} n_{15} $n_{16}n_{17}n_{18}n_{19}$ $n_{20}n_{21}$ n_{22} n_{23} $n_{24}n_{25}$ n_{26}
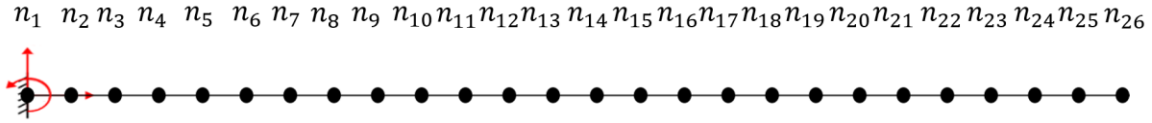
Figure 4.26   Initial model in physical space
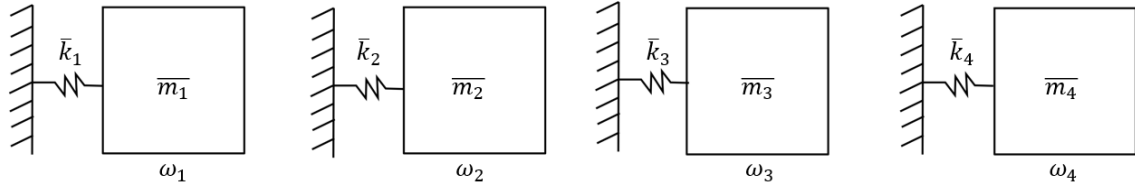
Figure 4.27   Initial model in modal space.

As the roller moves along the beam, the models are updated. Assuming the roller is at the midpoint of the beam, Figs. 4.28-4.30 illustrate the corresponding updated models. Where Fig. 4.28 represents the model in physical space, Fig. 4.29 is LEMP model with increased nodal stiffness, and Fig. 4.30 shows the model in modal space.

n_1 n_2 n_3 n_4 n_5 n_6 n_7 n_8 n_9 $n_{10}n_{11}n_{12}n_{13}$ n_{14} n_{15} $n_{16}n_{17}n_{18}n_{19}$ $n_{20}n_{21}$ n_{22} n_{23} $n_{24}n_{25}$ n_{26}
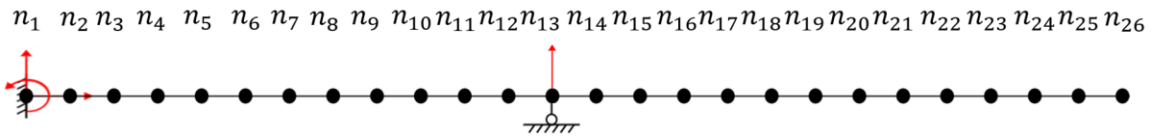
Figure 4.28   Altered model in physical space.

n_1 n_2 n_3 n_4 n_5 n_6 n_7 n_8 n_9 $n_{10}n_{11}n_{12}n_{13}$ n_{14} n_{15} $n_{16}n_{17}n_{18}n_{19}$ $n_{20}n_{21}$ n_{22} n_{23} $n_{24}n_{25}$ n_{26}
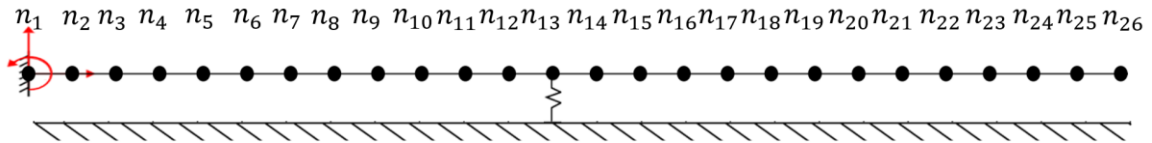
Figure 4.29   Altered LEMP model in physical space.

The initial model will remain constant; however, the altered models will adjust based on roller location. The initial and altered models will be used in LEMP and the Bayesian search space to determine the state of the system. Details of how this is accomplished are discussed further in the next chapter.
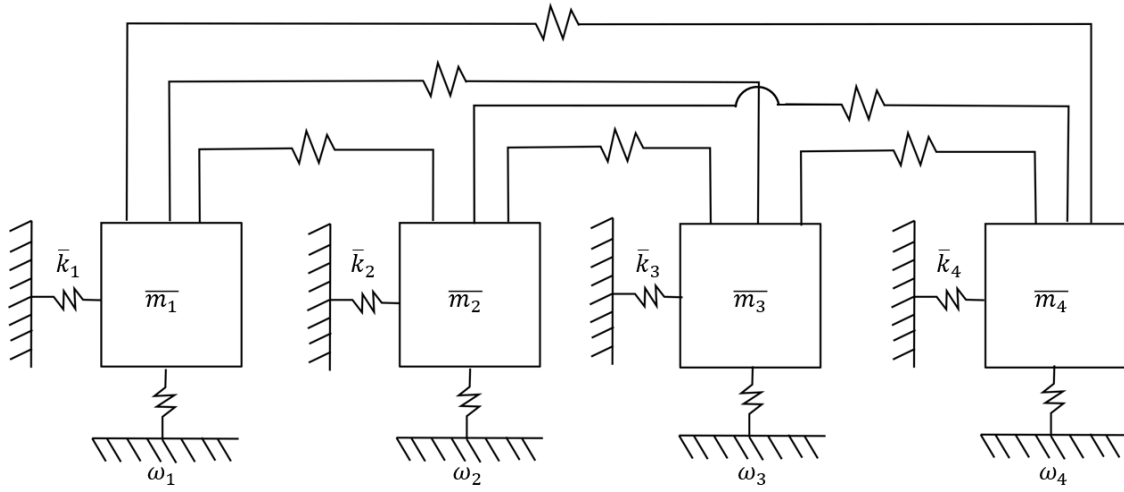
Figure 4.30   Altered model in modal space.

CHAPTER 5

METHODOLOGY

Once a surrogate model is created, the overall procedure can be divided into two main parts: the experimental procedure and the analytical procedure. The analytical procedure can be further decomposed into two procedures: selecting roller locations using the Bayesian search space and computing the modal state estimation using LEMP. The overall procedure and integral steps are shown in Fig. 5.1 below.
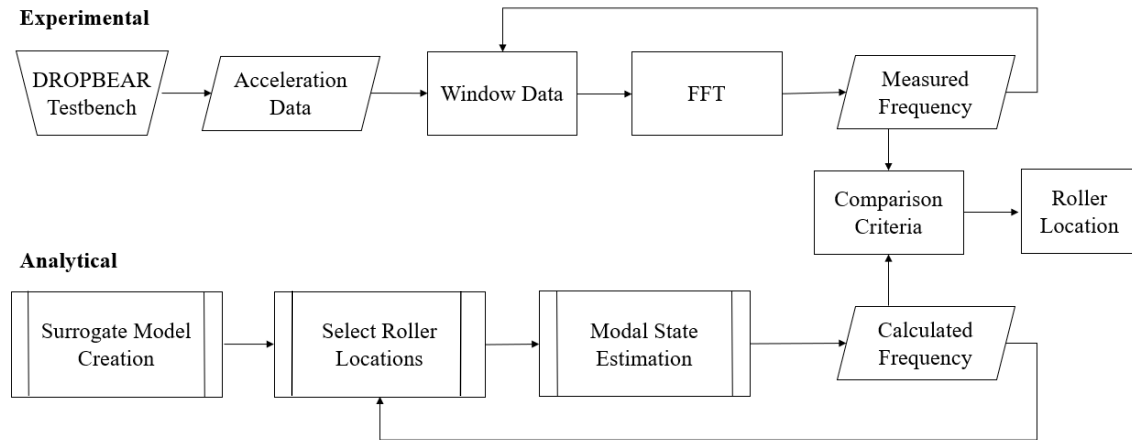
Figure 5.1   Flowchart of overall procedure and integral steps used in this work.

The experimental procedure will be covered in Section 5.1, selecting roller locations using the Bayesian search space will be covered in Section 5.2, and modal state estimation will be covered in Section 5.3. Surrogate model creation was covered entirely in chapter 4.

5.1 EXPERIMENTAL PROCEDURE

The purpose of the experimental procedure is to determine the "true" system response of the DROPBEAR testbed with varying boundary conditions. This is accomplished by collecting acceleration data from the system using the accelerometer mounted on the free end of the beam. Before the acceleration data is processed, a sliding Hann window is applied to smooth the time-series data. The natural frequency of the beam is then obtained by taking the Fast Fourier Transform (FFT) of the acceleration data. This "true" system response is then compared to the various analytically solved models and a state estimation is made using comparison criteria. The test profile used to define the roller location for this procedure can be seen in Fig. 5.2.
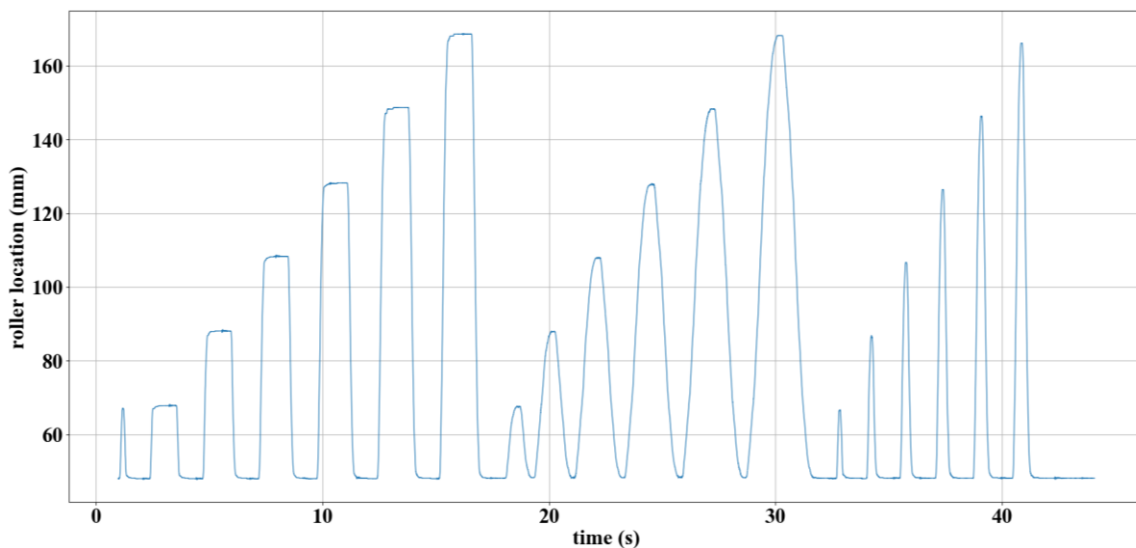
Figure 5.2   Roller testing parameters used in this work.

The experimental data collected from DROPBEAR allows for the evaluation of algorithms that create real-time models of systems experiencing high-rate dynamic events. These models can then be expanded to more complex structure with the goal of detecting and quantifying damage that occurs using natural frequency estimations.

5.2 BAYSIAN SEARCH SPACE

The function of the Bayesian search space is to select the most probable roller locations at which to apply LEMP. This is done to improve initial estimations and reduce the number of comparison points selected and error calculations required. Figure 5.3 illustrates the role of the Bayesian search space loop within the analytical procedure.
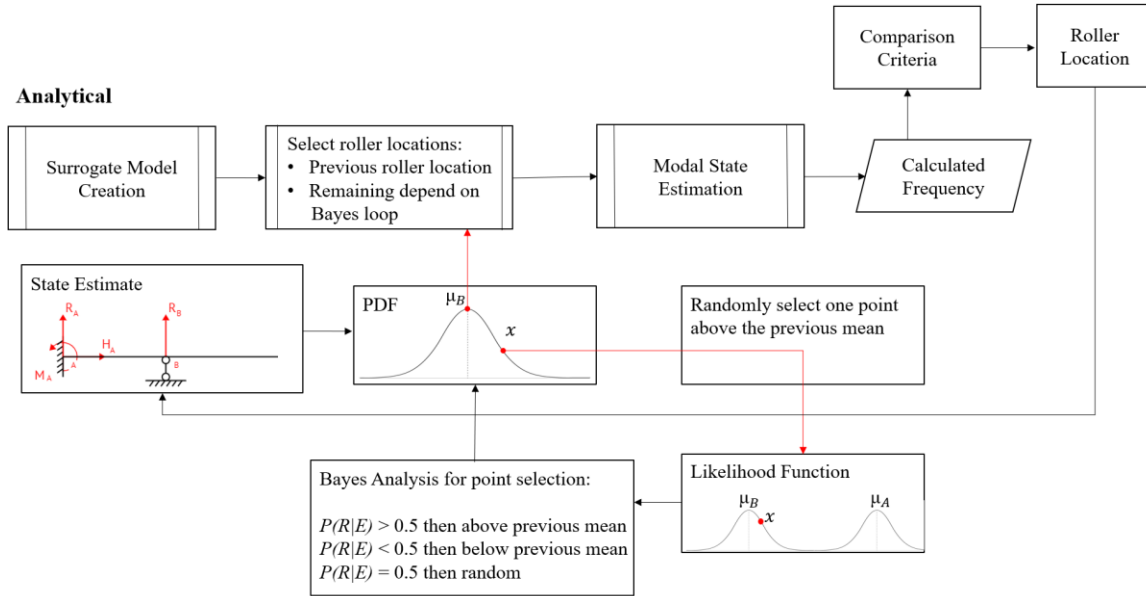
Figure 5.3   Bayesian search space loop within the analytical procedure.

When a state estimation is made, a new PDF is created about the updated roller location. Points are selected from this distribution and either accepted or rejected using the likelihood function and Bayes conditions (as discussed in Section 3.4). The Bayes procedure refines roller positions to select probable locations based on past estimates and uncertainty. The selected points are then used as input for LEMP which calculates the analytical frequency at each point. The analytical frequencies are then compared to the "true" experimental frequency to make state estimations and the analytical loop repeats itself.

56

5.3 REAL-TIME MODEL UPDATING

Real-time model updating can be completed in two steps: 1) calculating the analytical frequency at selected roller positions and 2) choosing the best estimation to represent the current system state using comparison criteria. Initially it is assumed that the roller is located at the midpoint of the beam and is moving to the right. Three comparison points are then selected at which to compare the analytically solved frequency with the true measured frequency.

Analytical solutions for system states in this work are calculated using three methods: GE solutions, LEMP solutions and LEMP solutions using a Bayesian search space. All three methods mentioned above utilize an adaptive standard deviation (SD) equal to the percentage error found in the frequency domain as shown in Eq. (41). This technique for altering the size of a search space is adopted from Hong et al. [5]. The ability to alter search space size is advantageous because it expands the search space when the sampled states differ from the measured states, allowing the algorithm to estimate sudden changes in systems. Additionally, the search space is reduced when sampled states and measured states are similar, allowing the algorithm to model constant system without much variation.

$$\sigma = \frac{\omega_{estimate}^{previous} - \omega_{true}^{current}}{\omega_{true}^{current}} \tag{41}$$

Here, σ is the SD of a normal distribution about the last roller position, $\omega_{true}^{current}$ is the current measured frequency from experimental data and $\omega_{estimate}^{previous}$ is the previously estimated frequency using the analytical methods and comparison criteria. As noted in Hong's study [5], Eq. (41) assumes that the percentage error in frequency is equivalent to the percentage error in position; however, since roller location and frequency are not

linearly related (as shown in Figs. 4.13-4.24), this assumption is not necessarily true for every case.

The analytical solutions discussed previously are used to estimate system states by two methods: error minimization and bounded regression, each using three comparison points. The error minimization method compares the "true" (measured) frequency with the frequency at each of the three testing points and selects the location that minimizes absolute error. The bounded regression approach was adopted from Hong et al. [5], where the linear model by least-squares method is given in its general form by Eq. (42) [37].

$$\binom{a}{b} = (X^T X)^{-1} X^T Y \tag{42}$$

For this work where three locations selected for comparison of frequency based on roller location, X and Y are defined as below:

$$X = \begin{pmatrix} x_1 & 1 \\ x_2 & 1 \\ x_3 & 1 \end{pmatrix} \tag{43}$$

$$Y = \begin{pmatrix} \omega_1 - \omega_{true} \\ \omega_2 - \omega_{true} \\ \omega_3 - \omega_{true} \end{pmatrix} \tag{44}$$

Where a and b are regression parameters such that $\omega - \omega_{true} = ax + b$. Therefore, $\omega = \omega_{true}$ when $x = -b/a$. However, because errors in the regression model propagate where sample data is limited, the estimated roller location is bound between the minimum and maximum comparison locations as shown in Eq. (45). Furthermore, for solutions using the Bayes approach, the past estimate will be the minimum comparison location if the roller is moving right or the maximum comparison location if the roller is moving left.

$$x_c = \begin{cases} x_{min} & -b/a < x_{min} \\ x_{max} & -b/a > x_{max} \\ -b/a & elsewhere \end{cases} \tag{45}$$

While the error minimization approach yields better estimations, the bounded

regression method allows estimations of roller locations that are not located on

preselected nodes. This advantage yields smoother estimation curves, which are shown in

the following chapter.

CHAPTER 6

RESULTS AND DISCUSSION

Roller locations obtained from each method: GE solutions, LEMP solutions and

LEMP solutions using a Bayesian search space are selected as state estimations using the

error minimization and bounded regression techniques as comparison criteria. For each

method three comparison points are selected, and the initial estimated roller position is

set to the center of the beam which accounts for the spike in error at the start of each test.

The estimated results are compared to the measured values by absolute mean error and

Time Response Assurance Criterion (TRAC) to assess the viability of each method.

TRAC was developed to quantify the similarity between time traces [38, 39]. In

this work it is used to compare the transient displacement responses of the various

estimation methods by considering the error and time delay of each as shown in Eq. (46).

$$TRAC \ = \ \frac{[\{t_m\}^T\{t_e\}]^2}{[\{t_m\}^T\{t_m\}][\{t_e\}^T\{t_e\}]} \tag{46}$$

Where t_m and t_e are time traces of the measured and estimated data, respectively. A

TRAC value of one indicates perfect correlation, and a value of zero indicates no

correlation.

Figures 6.1-6.3 illustrate GE estimations, LEMP estimations and LEMP

estimations using a Bayesian search space with error minimization approach used for

comparison criteria.
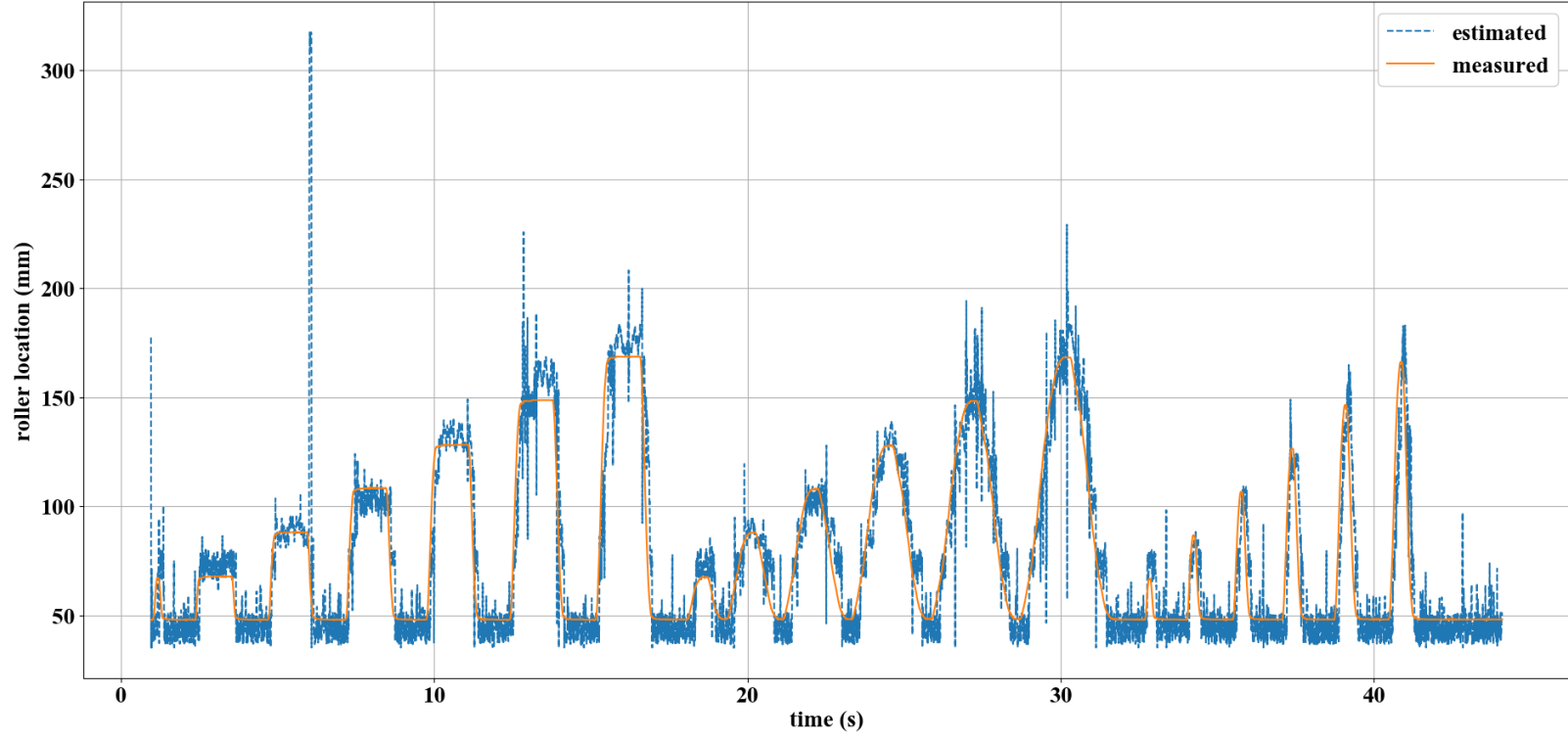
Figure 6.1   GE roller estimations using error minimization.
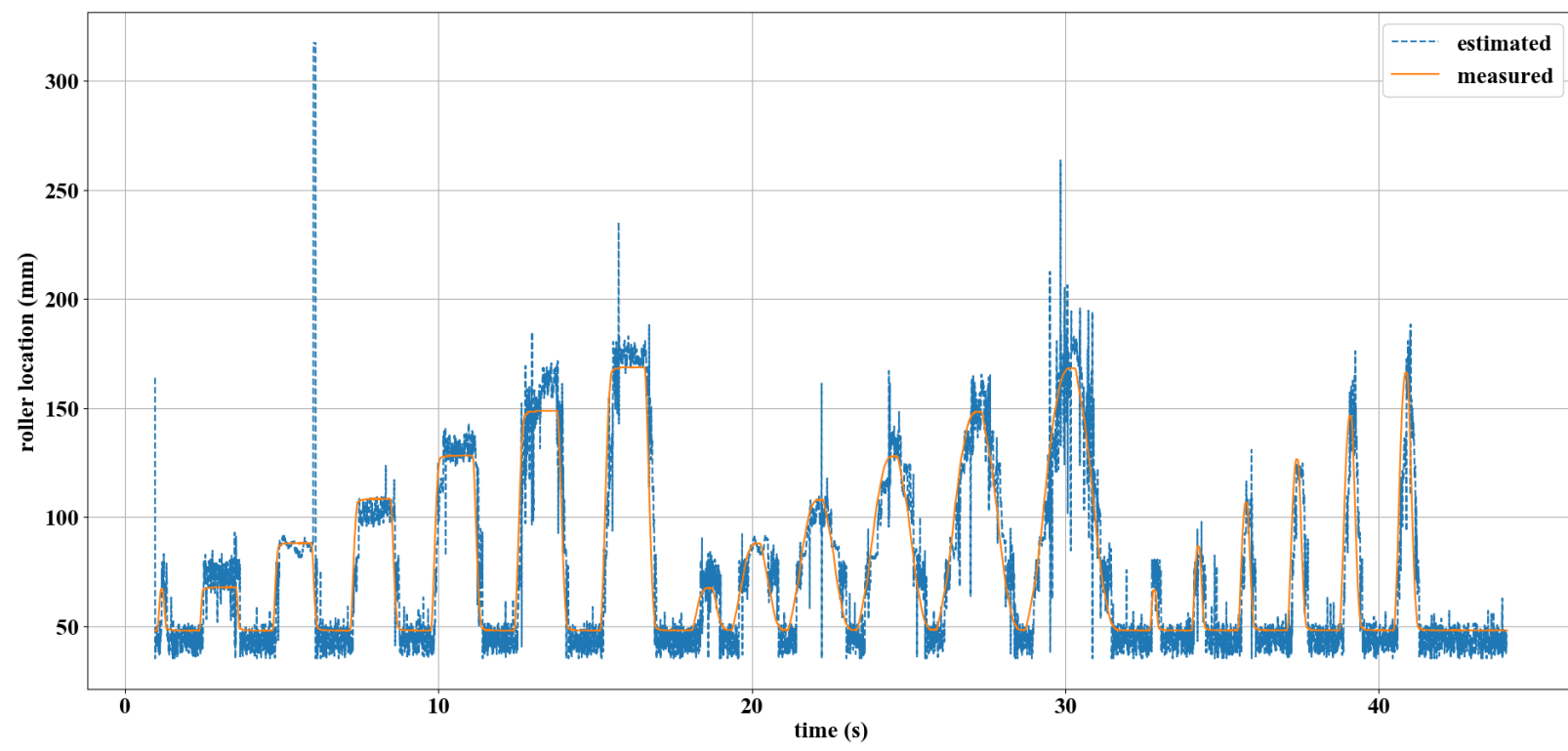
Figure 6.2   LEMP roller estimations using error minimization.
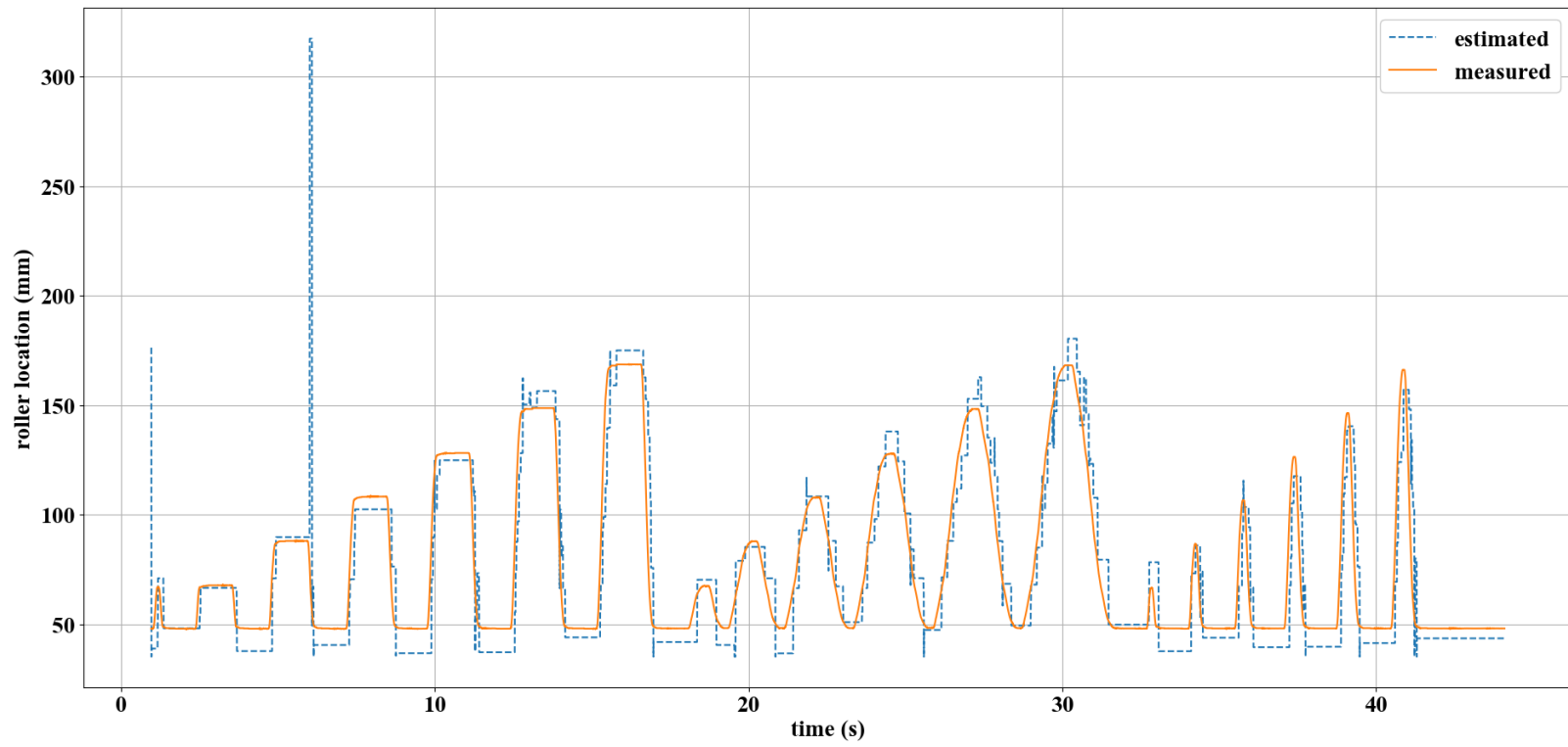
Figure 6.3   Bayesian LEMP roller using error minimization.

The fluctuation in estimations between Fig. 6.1 and Fig. 6.2 are similar, therefore it cannot be concluded that LEMP alone provides smooth estimates. However, as seen in Fig. 6.3 the implementation of a Bayesian search space with LEMP solutions allows for less fluctuation and smoother estimates since the comparison points are not selected at random, but rather by using a probabilistic approach. This is most advantageous when the roller is stationary as estimates remain constant for the most part.

The absolute mean error between the estimates and measured location and TRAC values are shown for each of the calculation methods using error minimization technique in Table 6.1 below.

Table 6.1   Assessment of error minimization as comparison criteria

Solution Type	Absolute Mean Error (mm)	TRAC
GE	49.721	.9596
LEMP	48.804	.9577
LEMP with Bayesian Search Space	48.121	.9592

The GE method has an absolute mean error of 49.721 mm with a TRAC value of .9596 compared to LEMP with an error of 48.804 mm with a TRAC value of .9577 and LEMP with a Bayesian search space error of 48.121 mm and TRAC value of .9592. Therefore, its concluded that LEMP somewhat improves the estimated value with Bayesian approach offering a slightly better estimate.

Figures 6.4-6.6 illustrate the GE solutions, LEMP solutions and LEMP solutions using a Bayesian search space with bounded regression approach used for comparison criteria.
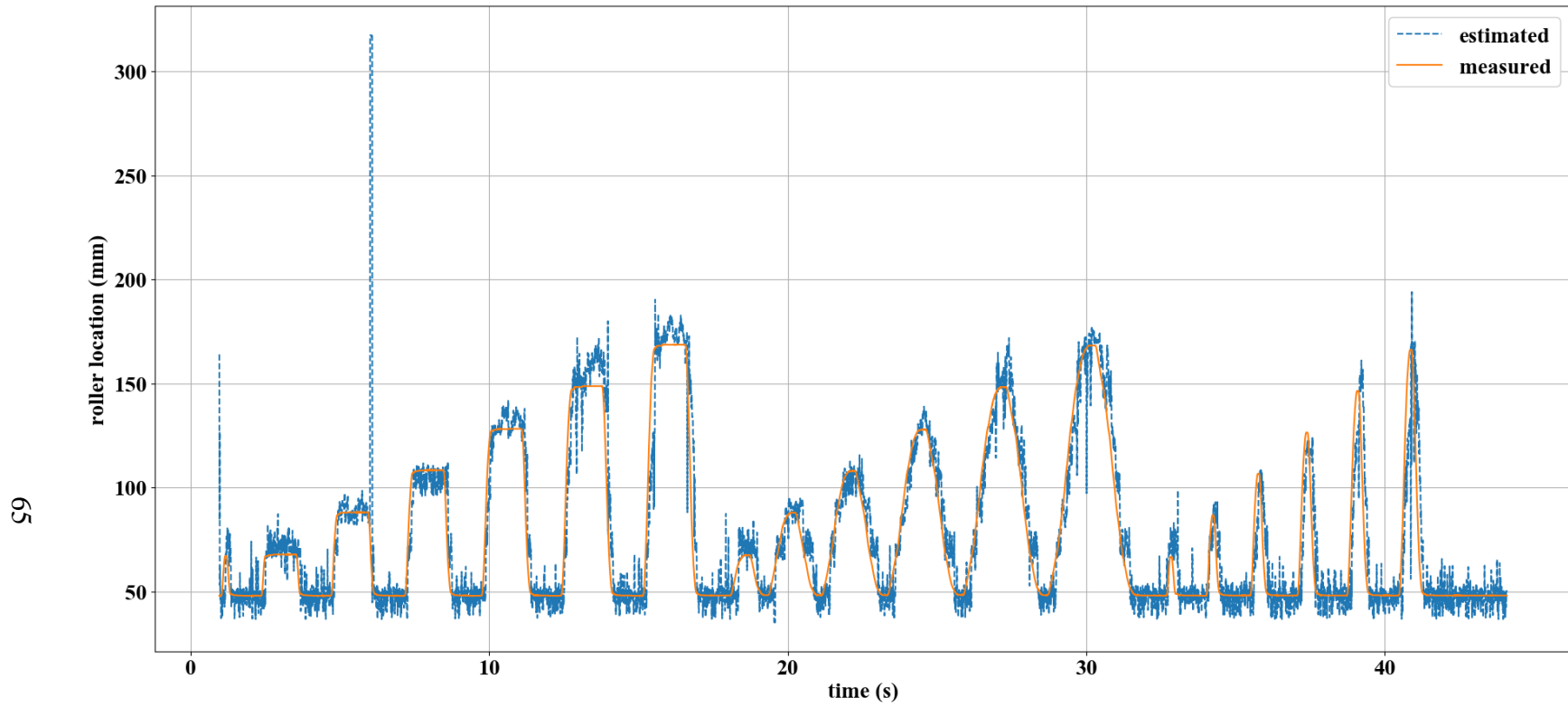
Figure 6.4   GE roller estimations using bounded regression.
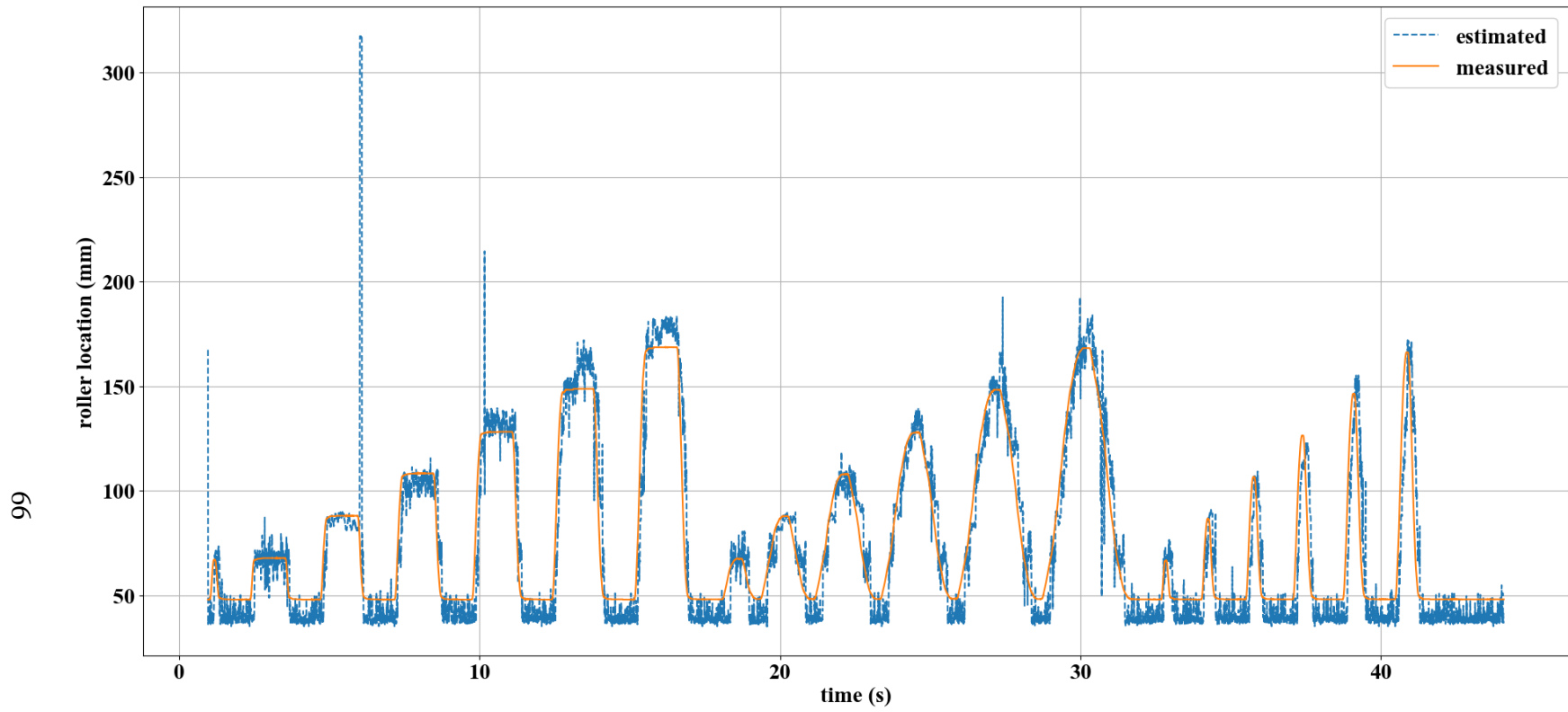
Figure 6.5   LEMP roller estimations using bounded regression.
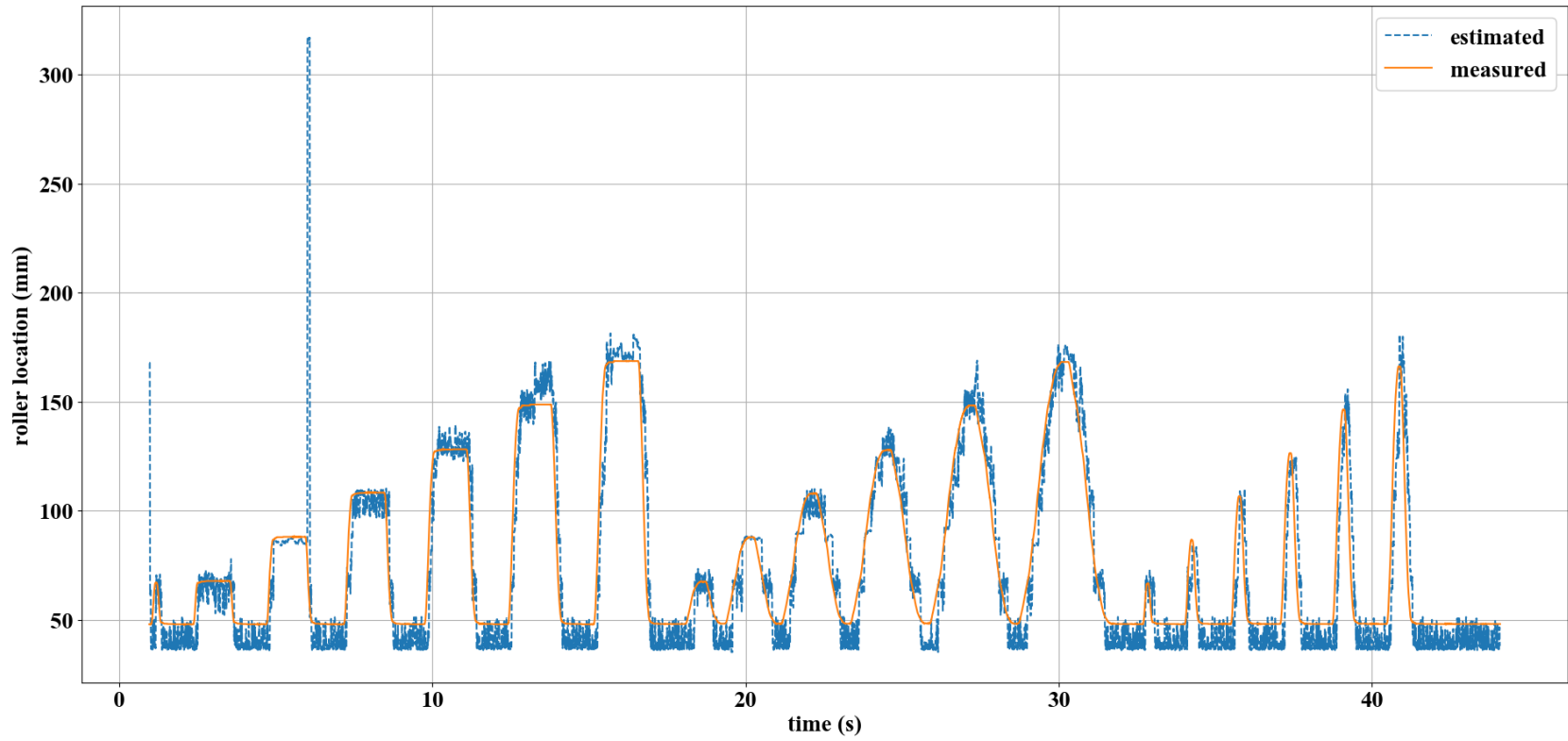
Figure 6.6   Bayesian LEMP roller using bounded regression.

Again, the fluctuation in estimations between Fig. 6.4, Fig. 6.5 and Fig. 6.6 are similar, but there is slightly less fluctuation in the LEMP approach that utilizes a Bayesian search space.

The absolute mean error between the estimates and measured location are shown for each of the calculation methods using bounded regression technique in Table 6.2.

Table 6.2   Assessment of bounded regression as comparison criteria

Solution Type	Absolut Mean Error (mm)	TRAC
GE	51.01	.9637
LEMP	46.564	.9580
LEMP with Bayesian Search Space	46.249	.9575

The GE method has an absolute mean error of 51.01 mm and TRAC value .9637 compared to LEMP with an error of 46.564 mm and TRAC value of .9580 and LEMP with a Bayesian search space with an error of 46.249 mm and TRAC value of .9575.

Note that the error for LEMP using a Bayesian search space is greater when linear regression is applied than when the error minimization technique is applied. This is due to the conflicting approaches of Bayes and linear regression when the roller is stationary. When minimizing error, the previous location is selected as a roller location and chosen as a state estimation when roller is stationary. However, for linear regression the approach creates a line of best fit which might not contain the previous location.

Overall, the bounded regression approach offers a better estimate of the roller's location; however, LEMP solution with a Bayesian search space utilizing error minimization as the comparison criteria offers the smoothest estimations with less fluctuation.

CHAPTER 7

USING LEMP TO MODEL UNSUPPORTED STRUCTURES

Chapters 4-6 propose and validate an algorithm that estimates the state of a

structure that is altered by the addition of a boundary condition. It is proposed here that

the procedure can be extended to altering structures by removing boundary conditions as

well. Extending LEMP to model the removal of boundary conditions would be beneficial

for modeling unsupported structures, such as potted printed circuit boards (PCB) with

gaps in the potting or large structures supported by eroding soil subjected to seismic

activity.

PCBs are potted to increase survivability when exposed to harsh environments

such as High-G forces or extreme thermal conditions [40]. Potting is a process of coating

a PCB with an epoxy to secure PCB components and eliminate contaminants. It increases

resistance to shock and vibration, adds protection from environmental factors and

insulates electrical leads. Potting electronics is one of the most viable and cost-effective

solutions to enhance electronic package survivability [41]. However, inconsistencies in

potting such as air bubbles, soft spots, or contaminants in the epoxy lead to unsupported

structures.

When modeling a PCB using LEMP the board components are represented by a

mass supported by a system of springs which represent the potting material. The presence

of airgaps or impurities within the potting supporting the PCB is represented by the

removal of a spring in the corresponding model location. Applying LEMP in this case

would allow researchers to determine the location of gaps more easily. In the case of large structures, LEMP allows for the modeling of unsupported structures such as those subject to erosion or seismic activity. One application is modeling steel or concrete storage tanks. Storage tanks are either buried or rest on topsoil and are used to hold water, gasoline, and other chemicals. To avoid failure and leakage that could pose a threat to plant operation, human safety and the environment, the interactions between the soil, tank foundation and walls must first be considered in the design and analysis phases [42]. Past works have used power series to describe soil infiltration, collocation methods to estimate remotely sensed moisture levels, as well as FEA and energy analysis to determine structure-soil interactions [43]. However, errors arise when the structure experiences changing conditions that are not taken into account in model parameters such as soil erosion. Another application is modeling bridges or building foundations subject to seismic activity. Current modeling techniques conduct seismic analysis by representing structures resting on the ground as masses supported by springs [44]. Expanding this technique using LEMP would allow for modeling shifting ground under foundations for damage analysis.

When modeling large structures using LEMP the structure itself represented by a mass supported by a system of springs which represent the soil. The redistribution of soil beneath the structure due to erosion or seismic activity is represented by the removal of a spring in the corresponding model location. Applying LEMP in these cases would allow engineers to determine the location of foundational damage more easily.

The procedure discussed for unsupported structured is illustrated using a modified version of the DROPBEAR model discussed in Section 4.2. The initial system is modeled

70

as a cantilever beam fixed on left end with 25 nodes. At each node a spring of stiffness

1E10 N/m is inserted connecting the system to ground. The initial model used for

analysis of an unsupported structure is shown in Fig. 7.1.

$n_1 \, n_2 \, n_3 \, n_4 \quad n_5 \quad n_6 \, n_7 \, n_8 \, n_9 \, n_{10} \, n_{11} \, n_{12} n_{13} \, n_{14} \, n_{15} \, n_{16} n_{17} n_{18} n_{19} n_{20} n_{21} \, n_{22} \, n_{23} \, n_{24} n_{25} \, n_{26}$
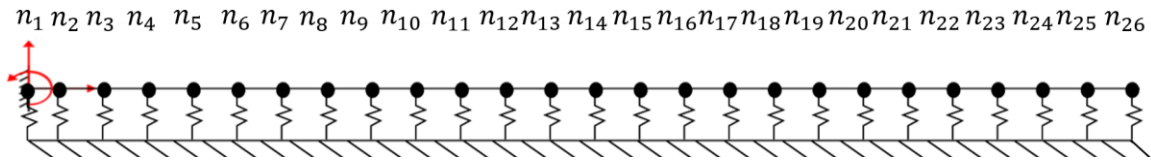
Figure 7.1   Initial model for a supported structure.

The first procedure tracked the response of the system as the stiffness value for a

single spring was varied. n_{25} was chosen as the location for spring modification because

removing the spring at the end of the beam yielded the largest frequency response change

for the system. The first four frequency responses of the system are shown in Figs. 7.2-

7.5. The figures plot the natural frequency of the system according to LEMP and GE

approaches for the spring at n_{25} with stiffness values ranging from zero to 1E10 N/m. The

plots are used to determine the frequency response of the system with and without a

spring which are summarized in Table 7.1 below.

Table 7.1   Frequency response for a system varying spring stiffness at n_{25}.

Frequency Response	Frequency with no spring at n_{25} (Hz)	Frequency with a spring of 1E9 N/m at n_{25} (Hz)	Change in Frequency
1	56.21	287.79	231.58
2	372.09	932.28	560.19
3	1073.85	1943.47	869.62
4	2149.76	3323.31	1173.55
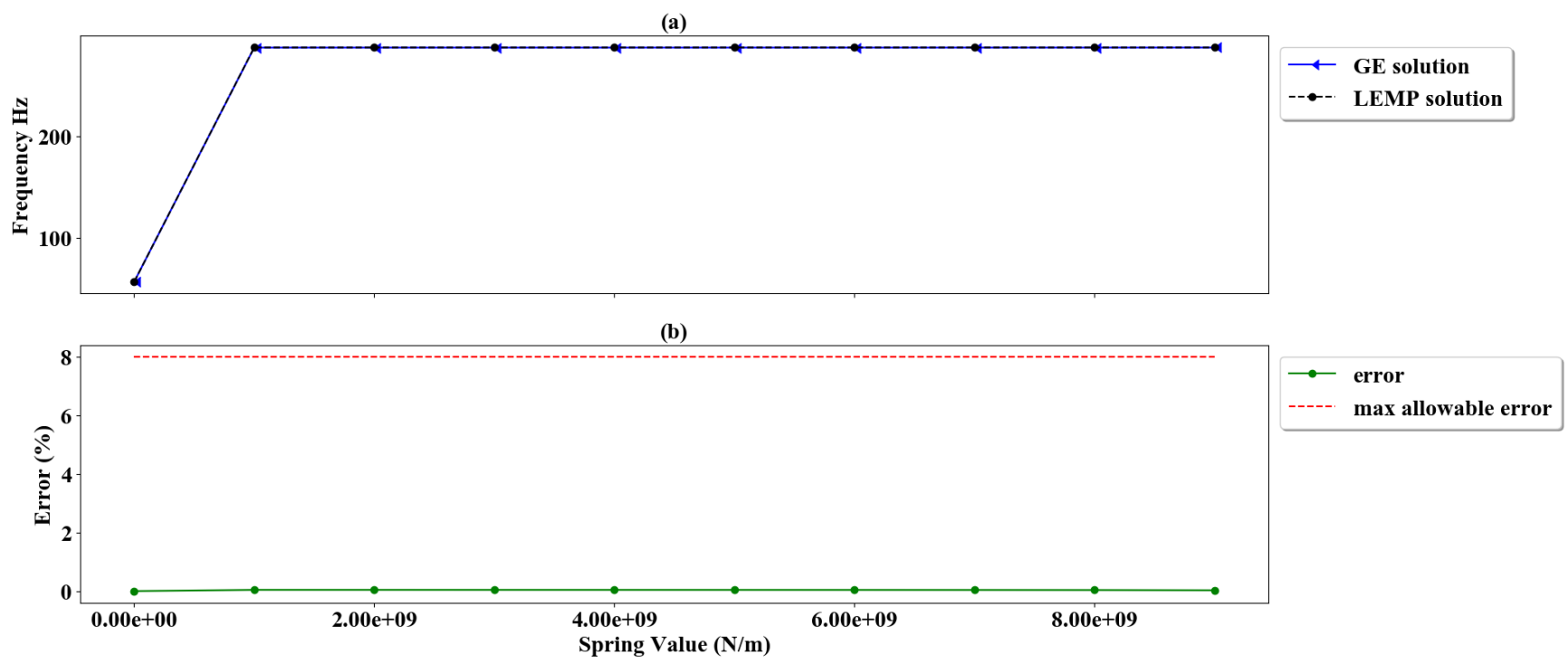
Figure 7.2   First frequency response for various spring values (a) and percent error (b).
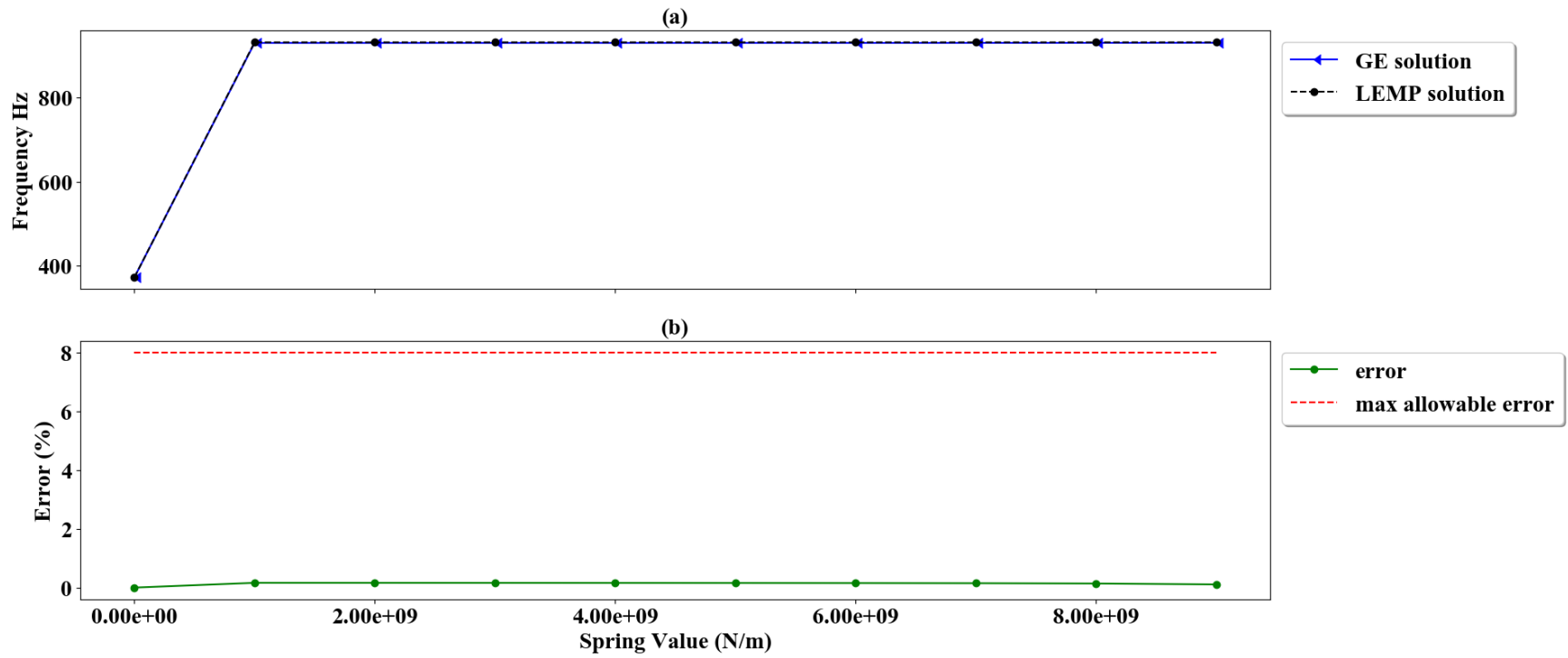
Figure 7.3   Second frequency response for various spring values (a) and percent error (b).
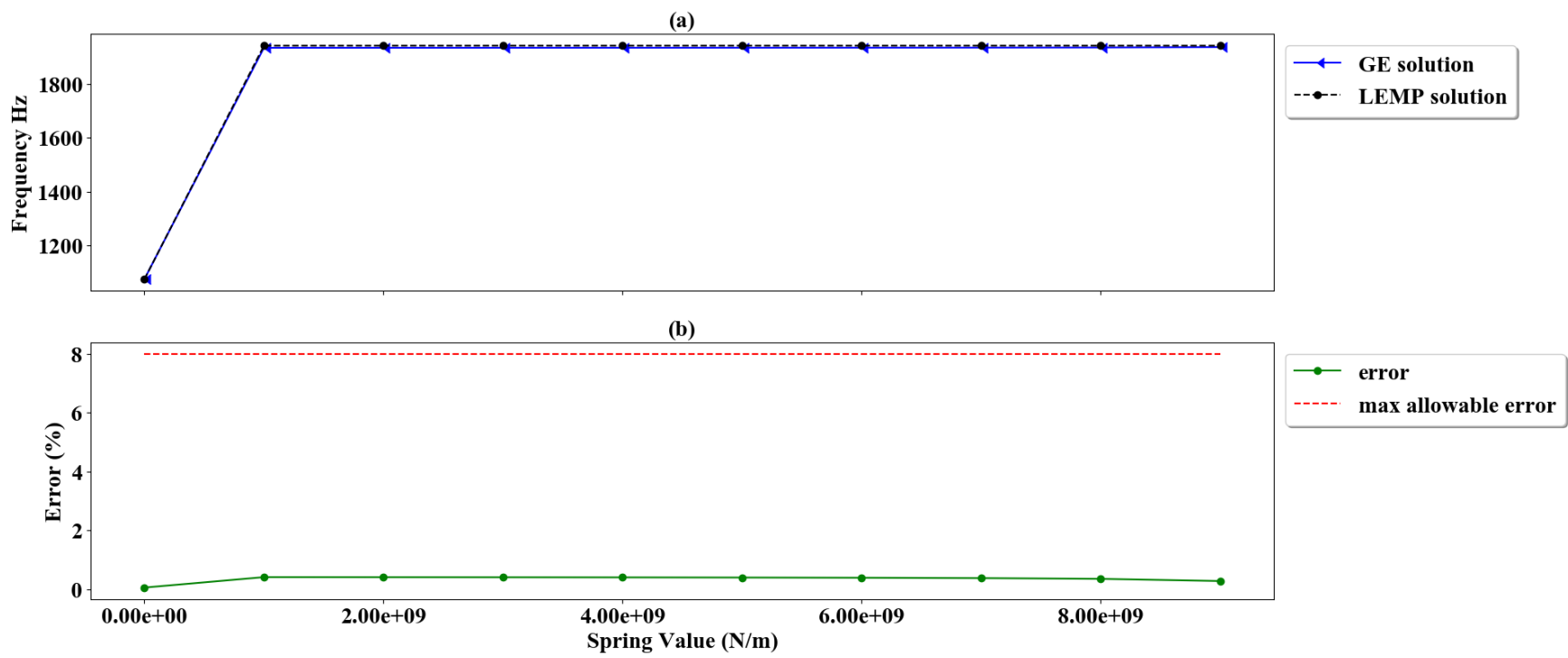
Figure 7.4   Third frequency response for various spring values (a) and percent error (b).
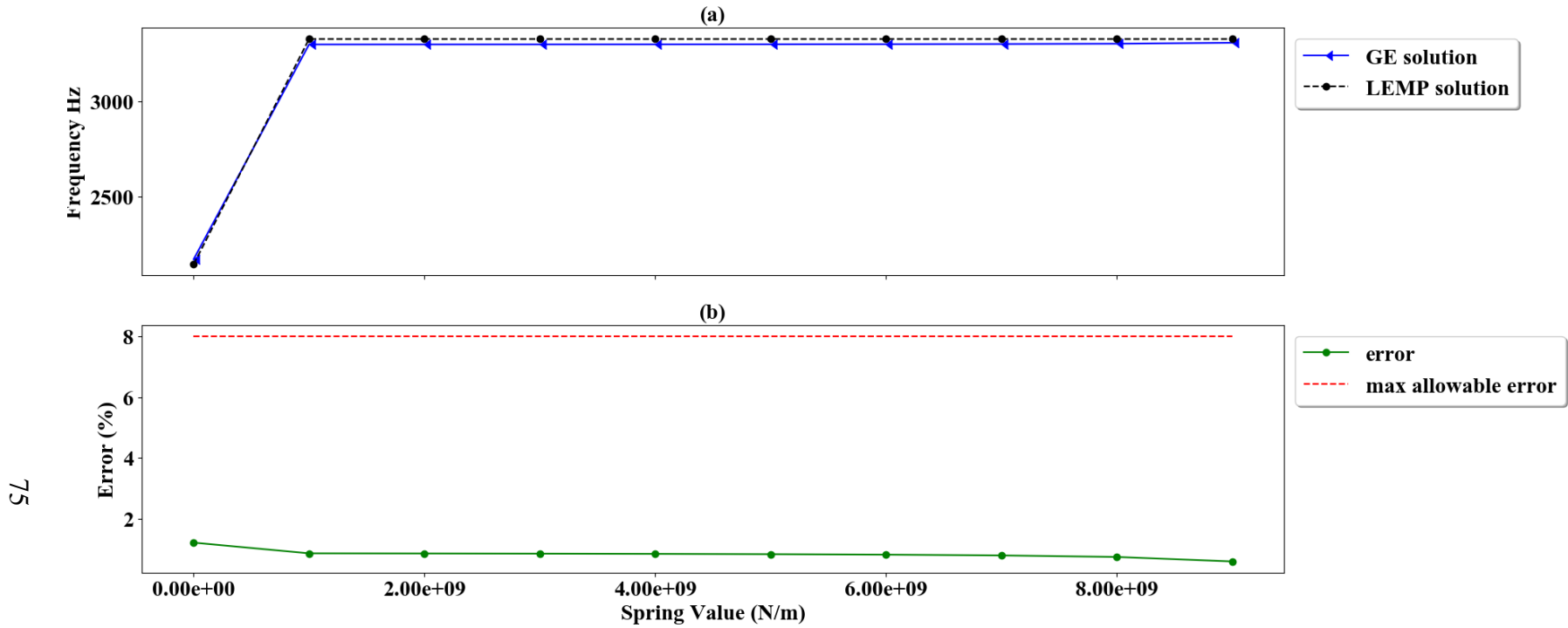
Figure 7.5   Fourth frequency response for various spring values (a) and percent error (b).

One challenge that arises when creating an analytical model of a structure is deciding the number and strength of springs to include. This is because models with more springs allow for smaller areas of damage detection, but also require that more springs be removed to achieve a change in dynamic system response. Additionally, if the spring stiffness is too small, the system will not deviate from cantilever beam behavior, but if the stiffness is too large the removal of one spring won't achieve a change in dynamic system response.

Figures 7.2-7.5 illustrate significant changes in system response between the initial system and the system with a spring stiffness reduction. This procedure effectively verifies the initial model. Based on the results from Table 7.1, using a 25-spring model with stiffness value of 1E10 N/m was sufficient for describing the system.

The second procedure tracked the response of the system as each spring support was removed, excluding n_1. The spring at the leftmost end of the beam was not removed because a fixed boundary condition already exists at that point and removing a spring at that location would not change the system response. The first four frequency responses of the system are shown in Figs. 7.6-7.9. The figures plot the natural frequency of the system according to LEMP and GE approaches for the removal of springs at different beam locations.

From the figures it is seen that the percent error between the true GE solution and the estimated LEMP solution remained below the maximum error of 8% for the first four frequency responses of the system. Therefore, it is concluded that LEMP offers an accurate estimate for the state of an unsupported structure.

76
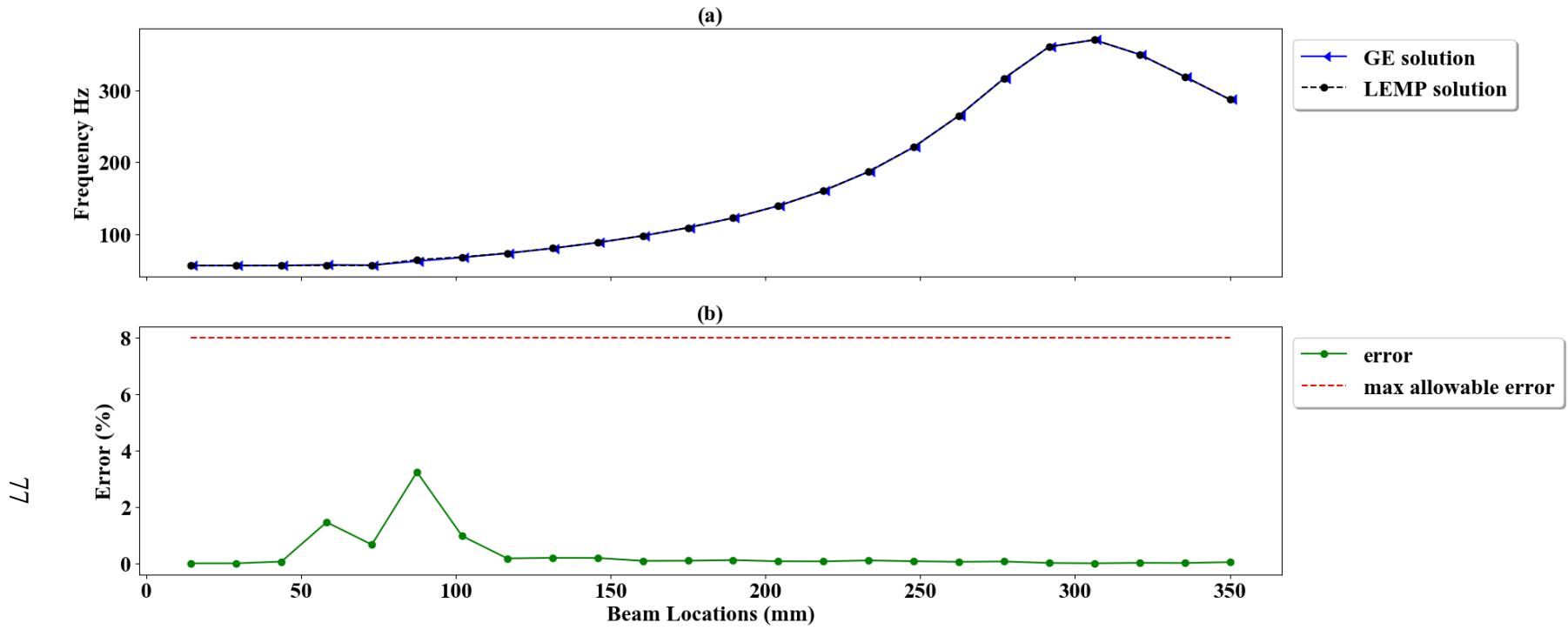
Figure 7.6   First frequency response for spring removal (a) and percent error (b).
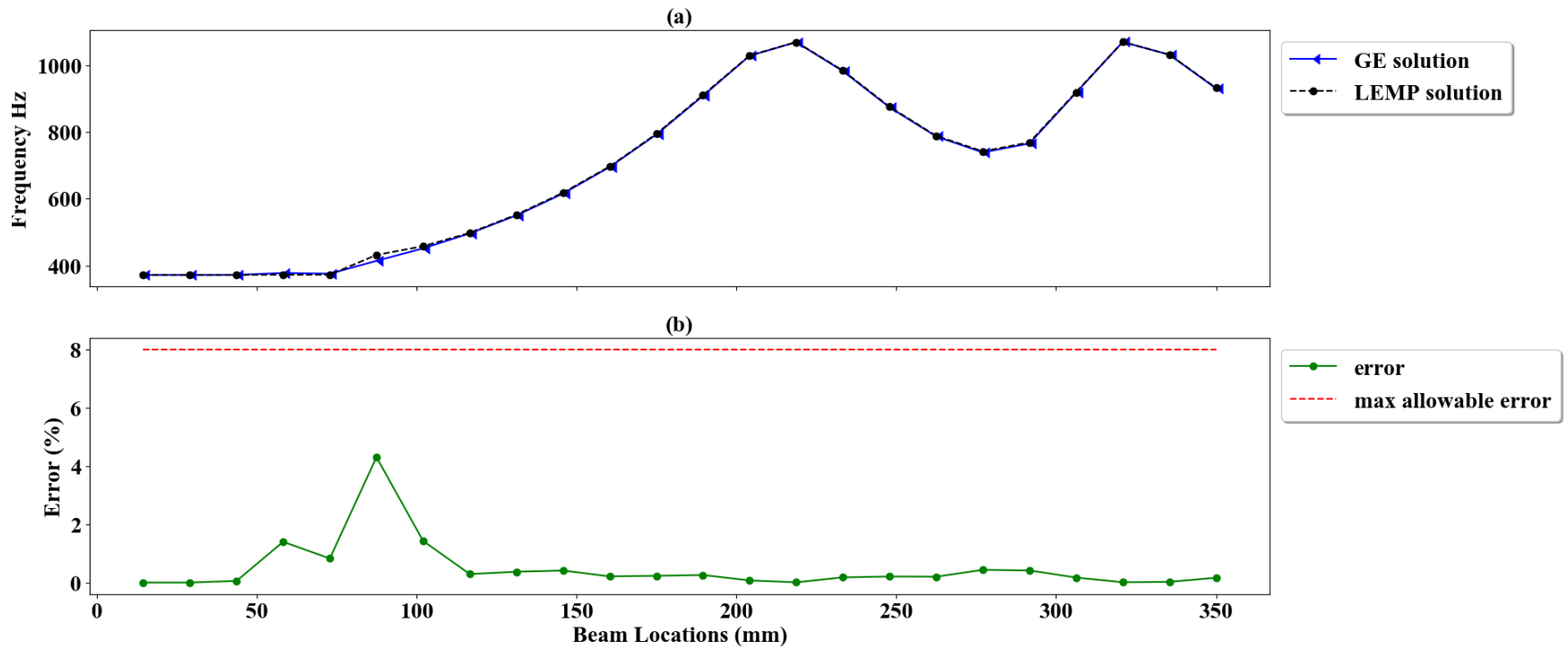
Figure 7.7   Second frequency response for spring removal (a) and percent error (b).
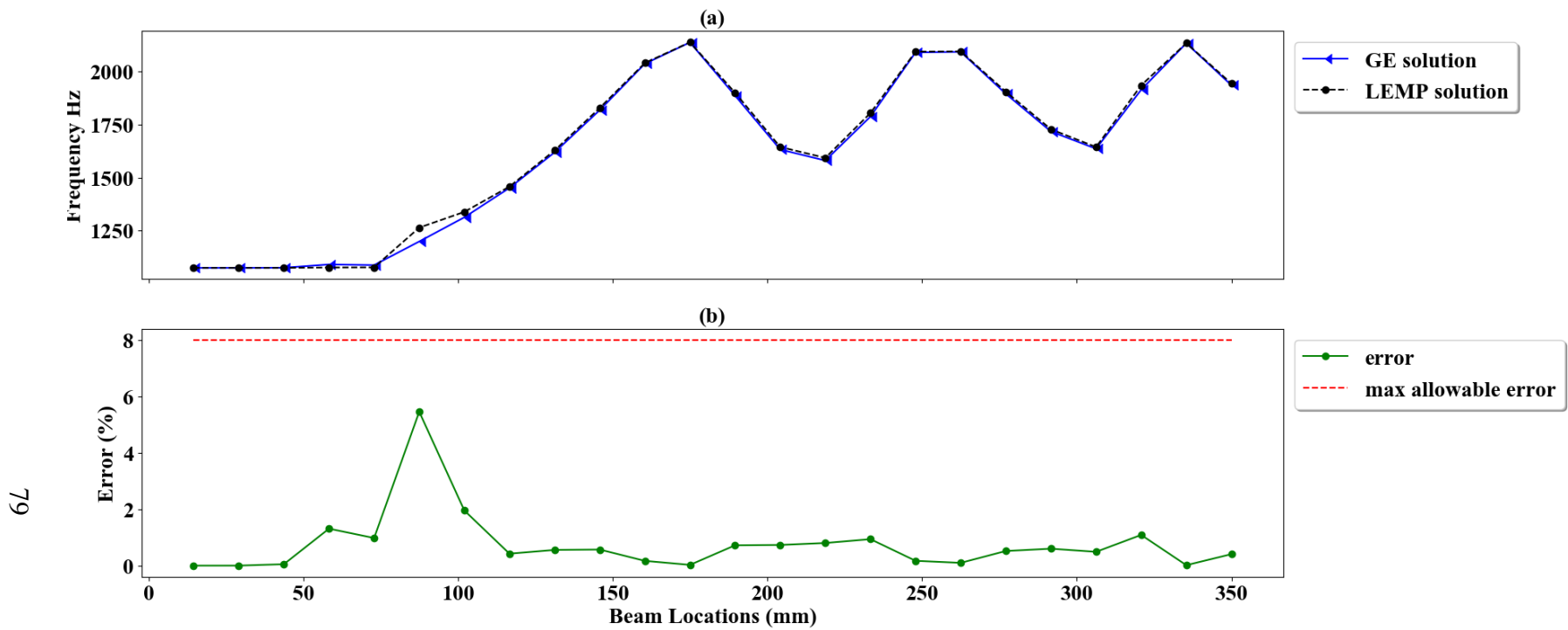
Figure 7.8   Third frequency response for spring removal (a) and percent error (b).
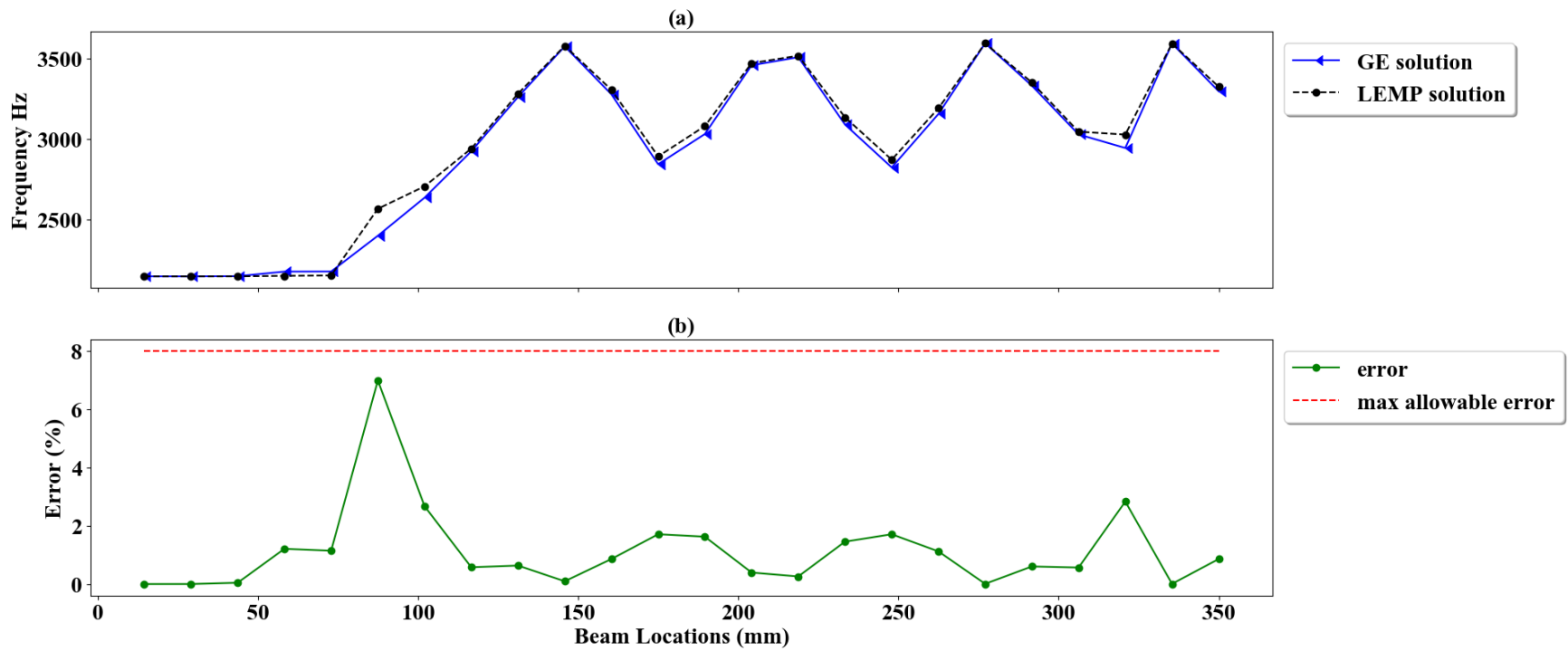
Figure 7.9   Fourth frequency response for spring removal (a) and percent error (b).

CHAPTER 8

CONCLUSION

Roller estimations were calculated by GE solutions, LEMP solutions and LEMP solutions utilizing a Bayesian search space using both error minimization and bounded regression as comparison criteria. In general, the error minimization technique resulted in sharp transient errors during roller movement and fluctuation when the roller remained stationary. The application of the bounded regression technique reduced estimation fluctuation during roller movement but not during stationary periods.

The GE and LEMP solutions offered similar accuracy, with LEMP preforming slightly better for both comparison criteria. The LEMP solutions with a Bayesian search space yielded smoother results with less fluctuation during roller movements and stationary periods which is advantageous when tracking an unchanging system as false reports of damage would be minimal.

From this work, it can be inferred that LEMP solutions with a Bayesian search space not only reduces the number and complexity of calculations required for state estimations, but also provides a better estimate for unchanging systems. Additionally, the bounded regression comparison criteria offer more consistent state estimations. It is concluded from this work that LEMP solutions with a Bayesian search space using bounded regression provides a viable method for updating models in real-time.

It was also concluded that LEMP can be applied to assess models that experience the removal of boundary conditions. Extending LEMP to model the removal of boundary conditions is beneficial for modeling unsupported structures. In small structures such as PCBs, the application of LEMP would allow for pinpointing the exact location of damage within the structure. In large structures such as bridges, buildings and storage tanks, the application of LEMP would narrow the search area for possible damage.

REFERENCES

[1] Hong J., Laflamme S., Dodson J. and Joyce B., 2018, "Introduction to State Estimation of High-Rate System Dynamics," *Sensors 18(1).*

[2] Mostert, F. J., 2018, "Challenges in Blast Protection Research," *Defense Technology,* **14**(5), pp. 426-432.

[3] Hong J., Laflamme S., Dodson J. and Joyce B., 2018, "Study of Input Space for State Estimation of High-Rate Dynamics," *Structural Control Health Monitoring, 25.*

[4] Richert, J., Coutellier, D., Götz, C. and Eberle, W., 2007, "Advanced smart airbags: The solution for real-life safety?," *International Journal of Crashworthiness,* **12**(2), pp. 159-171.

[5] Hong S. H., Drnek C., Downey A., Wang Y., Dodson J. and Hong J., 2020, "Real-Time Model Updating Algorithm for Structures Experiencing High-Rate Dynamic Events," *The ASME 2020 Conference on Smart Materials, Adaptive Structures and Intelligent Systems*, SMASIS Paper No. 2439

[6] He, J., 2001, "Structural modification," *Philosophical Transactions of the Royal Society A: Mathematical, Physical and Engineering Sciences,* **359**(1778), pp. 187-204.

[7] Sestieri, A., 2000, "Structural dynamic modification," *Sadhana,* **25**(3), pp. 247-259.

[8] Hurty, W. C., 1956, "Dynamic Analysis of Structural Systems Using Component Modes," *AIAA Journal,* **3**(4), pp. 678-685.

[9] Craig, R. J., 1987, "A Review of Time-Domain and Frequency-Domain Component Mode Synthesis Methods," *International Journal of Analytical and Experimental Modal Analysis*, **2**(2), pp. 59-72.
[10] Bilbao, S., 2009, *Numerical Sound Synthesis,* John Wiley & Sons, Ltd, West Sussex, pp. 152, Chap. 6

[11] Bilbao, S., Desvages, C., Ducceschi, M., Hamilton, B., Harrison-Harsley, R., Torin, A. and Webb, C., 2019, "Physical Modeling, Algorithms, and Sound Synthesis: The NESS Project," *Computer Music Journal,* **43**(2-3), pp. 15-30.

[12] Formenti, D. and Richardson, M., 2020, "Modal Modeling and Structural Dynamics Modification," Vibrant Technical Paper No. 71.

[13] Avitabile, P., 2003, "Twenty Years of Structural Dynamic Modification- A Review," *Sound and Vibration,* pp. 14-25.

[14] Nack, W. V., 1981, "Efficient reanalysis for structural dynamic response," *Computers & Structures,* **14**(1-2), pp. 153-155

[15] Weissenburger, J. T., 1968, "Effect of Local Modifications on the Vibration Characteristics of Linear Systems," *Journal of Applied Mechanics,* **35**(2), pp. 327.

[16] Pomazal, R. J. and Snyder, V. W., 1971, "Local Modifications of Damped Linear Systems," *AIAA Journal,* **9**(11), pp. 2216-2221.

[17] Hallquist, J., Snyder, V. 1973, "Synthesis of Two Discrete Vibratory Systems Using Eigenvalue Modification," *AIAA Journal,* **11**(2), pp. 247-249.

[18] Ozguven, H. N., 1990, "Structural Modifications Using Frequency Response Functions," *Mechanical Systems and Signal Processing,* **4**(1), pp. 53-63.

[19] Sabato, A., Poozesh, P., Avitabile, P. and Niezrecki, C., 2018, "Experimental modal analysis of a utility-scale wind turbine blade using a multi-camera approach," *Journal of Physics: Conference Series,* **1149**

[20] Pan, W., Mao, S., Haug, E. J. and Solis, D., 2003, "Efficient Modal Approach for Flexible Multibody Dynamic Simulation," *Mechanics Based Design of Structures and Machines,* **31**(1), pp. 1-23.

[21] Jesus, A., Brommer, P., Westgate, R., Koo, K., Brownjohn, J. and Laory, I., 2019, "Modular Bayesian damage detection for complex civil infrastructure," *Journal of Civil Structural Health Monitoring* **9**, pp. 201-215.

[22] Huang, Y., Shao, C. and Wu, B., 2018, "State-of-the-art review on Bayesian inference in structural system identification and damage assessment," *SAGE Jounrals,* **22**(6), pp. 1329-1351.

[23] Li, M. and Meeker, W., 2013, "Application of Bayesian Methods in Reliability Data Analyses," *Statistics Preprints,* **84**.

[24] Kurata, M., Kim, J., Lynch, J. P., Law, K. H. and Salvino, L. W., 2010, "A Probabilistic Model Updating Algorithm for Fatigue Damage Detection in Aluminum Hull Structures," *Proceedings of the ASME 2010 Conference on Smart Materials, Adaptive Structures and Intelligent Systems.*

[25] Hamada, M., 2005, "Using Degradation Data to Assess Reliability," *Quality Engineering,* **17**(4), pp.615-620.

[26] Behmanesh, I. and Moaveni, B., 2014, "Probabilistic identification of simulated damage on the Dowling Hall footbridge through Bayesian finite element model updating," *Structural Control and Health Monitoring,* **22**(3), pp. 463-483.

[27] Lam, H. F., Hu, Q. and Wong, M. T., 2014, "The Bayesian methodology for the detection of railway ballast damage under a concrete sleeper," *Engineering Structures,* **81**, pp. 289-301.

[28] Ramin, M. and Caicedo, J. M., 2015, "Reducing MCMC Computational Cost with a Two Layered Bayesian Approach," *Model Validation and Uncertainty Quantification,* **3**, pp. 291-297.

[29] Papadimitriou, C. and Ntotsios, E., 2009, "Bayesian Methodology for Structural Damage Identification and Reliability Assessment," *2009 International Operational Modal Analysis Conference.*

[30] Caicedo, J., Zarate, B., Giurgiotio, V., Yu, L. and Ziehl, P., 2011, "Bayesian Finite Element Model Updating for Crack Growth," *Structural Dynamics,* **3**, pp. 861-866.

[31] Joyce B., Dodson J., Laflamme S. and Hong, J., 2018, "An Experimental Test Bed for Developing High-Rate Structural Health Monitoring Methods" *Hindawi: Shock and Vibration.*

[32] Downey A., Hong J., Dodson J., Carroll M. and Scheppegrell J., 2020, "Millisecond Model Updating for Structures Experiencing Unmodeled High-Rate Dynamic Events" *Mechanical Systems and Signal Processing 138.*

[33] Carroll, M., Downey, A., Dodson, J., Hong, J. and Scheppegrell, J., "Analysis of Computation Speeds of Eigenvalue Solutions for High-Rate Structural Health Monitoring."

[34] Inman, D. J., 2007, *Engineering Vibration*, Pearson Education, Inc., Upper Saddle River, NJ.

[35] Avitabile, P., 2000, "Modal Space: Back to Basics," *Experimental Techniques,* **24**(5), pp. 15–18.

[36] PCB Model 393B04, n.d., from https://www.pcb.com/products?model=393b04.

[37] Hastie, T., Tibshirani, R. and Friedman, J., 2001, *The Elements of Statistical Learning*, Springer, New York, NY.

[38] Van Zandt, T., 2006, "Development of efficient reduced models for multi-body dynamics simulations of helicopter wing missile configurations," M.S. thesis, Department of Mechanical Engineering, University of Massachusetts Lowell.

[39] Avitabile, P., and Pingle P., 2012, "Prediction of Full Field Dynamic Strain from Limited Sets of Measured Data," *Shock and Vibration,* **19**, pp. 765-785.

[40] Lall, P., Dornala, K., Lowe, R., and Foley, J., 2016, "Survivability Assessment of Electronics Subjected to Mechanical Shock Up to 25,000g," *IEEE ITHERM Conference*, pp. 507-518.

[41] Lall, P., Dornala, K., Suhling, J., Deep, J., and Lowe, R., 2019, "Fatigue Delamination Crack Growth of Potting Compounds in PCB/ Epoxy Interfaces Under Flexure Loading," *ASME InterPACK Conference,* pp. 1-6.

[41] Kukreti, A. and Siddiqi, Z., 1997, "Analysis of fluid storage tanks including foundation-superstructure interaction using differential quadrature method," *Applied Mathematical Modeling,* **21**, pp. 193-205.

[42] Selvadurai, A. P. S., 1979, Elastic Analysis of Soil-Foundation Interaction, Elsevier Scientific Publishing Company, NY.

[43] Cofer, W. F., McGuire, J. W. and McLean, D. I., 1994, "Analytical Modeling of Foundations for Seismic Analysis of Bridges," WA-RD 328.1, Washington State University, Pullman, WA.

APPENDIX A

LEMP IMPLEMENTATION USING EXPERIMENTAL VALUES

The example discussed here assumes a beam with similar properties as the one used in the body of this work; therefore, material properties are the same as those shown in Table 3.1. The model contains eight nodes, which corresponds to 16 DOF for a Euler-Bernoulli beam ($n = 16$). Additionally, only the first five modes are utilized for tracking the state of the system ($m = 5$). The initial model is shown below.

Figure A.1   Model used in LEMP example.

The elemental mass and stiffness matrices are calculated using the beam properties according to Eqs. (34) and (35) and combined to define the global mass matrix and global stiffness matrix as Eq. (A1) and Eq. (A2) respectively. The global mass and stiffness matrix are then used in the initial EOM represented by Eq (1), for which the GE problem is defined as $K_1 U_1 = M_1 U_1 \lambda$. Here, λ are the eigenvalues and U_1 are the eigenvectors. The GE solution is solved using Eqs. (2) and (3), which yields the squares of the first n natural frequencies and the first n modal vectors for the initial system. In this case $n=16$, so the squares of the first 16 natural frequencies are given along the diagonal in Eq. (A3).

$$\mathbf{M_1} =$$

$$
\begin{pmatrix}
0.0476651 & 0.000338501 & 0.0164995 & -0.000200023 & 0 & 0 & 0 & 0 & 0 & 0 & 0 & 0 & 0 & 0 & 0 & 0 \\
 & 0.00000309926 & 0.000200023 & -0.00000232445 & 0 & 0 & 0 & 0 & 0 & 0 & 0 & 0 & 0 & 0 & 0 & 0 \\
 & & 0.0953303 & 0 & 0.0164995 & -0.000200023 & 0 & 0 & 0 & 0 & 0 & 0 & 0 & 0 & 0 & 0 \\
 & & & 0.00000619853 & 0.000200023 & -0.00000232445 & 0 & 0 & 0 & 0 & 0 & 0 & 0 & 0 & 0 & 0 \\
 & & & & 0.0953303 & 0 & 0.0164995 & -0.000200023 & 0 & 0 & 0 & 0 & 0 & 0 & 0 & 0 \\
 & & & & & 0.00000619853 & 0.000200023 & -0.00000232445 & 0 & 0 & 0 & 0 & 0 & 0 & 0 & 0 \\
 & & & & & & 0.0953303 & 0 & 0.0164995 & -0.000200023 & 0 & 0 & 0 & 0 & 0 & 0 \\
 & & & & & & & 0.00000619853 & 0.000200023 & -0.00000232445 & 0 & 0 & 0 & 0 & 0 & 0 \\
 & & & & & & & & 0.0953303 & 0.00000619853 & 0.0164995 & -0.000200023 & 0 & 0 & 0 & 0 \\
 & & & & & & & & & 0.000200023 & 0.000200023 & -0.00000232445 & 0 & 0 & 0 & 0 \\
 & & & & & & & & & & 0.0953303 & 0 & 0.0164995 & -0.000200023 & 0 & 0 \\
 & & & & & & & & & & & 0.00000619853 & 0.000200023 & -0.00000232445 & 0 & 0 \\
 & & & & & & & & & & & & 0.12133 & 0.000184643 & 0.0254995 & -0.000309131 \\
 & & & & & & & & & & & & & 0.00000788909 & 0.000309131 & -0.00000359237 \\
 & & & & & & & & & & & & & & 0.0736651 & -0.000523144 \\
 & & & & & & & & & & & & & & & 0.00000478982
\end{pmatrix}
$$

(A1)

$$\mathbf{K_1} =$$

$$
\begin{pmatrix}
10000000000 & 537300 & -21339600 & 537300 & 0 & 0 & 0 & 0 & 0 & 0 & 0 & 0 & 0 & 0 & 0 & 0 \\
 & 10000000000 & -537300 & 9018.96 & 0 & 0 & 0 & 0 & 0 & 0 & 0 & 0 & 0 & 0 & 0 & 0 \\
 & & 42679100 & 0 & -21339600 & 537300 & 0 & 0 & 0 & 0 & 0 & 0 & 0 & 0 & 0 & 0 \\
 & & & 36075.9 & -537300 & 9018.96 & 0 & 0 & 0 & 0 & 0 & 0 & 0 & 0 & 0 & 0 \\
 & & & & 42679100 & 0 & -21339600 & 537300 & 0 & 0 & 0 & 0 & 0 & 0 & 0 & 0 \\
 & & & & & 36075.9 & -537300 & 9018.96 & 0 & 0 & 0 & 0 & 0 & 0 & 0 & 0 \\
 & & & & & & 42679100 & 0 & -21339600 & 537300 & 0 & 0 & 0 & 0 & 0 & 0 \\
 & & & & & & & 36075.9 & -537300 & 9018.96 & 0 & 0 & 0 & 0 & 0 & 0 \\
 & & & & & & & & 42679100 & 0 & -21339600 & 537300 & 0 & 0 & 0 & 0 \\
 & & & & & & & & & 36075.9 & -537300 & 9018.96 & 0 & 0 & 0 & 0 \\
 & & & & & & & & & & 42679100 & 0 & -21339600 & 537300 & 0 & 0 \\
 & & & & & & & & & & & 36075.9 & -537300 & 9018.96 & 0 & 0 \\
 & & & & & & & & & & & & 42679100 & 0 & -21339600 & 537300 \\
 & & & & & & & & & & & & & 36075.9 & -537300 & 9018.96 \\
 & & & & & & & & & & & & & & 21339600 & -537300 \\
 & & & & & & & & & & & & & & & 18037.9
\end{pmatrix}
$$

(A2)

$\boldsymbol{\lambda} =$

$$
\begin{pmatrix}
56841.4 & 0 & 0 & 0 & 0 & 0 & 0 & 0 & 0 & 0 & 0 & 0 & 0 & 0 & 0 & 0 \\
 & 2502950 & 0 & 0 & 0 & 0 & 0 & 0 & 0 & 0 & 0 & 0 & 0 & 0 & 0 & 0 \\
 & & 20521600 & 0 & 0 & 0 & 0 & 0 & 0 & 0 & 0 & 0 & 0 & 0 & 0 & 0 \\
 & & & 79947500 & 0 & 0 & 0 & 0 & 0 & 0 & 0 & 0 & 0 & 0 & 0 & 0 \\
 & & & & 2.18947E8 & 0 & 0 & 0 & 0 & 0 & 0 & 0 & 0 & 0 & 0 & 0 \\
 & & & & & 4.92401E8 & 0 & 0 & 0 & 0 & 0 & 0 & 0 & 0 & 0 & 0 \\
 & & & & & & 9.71232E8 & 0 & 0 & 0 & 0 & 0 & 0 & 0 & 0 & 0 \\
 & & & & & & & 2.07264E9 & 0 & 0 & 0 & 0 & 0 & 0 & 0 & 0 \\
 & & & & & & & & 3.57992E9 & 0 & 0 & 0 & 0 & 0 & 0 & 0 \\
 & & & & & & & & & 6.19089E9 & 0 & 0 & 0 & 0 & 0 & 0 \\
 & & & & & & & & & & 1.05039E10 & 0 & 0 & 0 & 0 & 0 \\
 & & & & & & & & & & & 1.73962E10 & 0 & 0 & 0 & 0 \\
 & & & & & & & & & & & & 2.70764E10 & 0 & 0 & 0 \\
 & & & & & & & & & & & & & 3.75065E10 & 0 & 0 \\
 & & & & & & & & & & & & & & 2.6818E11 & 0 \\
 & & & & & & & & & & & & & & & 2.35413E16
\end{pmatrix}
$$

(A3)

68

As noted in section 3.2, simplification of state equations occurs by reducing the initial state to only include the modes of interest. As a result, λ is reduced to a matrix of size (m x m) and U_1 is reduced to a matrix of (n x m). In the case of this example n=16 and m=5. Therefore, the eigenvalue matrix is reduced to a (5x5) matrix and a modal matrix is reduced to a matrix with dimensions (16x5). The reduced matrices are shown in Eq. (A4) and (A5).

To find the natural frequency in rad/s, the square root of each eigenvalue is taken and to convert to Hz, Eq. (A6) is applied. The first five natural frequencies for the initial system in Hz are summarized in Eq. (A7).

$$\lambda = \begin{pmatrix} 56841.4 & 0 & 0 & 0 & 0 \\ & 2502950 & 0 & 0 & 0 \\ & & 20521600 & 0 & 0 \\ & & & 79947500 & 0 \\ & & & & 218947000 \end{pmatrix} \tag{A4}$$

$$U_1 = \begin{pmatrix} 0.00000444313 & 0.000105744 & -0.000504132 & -0.0013903 & -0.00294468 \\ 0.00000118569 & 0.00000802108 & -0.0000229865 & -0.0000451469 & -0.0000746068 \\ 0.0620527 & 0.349269 & -0.816928 & -1.25315 & -1.54163 \\ 2.38187 & 11.9194 & -23.3996 & -26.2011 & -15.5753 \\ 0.231619 & 1.01204 & -1.59513 & -1.1493 & 0.0438785 \\ 4.27116 & 12.6763 & -2.44326 & 32.2782 & 59.6107 \\ 0.484142 & 1.47835 & -0.91485 & 0.968009 & 1.34074 \\ 5.67982 & 4.71355 & 27.2397 & 34.944 & -25.848 \\ 0.796067 & 1.41495 & 0.651034 & 1.15596 & -1.14801 \\ 6.63702 & -7.50038 & 28.5669 & -28.7843 & -38.1148 \\ 1.14587 & 0.739498 & 1.39865 & -0.876493 & -0.452089 \\ 7.19489 & -18.7738 & -2.35769 & -34.5521 & 55.3922 \\ 1.5153 & -0.393289 & 0.382619 & -0.979679 & 1.2892 \\ 7.43253 & -25.2407 & -35.2469 & 33.9712 & -15.0867 \\ 1.891 & -1.71165 & -1.71428 & 1.79216 & -1.85613 \\ 7.47023 & -26.5139 & -44.0478 & 63.5753 & -83.3884 \end{pmatrix} \tag{A5}$$

$$f_n = \frac{1}{2\pi}\omega_n \tag{A6}$$

$$\vec{f_1} = (37.9448 \quad 251.794 \quad 720.984 \quad 1423.06 \quad 2354.99) \tag{A7}$$

The altered case for this example is defined as the addition of a roller at node 4 which can be modeled as the addition of a spring with an equivalent stiffness of 1e10 N/m.

Based on the definition of a Euler-Bernoulli beam, the addition of a roller at node 4 corresponds to applying a boundary condition at DOF 8. The EOM for the altered state in physical space was given by Eq. (14).

As discussed in Section 3.2, ΔK_{12} represents the changes made in the physical space from the initial state to the altered state where diagonal values represent spring stiffness change from each elemental mass to ground and off-diagonal values couple elemental masses together. Because this example sets the roller at DOF 8, the only non-zero term in the ΔK_{12} matrix is the 8th diagonal value. This term will have a value equal to the equivalent spring stiffness used to model the roller i.e. 1e10 N/m as shown in Eq. (A8). The simplified EOM in modal space is given by Eq. (16) where $\overline{\Delta K_{12}}$ is obtained by pre-multiplying the $\Delta K_{12} U_1$ term by U_1^{T} and is given by Eq. (A9). Here, $\overline{\Delta K_{12}}$ represents the changes made in modal space from the initial to altered state.

The next step is to spectrally decompose the ΔK_{12} matrix according to Eq. (20). For this example, the spectral decomposition yields a simple tie and alpha matrix; however, for more complex changes between system states, the matrices will also be more complex. The tie and alpha matrices for this example can be seen in Eq. (A10) and (A11) respectively. The stiffness change matrix is then transformed into modal space and simplified with the contributing DOF using Eq. (24).

Recall from Eq. (22) that $\vec{v} = U_c^{\mathrm{T}} \vec{t}$. Noting that only DOF 8 is affected by the addition of a spring at the 4th node, the contributing vectors are reduced to only those values in the 8th row of each matrix. Therefore, the contributing modal and tie vectors can be written according to Eqs. (A12) and (A13) respectively which results in a change vector $\vec{v}$ as shown in Eq. (A14). Rearranging the terms in the eigen solution problem for

the altered state yields Eq. (33), which represents five second degree equations bounded

by the initial frequencies of the system. Solving for Ω^2 yields the squares of the updated

natural frequencies shown in Eq. (A15). The conversion in Eq. (A6) is then applied to

find the updated natural frequencies in Hz as shown in Eq. (A16).

The model used in this example consisted of eight nodes and five modes.

Applying LEMP to this example reduced the original 16th order GE problem to a set of 5

second order equations that can be solved using Eq. (33), thereby simplifying the

complexity of the associated state equation. All equations referenced in this appendix

were originally presented in Section 3.2. The purpose of this appendix is to provide a

detailed example with experimental values to illustrate the steps in LEMP. Providing an

example allows readers to fully understand the algorithm presented in the body of this

work.

$$
\Delta K_{12} = \begin{pmatrix}
0 & 0 & 0 & 0 & 0 & 0 & 0 & 0 & 0 & 0 & 0 & 0 & 0 & 0 & 0 & 0 \\
 & 0 & 0 & 0 & 0 & 0 & 0 & 0 & 0 & 0 & 0 & 0 & 0 & 0 & 0 & 0 \\
 & & 0 & 0 & 0 & 0 & 0 & 0 & 0 & 0 & 0 & 0 & 0 & 0 & 0 & 0 \\
 & & & 0 & 0 & 0 & 0 & 0 & 0 & 0 & 0 & 0 & 0 & 0 & 0 & 0 \\
 & & & & 0 & 0 & 0 & 0 & 0 & 0 & 0 & 0 & 0 & 0 & 0 & 0 \\
 & & & & & 0 & 0 & 0 & 0 & 0 & 0 & 0 & 0 & 0 & 0 & 0 \\
 & & & & & & 0 & 0 & 0 & 0 & 0 & 0 & 0 & 0 & 0 & 0 \\
 & & & & & & & 1e10 & 0 & 0 & 0 & 0 & 0 & 0 & 0 & 0 \\
 & & & & & & & & 0 & 0 & 0 & 0 & 0 & 0 & 0 & 0 \\
 & & & & & & & & & 0 & 0 & 0 & 0 & 0 & 0 & 0 \\
 & & & & & & & & & & 0 & 0 & 0 & 0 & 0 & 0 \\
 & & & & & & & & & & & 0 & 0 & 0 & 0 & 0 \\
 & & & & & & & & & & & & 0 & 0 & 0 & 0 \\
 & & & & & & & & & & & & & 0 & 0 & 0 \\
 & & & & & & & & & & & & & & 0 & 0 \\
 & & & & & & & & & & & & & & & 0
\end{pmatrix} \tag{A8}
$$

$$\overline{\Delta K_{12}} =$$

$$
\begin{pmatrix}
6337230000 & 11263900000 & 0.01649955182670000 & 9202200000 & -9138930000 & 6196220000 & 011953600000 & -1427190000 & -11439700000 & -2790240000 & 9999260000 & 5596650000 & 4352020000 & 2356790000 & 199783000 & 241627000 \\
11263900000 & 20020700000 & 9211780000 & 16356200000 & -16243700000 & 11013300000 & 021246500000 & -2536720000 & -20333100000 & -4959420000 & 17772900000 & 9947600000 & 7735370000 & 4189010000 & 355099000 & 429473000 \\
5182670000 & 9211780000 & 4238460000 & 7525680000 & -7473940000 & 5067360000 & 9775800000 & -1167170000 & -9355520000 & -2281890000 & 8177530000 & 4577020000 & 3559140000 & 1927420000 & 163385000 & 197606000 \\
9202200000 & 16356200000 & 7525680000 & 13362400000 & -13270500000 & 8997450000 & 17357600000 & -2072400000 & -16611400000 & -4051660000 & 14519800000 & 8126820000 & 6319510000 & 3422260000 & 290102000 & 350863000 \\
-9138930000 & -16243700000 & -7473940000 & -13270500000 & 13179300000 & -8935590000 & -17238300000 & 2058150000 & 16497200000 & 4023810000 & -14420000000 & -8070940000 & -6276060000 & -3398730000 & -288108000 & -348451000 \\
6196220000 & 11013300000 & 5067360000 & 8997450000 & -8935590000 & 60583600003 & 11687600000 & -1395430000 & -11185100000 & -2728150000 & 9776780000 & 5472130000 & 4255190000 & 2304350000 & 195338000 & 236251000 \\
11953600000 & 21246500000 & 9775800000 & 17357600000 & -17238300000 & 11687600000 & 22547400000 & -2692030000 & -21578100000 & -5263080000 & 18861100000 & 10556700000 & 8208990000 & 4445490000 & 376841000 & 455769000 \\
-1427190000 & -2536720000 & -1167170000 & -2072400000 & 2058150000 & -1395430000 & -2692030000 & 321413000 & 2576300000 & 628382000 & -2251900000 & -1260410000 & -980106000 & -530766000 & -44992600 & -54416200 \\
-11439700000 & -20333100000 & -9355520000 & -16611400000 & 16497200000 & -11185100000 & -21578100000 & 2576300000 & 20650400000 & 5036810000 & -18050200000 & -10102800000 & -7856060000 & -4254370000 & -360639000 & -436174000 \\
-2790240000 & -4959420000 & -2281890000 & -4051660000 & 4023810000 & -2728150000 & -5263080000 & 628382000 & 5036810000 & 1228520000 & -4402600000 & -2464170000 & -1916160000 & -1037680000 & -87963100 & -106387000 \\
9999260000 & 17772900000 & 8177530000 & 14519800000 & -14420000000 & 9776780000 & 18861100000 & -2251900000 & -18050200000 & -4402600000 & 15777400000 & 8830730000 & 6866880000 & 3718690000 & 315230000 & 381254000 \\
5596650000 & 9947600000 & 4577020000 & 8126820000 & -8070940000 & 5472130000 & 10556700000 & -1260410000 & -10102800000 & -2464170000 & 8830730000 & 4942620000 & 3843440000 & 2081370000 & 176436000 & 213390000 \\
4352020000 & 7735370000 & 3559140000 & 6319510000 & -6276060000 & 4255190000 & 8208990000 & -980106000 & -7856060000 & -1916160000 & 6866880000 & 3843440000 & 2988700000 & 1618500000 & 137199000 & 165935000 \\
2356790000 & 4189010000 & 1927420000 & 3422260000 & -3398730000 & 2304350000 & 4445490000 & -530766000 & -4254370000 & -1037680000 & 3718690000 & 2081370000 & 1618500000 & 876481000 & 74298600 & 89860200 \\
199783000 & 355099000 & 163385000 & 290102000 & -288108000 & 195338000 & 376841000 & -44992600 & -360639000 & -87963100 & 315230000 & 176436000 & 137199000 & 74298600 & 6298230 & 7617370 \\
241627000 & 429473000 & 197606000 & 350863000 & -348451000 & 236251000 & 455769000 & -54416200 & -436174000 & -106387000 & 381254000 & 213390000 & 165935000 & 89860200 & 7617370 & 9212810
\end{pmatrix}
$$

(A9)

$$
T =
\begin{pmatrix}
1 & 0 & 0 & 0 & 0 & 0 & 0 & 0 & 0 & 0 & 0 & 0 & 0 & 0 & 0 & 0 \\
 & 1 & 0 & 0 & 0 & 0 & 0 & 0 & 0 & 0 & 0 & 0 & 0 & 0 & 0 & 0 \\
 & & 1 & 0 & 0 & 0 & 0 & 0 & 0 & 0 & 0 & 0 & 0 & 0 & 0 & 0 \\
 & & & 1 & 0 & 0 & 0 & 0 & 0 & 0 & 0 & 0 & 0 & 0 & 0 & 0 \\
 & & & & 1 & 0 & 0 & 0 & 0 & 0 & 0 & 0 & 0 & 0 & 0 & 0 \\
 & & & & & 1 & 0 & 0 & 0 & 0 & 0 & 0 & 0 & 0 & 0 & 0 \\
 & & & & & & 1 & 0 & 0 & 0 & 0 & 0 & 0 & 0 & 0 & 0 \\
 & & & & & & & 1 & 0 & 0 & 0 & 0 & 0 & 0 & 0 & 0 \\
 & & & & & & & & 1 & 0 & 0 & 0 & 0 & 0 & 0 & 0 \\
 & & & & & & & & & 1 & 0 & 0 & 0 & 0 & 0 & 0 \\
 & & & & & & & & & & 1 & 0 & 0 & 0 & 0 & 0 \\
 & & & & & & & & & & & 1 & 0 & 0 & 0 & 0 \\
 & & & & & & & & & & & & 1 & 0 & 0 & 0 \\
 & & & & & & & & & & & & & 1 & 0 & 0 \\
 & & & & & & & & & & & & & & 1 & 0 \\
 & & & & & & & & & & & & & & & 1
\end{pmatrix}
$$

(A10)

$$
\alpha =
\begin{pmatrix}
0 & 0 & 0 & 0 & 0 & 0 & 0 & 0 & 0 & 0 & 0 & 0 & 0 & 0 & 0 & 0 \\
0 & 0 & 0 & 0 & 0 & 0 & 0 & 0 & 0 & 0 & 0 & 0 & 0 & 0 & 0 & 0 \\
0 & 0 & 0 & 0 & 0 & 0 & 0 & 0 & 0 & 0 & 0 & 0 & 0 & 0 & 0 & 0 \\
0 & 0 & 0 & 0 & 0 & 0 & 0 & 0 & 0 & 0 & 0 & 0 & 0 & 0 & 0 & 0 \\
0 & 0 & 0 & 0 & 0 & 0 & 0 & 0 & 0 & 0 & 0 & 0 & 0 & 0 & 0 & 0 \\
0 & 0 & 0 & 0 & 0 & 0 & 0 & 0 & 0 & 0 & 0 & 0 & 0 & 0 & 0 & 0 \\
0 & 0 & 0 & 0 & 0 & 0 & 0 & 0 & 0 & 0 & 0 & 0 & 0 & 0 & 0 & 0 \\
1e10 & 0 & 0 & 0 & 0 & 0 & 0 & 0 & 0 & 0 & 0 & 0 & 0 & 0 & 0 & 0 \\
 & 0 & 0 & 0 & 0 & 0 & 0 & 0 & 0 & 0 & 0 & 0 & 0 & 0 & 0 & 0 \\
 & & 0 & 0 & 0 & 0 & 0 & 0 & 0 & 0 & 0 & 0 & 0 & 0 & 0 & 0 \\
 & & & 0 & 0 & 0 & 0 & 0 & 0 & 0 & 0 & 0 & 0 & 0 & 0 & 0 \\
 & & & & 0 & 0 & 0 & 0 & 0 & 0 & 0 & 0 & 0 & 0 & 0 & 0 \\
 & & & & & 0 & 0 & 0 & 0 & 0 & 0 & 0 & 0 & 0 & 0 & 0 \\
 & & & & & & 0 & 0 & 0 & 0 & 0 & 0 & 0 & 0 & 0 & 0 \\
 & & & & & & & 0 & 0 & 0 & 0 & 0 & 0 & 0 & 0 & 0 \\
 & & & & & & & & & & & & & & & 0
\end{pmatrix}
$$

(A11)

$$\boldsymbol{U}_c^{\mathrm{T}} = (5.67982 \quad 4.71355 \quad 27.2397 \quad 34.944 \quad -25.848) \qquad \text{(A12)}$$

$$\vec{t} = (0 \quad 0 \quad 0 \quad 0 \quad 0 \quad 0 \quad 0 \quad 1 \quad 0 \quad 0 \quad 0 \quad 0 \quad 0 \quad 0 \quad 0 \quad 0) \qquad \text{(A13)}$$

$$\vec{v} = \begin{pmatrix} 5.67982 \\ 4.71355 \\ 27.2397 \\ 34.944 \\ -25.848 \end{pmatrix} \qquad \text{(A14)}$$

$$\Omega^2 = \begin{pmatrix} 15881.79 & 0 & 0 & 0 & 0 \\ & 443939.69 & 0 & 0 & 0 \\ & & 1395068.08 & 0 & 0 \\ & & & 4483806.25 & 0 \\ & & & & 1449142170 \end{pmatrix} \qquad \text{(A15)}$$

$$\vec{f_2} = (126.023 \quad 666.288 \quad 1181.13 \quad 2117.5 \quad 38067.6) \qquad \text{(A16)}$$